UNIVERSITY OF CALIFORNIA,
IRVINE

Multicomponent DNAzyme-mediated Nucleic Acid Detection and Genotyping

DISSERTATION

submitted in partial satisfaction of the requirements
for the degree of

DOCTOR OF PHILOSOPHY

in Chemical and Biomolecular Engineering

by

Kefan Yang

Dissertation Committee:
Professor John C. Chaput, Chair
Professor Nancy Da Silva
Professor Han Li

2023

DEDICATION

To

my parents Yaohua Wang, and Yongzhi Yang

for their endless support and trust.

Life is trying things to see if they work. -Ray Bradbury

Table of Contents

LIST OF ABBREVIATIONS

ALP	alkaline phosphatase
aM	attomolar
ATP	adenosine triphosphate
au	arbitrary unit
BHQ	black hole quencher
CDC	centers for disease control and prevention
CHA	catalytic hairpin assembly reaction
COVID-19	coronavirus disease 2019
cp/uL	copy per microliter
CRISPR	clustered regularly interspaced short palindromic repeats
crRNA	small CRISPR RNA
Ct	cycle threshold
Cy5	Cyanine-5
ddPCR	droplet digital polymerase chain reaction
ddREVEALR	digital droplet REVEALR
DETECTR	DNA endonuclease targeted CRISPR trans reporter
DNA	deoxyribonucleic acid
DNase	deoxyribonuclease
DNAzyme	deoxyribozyme
dNTPs	deoxynucleoside triphosphate
EUA	emergency use authorization

EXPAR	exponential amplification reaction
FAM	fluorescein amidites
FANA	2′-deoxy-2′-fluoroarabino nucleic acid
FDA	U.S. food and drug administration
fM	femtomolar
GNP	gold nanoparticles
h	hour (s)
HCR	hybridization chain reaction
HDA	helicase-dependent amplification
HEX	Hexachloro-fluorescein
hr (s)	hour (s)
IVT	in vitro transcription
L	liter
LAMP	loop-mediated isothermal amplification
LFA	lateral flow assay
LNA	locked nucleic acid
LoD	limit of detection
M	molar
M-MuLV	Moloney murine leukemia virus
MERS	middle east respiratory syndrome
Mg	magnesium
$MgCl_2$	magnesium chloride

Min	minute
mM	millimolar
MNAzyme	multicomponent deoxyribozyme
MOE	2'-o-methoxy-ethylribonucleic acid
MT	mutant type
Mz	multicomponent deoxyribozyme
N/A	not applicable
n	nucleic acid amplification test
NaCl	sodium chloride
NASBA	nucleic acid sequenced based amplification
NEAR	nicking and extension amplification reaction
NGS	next-generation sequencing
nM	nanomolar
NPV	negative predictive value
NTC	no template control
NTP	ribonucleoside triphosphate
°C	Celsius
OMe	2'-o-methylribonucleic acid
OTC	over the counter
PAGE	polyacrylamide gel electrophoresis
PAM	protospacer adjacent motif
PCR	polymerase chain reaction

PFS	protospacer flanking site
pM	picomolar
PNA	peptide nucleic acid
POCT	point-of-care testing
PPD	proportion of positive droplets
PPV	positive predictive value
PS	phosphorothioate
qPCR	quantitative polymerase chain reaction
qRT-PCR	quantitative reverse transcription PCR
RAA	recombinase-aided amplification
RCA	rolling circle amplification
REVEALR	RNA-encoded viral nucleic acid analyte reporter
RNA	ribonucleic acid
Rnase H	ribonuclease H
RPA	recombinase polymerase amplification
RT	reverse transcription
SARS-CoV-2	severe acute respiratory syndrome coronavirus 2
SD	standard deviation
SDA	strand displacement amplification
SEM	standard error of the mean
SHERLOCK	specific high-sensitivity enzymatic reporter unlocking
SNP	single nucleotide polymorphisms

SSB	single-stranded DNA binding protein
STD	sexually transmitted diseases
T7 Trxn	T7 transcription
TMA	transcription-mediated amplification
TNA	threose nucleic acid
Tris-HCl	Tris hydrochloride
uL	microliter
uM	micromolar
um	micrometer
VOC	variant of concern
WT	wild type
XNAzyme	Xeno-nucleic acids enzyme

LIST OF FIGURES

LIST OF TABLES

ACKNOWLEDGEMENTS

I would like to express my deepest appreciation to my committee chair, Professor John Chaput for giving me the chance to join the lab from the chemical and biomolecular engineering department. I thank him for giving me unlimited trust and support to explore new directions. His insight knowledge, generosity on instruments/reagents, and tolerance to failures make my Ph.D. life much easier and more fruitful. The REVEALR systems could not be discovered without endless failures. Thank you again for all the helps, John.

I would like to thank my committee members, Prof. Weian Zhao, Prof. Nancy Da Silva, Prof. Han Li, and Prof. Chang Liu. Specifically, I would like to thank Prof. Nancy Da Silva who helped me have a smooth transfer to Chaput lab by serving as a co-advisor in the beginning, I really appreciate it! Also, I want to thank Prof. Weian Zhao who shared recourses of SARS-CoV-2 clinical samples that elevated my detection systems, making them more convincing. Thank you!

I would like to thank all current and former Chaput lab members for their physical and mental support. Specifically, I would like to thank Dr. Nicholas Chim, Dr. Cailen McCloskey, Dr. Ali Nikoomanzar, Dr. Derek Vallejo, and Eric Yik for their mentoring. I'm eternally grateful to lab manager Arlene Ngor for her help with interpersonal relationships, purchasing, and manuscript revision. Thank Daniel Schuder for working together with me on the assay development. Time flies when working in a nice research family here.

I would like to thank Prof. Brian M. Paegel and his group members for their guidance and accompany. Special thanks to Dr. Valerie Cavett, and Dr. Juan Hu for their educational suggestions that help move my project forward.

I would like to thank the Genomic High Throughput Sequencing Facility, Jenney Wu, and Whitney England at UCI for the support of NGS sequencing and trained me on bioinformatic analysis. Thank the Chao Family Comprehensive Cancer Center Experimental Tissue Shared Resource and Delia Tifrea for their clinical patient samples.

Thank the UCI Beall Applied Innovation for awarding me the Graduate Innovation Fellowship. It gave me a great opportunity to learn how the entrepreneur works.

I would like to thank all my friends for their love and support, especially Wenrui Lin, Xiao Nie, and Yue Zhao. You made my life at UCI much more colorful.

In the end, I would like to thank the American Chemical Society for the permission to include copyrighted paragraphs and figures of the chapter 2 and 3, which were originally published in the *Journal of the American Chemical Society.*[1,2] The co-authors listed in the publications are Dr. John Chaput, Daniel Schuder, and Arlene Ngor.

VITA

Kefan Yang

EDUCATION

Ph.D. in Chemical and Biomolecular Engineering, University of California, Irvine
Thesis Advisor: Professor John C. Chaput 2018 – 2023
Dissertation Title: *Multicomponent DNAzyme-mediated Nucleic Acid Detection and Genotyping.*

M.S. in Chemical Engineering, Texas A&M University 2015 – 2017

B.S. in Chemical Engineering and Technology, Tianjin University 2011 – 2015

RESEARCH PROJECTS

Assay Development of SARS-CoV-2 Nucleic Acid Detection Systems 08/2020-03/2023
Established a novel nucleic acid detection system, named REVEALR, capable of SARS-CoV-2 detection and genotyping and accurately identifying SARS-CoV-2 variants (Alpha, Beta, Gamma, Delta, Omicron).

- Optimized the assay for isothermal amplification (RPA, LAMP, RCA, NASBA, etc).
- Optimized DNAzyme sensor by nucleic acid modifications.
- Currently establishing an amplification-free detection system with microfluidic droplets.

Kinetic Analysis of *Bst* DNA Polymerase 05/2020 – 08/2020
Investigated *Bst* DNA polymerase to understand the order and transition of intermediates in the catalytic cycle of DNA synthesis.

- Designed plasmid constructs, which were then expressed in *E. coli* and protein purified.
- Assayed the polymerase activity of the various protein variants via primer extension.

Nucleic Acid Data Storage 03/2019 – 09/2020
Encoded, stored, and decoded digital information using nucleic acids (DNA and TNA).

- Performed NGS data analysis using bioinformatic tools and statistical analysis using Python.
- Demonstrated how nuclease-resistant TNA is a better alternative than DNA for long-term information storage.

PUBLICATIONS

5. **Yang K** and Chaput JC 2022. Droplet REVEALR: an ultrasensitive amplification-free nucleic acid detection platform, in preparation.

4. **Yang K**, Schuder DN, Ngor AK, and Chaput JC 2022. REVEALR-based genotyping of SARS-CoV-2 variants of concern in clinical samples. *J. Am. Chem. Soc.* 144, 11685-11692.
   - *University of California Announcements and News: "UCI-developed COVID-19 test detects, identifies specific variants with 100% accuracy" (Aug. 3, 2022)*

3. **Yang K** and Chaput JC 2021. REVEALR: A multicomponent XNAzyme-based nucleic acid detection system for SARS-CoV-2. *J. Am. Chem. Soc.* 143, 8957-8961.
   - *University of California Announcements and News: "Professor John Chaput and grad student Kefan Yang developed a nucleic acid detection system named REVEALR" (July 9, 2021)*
2. **Yang K**, McCloskey CM, and Chaput JC 2020. Reading and writing digital information in TNA. *ACS Synth. Bio.* 9, 2936-2942.

1. Chim N, Meza RA, Trinh AM, **Yang K**, and Chaput JC 2021. Following replicative DNA synthesis by time-resolved X-ray crystallography. *Nat. Commun.* 12: 2641.
   - *Berkeley National Labs ALS Scientific Brief: "DNA Synthesis: Flip it and Reverse it" (Dec. 2, 2021)*

PATENTS

- John C. Chaput, **Kefan Yang**, "Multicomponent XNAzyme-based Nucleic Acid Detection System", UC Case Number: 2021-789

- John C. Chaput, **Kefan Yang**, "REVEALR-based Genotyping of SARS-CoV-2 Variants of Concern in Clinical Samples", UC Case Number: 2022-961

AWARDS & HONORS

Graduate Innovation Fellowship, UCI Beall Applied Innovation, April 2022
- Trained to commercialize a startup idea from the research lab into potential business ventures.

TEACHING & PROFESSIONAL EXPERIENCE

Teaching Assistant, Department of Chemical and Biomolecular Engineering, UCI
Spring 2021
- Held office hours for detailed discussions and student support outside of lectures.
- Graded course assessments to ensure students understood the material and stayed on track.

Judge, International Genetically Engineered Machine (iGEM) Competition Fall 2021
- Invited judge for 2021 iGEM competition, which gathers and trains the next generation of student researchers for the synthetic biology field.

Intern, Institute of Microbiology, Chinese Academy of Sciences, Beijing, China
07/2018– 08/2018

- Used Golden Gate methods to optimize the yield of shikimic acid.
- Trained in gene knockout using the CRISPR-Cas9 system in *E. coli*.

Lab Technician, EK Laboratories, FL, USA 09/2017 – 06/2018

- Produced biofuel (ethanol) with pretreating biomass (hay, yard waste) through hot water/acid/alkali/microwave.
- Developed fermentation process using *Saccharomyces cerevisiae* yeast to produce bioethanol.
- Trained in HPLC for the testing of sugar concentration.

PRESENTATIONS

- "SARS-CoV-2 Nucleic Acid Detection and Genotyping", Synthetic and Chemical Biology Club (SCBC), Irvine, CA. Feb. 18, 2022.
- "Effect of Extraction Using Ion-Exchange Resins on Countercurrent Mixed-Acid Fermentations", 2016 Texas A&M Conference on Energy, College Station, TX, Sept. 16, 2016.

SELECTED SKILLS & TECHNIQUES

- Molecular diagnostics: PCR, qPCR, ddPCR, RPA, LAMP, RCA, NASBA, EXPAR
- Microfluidics: PDMS chip fabrication, droplet generation and sorting
- Data analysis: Python, MATLAB, bioinformatic tools, JMP, ImageJ
- Characterization: Confocal & Fluorescence Microscopy; GC; Mass-Spec; PAGE/SDS-PAGE
- Wet lab techniques: DNA and RNA extraction/purification, Protein expression and purification

ABSTRACT OF THE DISSERTATION

Multicomponent DNAzyme-mediated Nucleic Acid Detection and Genotyping

by

Kefan Yang

Doctor of Philosophy in Chemical and Biomolecular Engineering

University of California, Irvine, 2023

Professor John C. Chaput, Chair

The coronavirus disease 2019 (COVID-19) pandemic caused millions of deaths and serious socioeconomic disruptions, and boosted the unprecedented development of novel nucleic acid detection methods. Although polymerase chain reaction (PCR) is the golden standard and has been widely used for practical nucleic acid detection, isothermal amplification strategies capable of rapid, inexpensive, and accurate nucleic acid detection also provide new options for large-scale pathogen detection, disease diagnosis, and genotyping. Here we are going to describe an assay development journey from a simple COVID-19 detection assay to a genotyping strategy and eventually to a droplet-based amplification-free assay.

Chapter 1 reviews the general strategies for nucleic acids detection. Starts from the most well-known PCR reaction to a variety of isothermal amplification-based techniques that have been applied for severe acute respiratory syndrome coronavirus 2 (SARS-CoV-2)

nucleic acid detection. Specifically, the clustered regularly interspaced short palindromic repeats (CRISPR)-based biosensor systems and the DNAzyme-based biosensor systems are further described that could be coupled with amplification strategies for ultra-sensitivity and specificity.

Chapter 2 describes a highly sensitive multicomponent XNA-based nucleic acid detection platform that combines analyte preamplification with X10–23 mediated catalysis to detect the viral pathogen responsible for COVID-19. It is termed RNA-Encoded Viral Nucleic Acid Analyte Reporter (REVEALR), and functions with a detection limit of ≤20 aM (~10 copies/μL) using conventional fluorescence and paper-based lateral flow readout modalities. With a total assay time of 1 h, REVEALR provides a convenient nucleic acid alternative to equivalent CRISPR-based approaches, which have become popular methods for SARS-CoV-2 detection. The assay shows no cross-reactivity for other in vitro transcribed respiratory viral RNAs and functions with perfect accuracy against COVID-19 patient-derived clinical samples.

Chapter 3 describes how we design REVEALR into a novel genotyping assay that detects single-base mismatches corresponding to each of the major SARS-CoV-2 strains found in the United States. Of 34 sequence-verified patient samples collected in early, mid, and late 2021 at the UCI Medical Center in Orange, California, REVEALR identified the correct variant with 100% accuracy. The assay, which is programmable and amenable to multiplexing, offers an important new approach to personalized diagnostics.

Chapter 4 describes an improved REVEALR platform, termed digital droplet REVEALR (ddREVEALR), that can achieve direct viral detection and absolute quantitation

utilizing a signal amplification strategy that relies on DNAzyme multiplexing and volume compression. Using an AI-assisted image-based readout, ddREVEALR was found to achieve 95% positive predictive agreement from a set of 20 nasal pharyngeal swabs collected at UCI Medical Center in Orange, California. We suggest that the combination of amplification-free and protein-free analysis makes ddREVEALR a promising approach for direct viral RNA detection of clinical samples.

Chapter 5 summarizes the developed DNAzyme-based nucleic acid detection methods, offers some alternatives, compares the DNAzyme-based platforms with CRISPR-based platforms, and gives insight into potential future directions to further elevate the REVEALR system.

CHAPTER 1:

Introduction of nucleic acid detection for SARS-CoV-2

1.1. Introduction

Natural nucleic acids, including deoxyribonucleic acid (DNA) and ribonucleic acid (RNA), encode genetic information and play very important roles in all living creatures. Thus, they are commonly used as biomarkers for diagnostics[3]. Compared with the detection of other biomarkers like antigens detection, nucleic acid detection is more sensitive because they could be amplified to a tremendous amount before detection. [4]

In general, COVID-19 nucleic acid test includes 3 steps. First, the patent specimens could be collected through nasopharyngeal swabs, throat swabs, or saliva. Second, the clinical sample will be lysed and purified through an RNA purification kit. Last, the purified sample will be moved forward to nucleic acid amplification test (NAAT) based detection. Here we are mainly focused on the detection step after RNA purification.

1.2. Amplification-based methods

1.2.1 Summary of amplification methods

Nucleic acid amplification tests (NAATs) are the most used methods for nucleic acid detection. A small amount of nucleic acid analytes is amplified using sequence-specific primers and polymerases. The amplicons could be detected through fluorescent signal, colorimetric signal, lateral flow assay, etc. The most popular NAAT is the PCR, followed by isothermal amplifications like loop-mediated isothermal amplification (LAMP), recombinase

polymerase amplification (RPA), transcription-mediated amplification (TMA), nucleic acid sequence-based amplification (NASBA), nicking and extension amplification reaction (NEAR), rolling circle amplification (RCA), helicase-dependent amplification (HDA), strand displacement amplification (SDA), etc. There are several additional proteins, like reverse transcription (RT), helicase, recombinase, single-stranded DNA binding protein (SSB), and RNase H that involve in detecting RNA under isothermal conditions.

For COVID-19 detection, there are 275 U.S. food and drug administration (FDA) approved NAAT-based methods till 11/02/22, among which ~90% of the FDA-approved SARS-CoV-2 nucleic acid detection methods are PCR based. Among all the other NAAT-based methods, LAMP and TMA are the most popular strategies (Figure 1.1, Table 1.1).

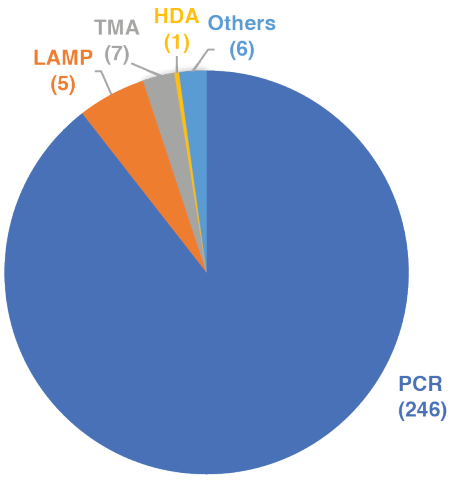

Figure 1.2.1. FDA-approved NAAT cases. Data was collected till 11/4/2022. In total, there are 275 FDA-approved NAAT methods.

Table 1.1. Summary of amplification methods for SARS-CoV-2 detection

No	Name	Enzyme	Limit of detection (LoD)	Reaction time (min)	Companies	Reference
1	PCR	polymerase	1-10 copies/reaction	30 - 90	Roche; Cepheid; Quest Diagnostics	[5,6]
2	NASBA	RT, RNA polymerase, RNase H	50 copies/reaction	90	N/A	[7]
4	LAMP	polymerase	10 copies/reaction	30 - 60	Detect; Lucira Health	[8]
5	HDA	polymerase, helicase, SSB	6 copies/uL	30 - 120	Quidel Corporation	[9]
6	RPA	polymerase, recombinase, SSB	5 - 10 copies/reaction	30 - 90	Synsorbio	[10]
8	NEAR	Polymerase, Nicking enzyme	20 copies/ uL	10 - 30	Abbott	[11]
10	TMA	RT, RNA polymerase	<1 copy/ uL	210	Grifols; Hologic; Quest Diagnostics	[12]

1.1.1. PCR

PCR was first described as a paper in 1986 by Kary Mullis[13] who received the 1993 Nobel prize in chemistry for this discovery. Since then, PCR was considered the golden-standard method for nucleic acid detection[14]. It uses a thermocycler to obtain the optimized temperature for denaturation, annealing, and primer extension (Figure 1.2). And by coupling with intercalating dye (e.g., SYBR) or the TaqMan probe, it could even do quantitative analysis by comparing the cycle of a threshold. For COVID-19 detection, PCR-based methods occupy most of the FDA-approved nucleic acid test cases. Companies like Roche and Cepheid are selling kits that proved to be accurate and reliable.

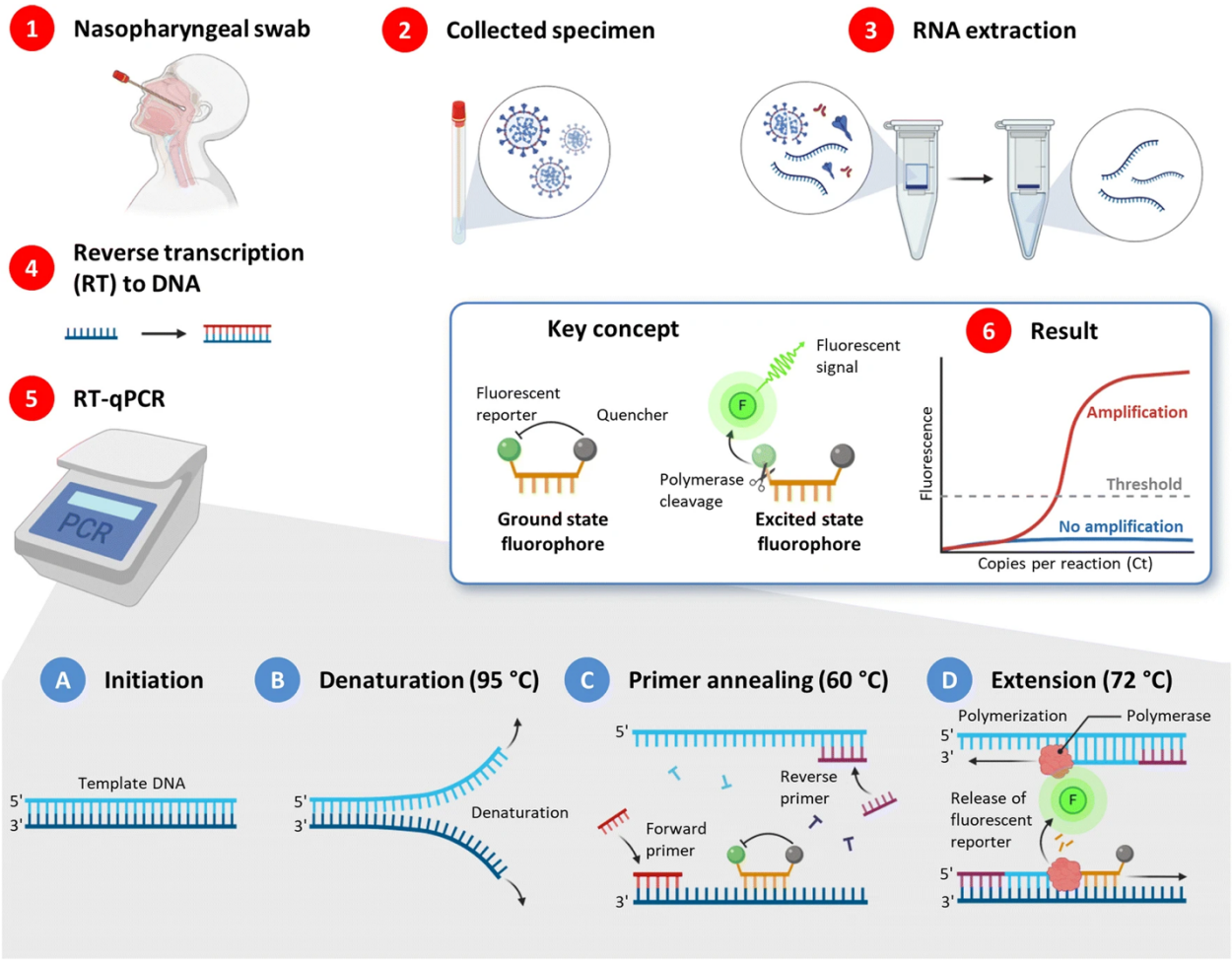

Figure 1.2.1. PCR test for COVID-19. The figure was adapted from Majumder, J.; Minko, T. *AAPS Journal*[15]. Reprinted with permission from Springer Nature.

1.2.2. LAMP

LAMP was first proposed in 2000 for the highly specific and rapid detection of nucleic acids. The reaction is usually performed under 65°C for 30 to 60 minutes and yield ~10^9 cauliflower-like dsDNA copies with a strand displacing polymerase and 4-6 primers are involved to generate (Figure 1.3). There is a large number of amplicons, resulting in pyrophosphate ion by-product and pH change. By coupling with a fluorescent metal indicator or pH-sensitive dye, the LAMP reaction enables visual result discrimination[16]. Also, LAMP shows higher tolerance for the inhibitors in the clinical samples[17], making it one of the ideal

NAAT methods for point-of-care testing (POCT) devices. Till now, LAMP is the most popular NAAT method for COVID-19 detection other than PCR. Several related products from companies like Lucira health and DETECT have been practically used to fight against COVID-19.

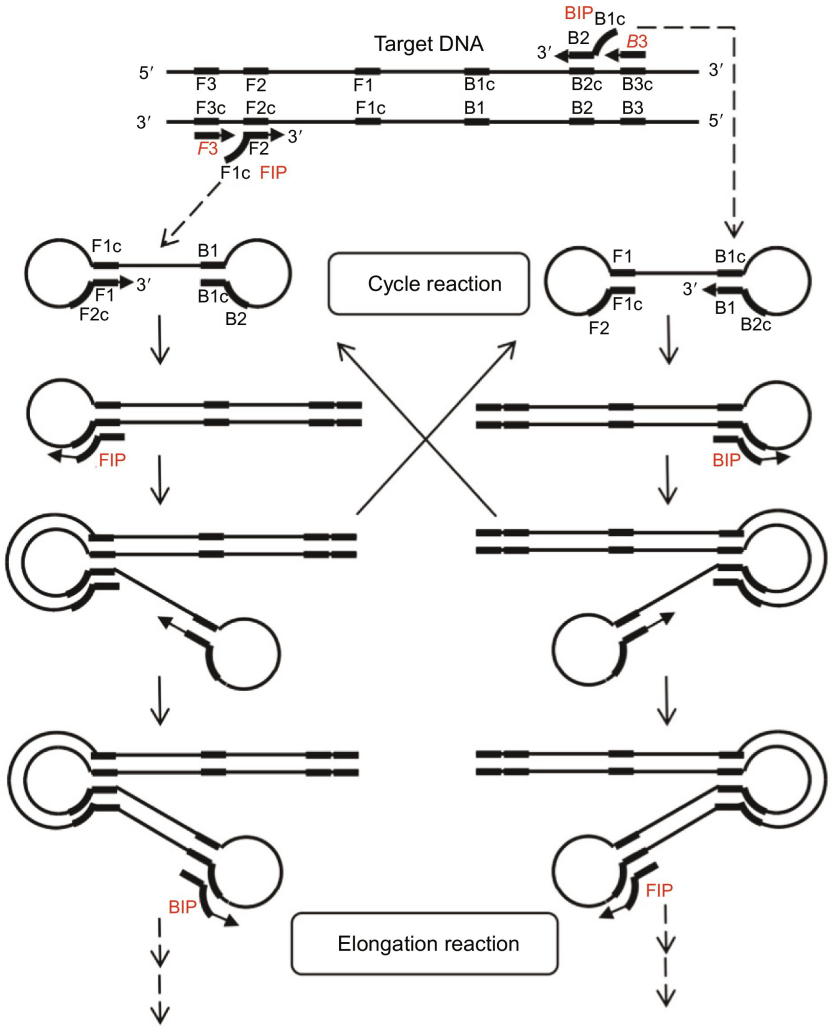

Figure 1.2.2. Scheme for LAMP reaction. This figure was adapted from Zheng, Z.; Cheng, Z. *Advances in Clinical Chemistry*; 2017; Vol. 80[18]. Reprinted with permission from Elsevier.

1.2.3. RPA

RPA was first discovered in 2006 utilizing recombinase to separate the dsDNA template that avoids the need for thermocycling steps in PCR[19]. The recombinase-primer

complexes can scan the dsDNA template, find the corresponding primer binding sites, and insert the primer. SSB is used to stabilize the ssDNA template and primer extension happens with strand displacing polymerase (Figure 1.4). With 20 min to 60 min incubation under 37°C to 42°C, RPA could detect the attomolar level of the analyte through florescent probe-based detection or lateral flow-based detection. The commercial RPA kit is available through TwistDx (Cambridge, U.K.) and some companies (e.g., Synsorbio) developed RPA based assay for COVID-19 detection.

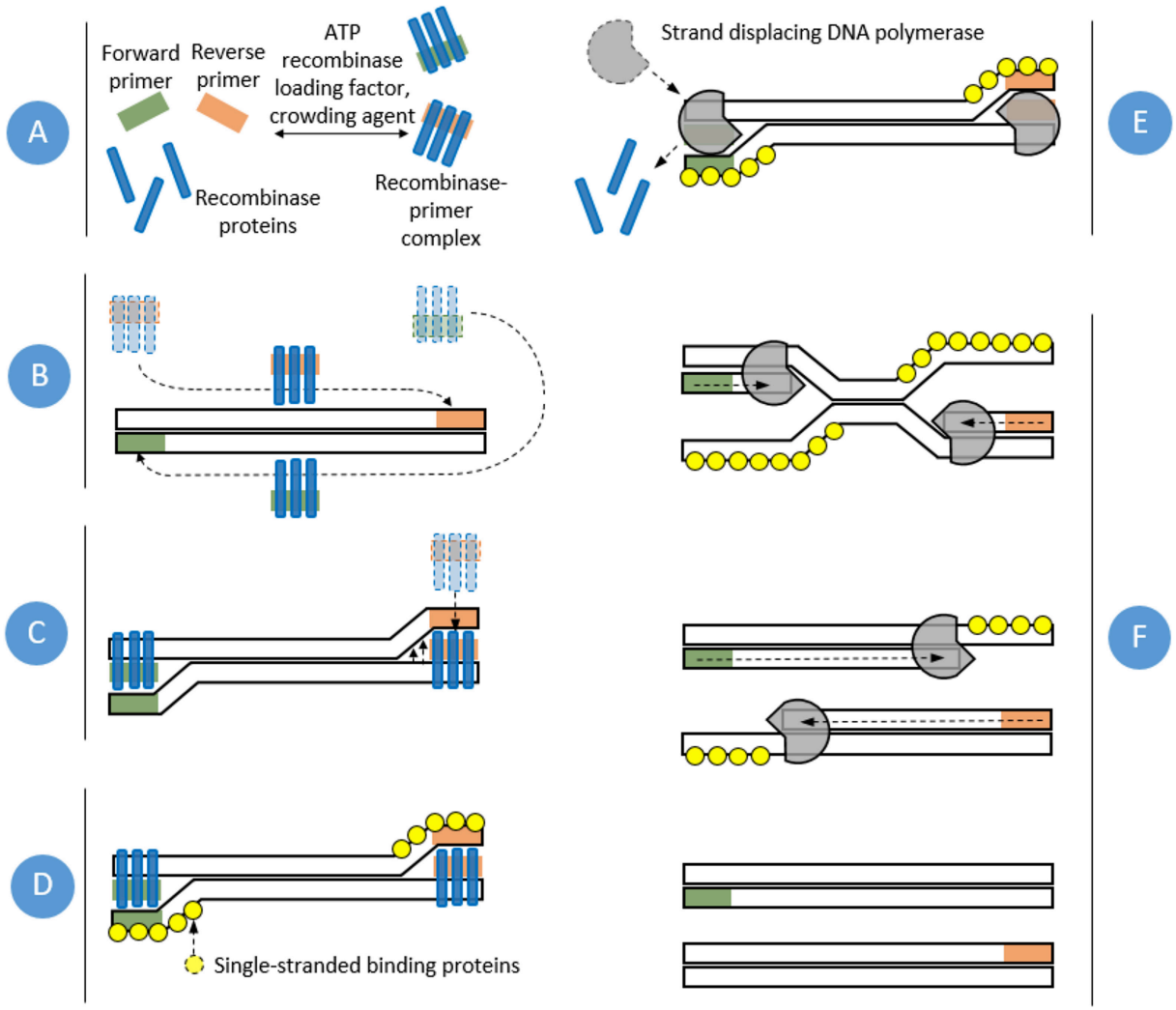

Figure 1.2.3. RPA amplification scheme. This figure was adapted from Lobato, I. M.; O'Sullivan, C. K. *Trends in Analytical Chemistry* 2018, 98, 19–35[20]. Reprinted with permission from Elsevier.

1.2.4. NASBA and TMA

NASBA was first discovered in 1991 as an alternative nucleic acid amplification yielding an RNA amplification of 10^6 to 10^9-fold under 41°C within 2 hours.[21] It requires three enzymes: RT, T7 RNA polymerase, and RNase H. The target RNA will first bind to primers and do primer extension with RT to generate cDNA. After RNase H digestion, the single-stranded cDNA will serve as the template for primer extension after binding to the second primer that contains the T7 promoter overhang. With T7 RNA polymerase, there will be many antisense RNA generated which will also serve as templates for the original RT reaction (Figure 1.5). The NASBA reaction targets RNA and does the exponential accumulation of the antisense RNA.[22] TMA is a very similar method, and the only difference is the lack of RNase H which was replaced by the RT that has the RNase H activity. TMA-based method has been used for practical COVID-19 detection by companies like Grifols, Hologic, and Quest Diagnostics.

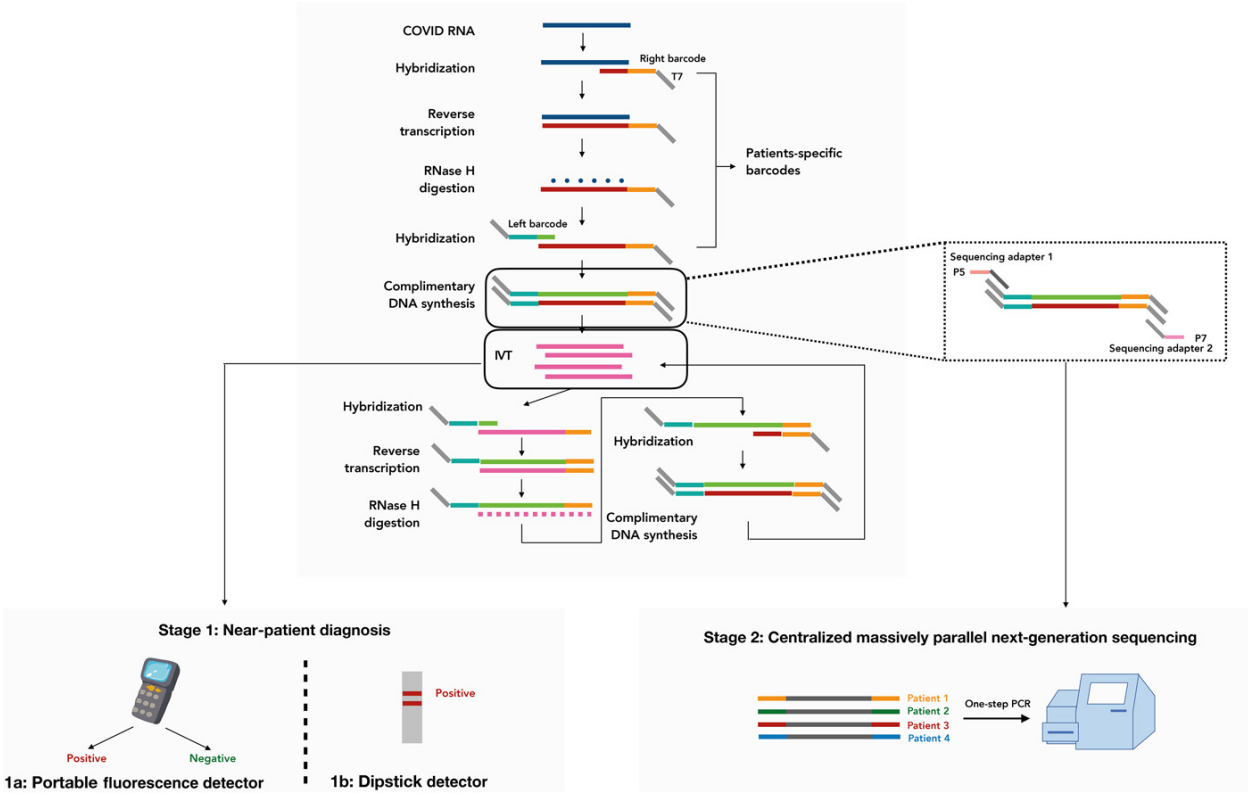

Figure 1.2.4. NASBA assay for SARS-CoV-2 detection. This Figure was adapted from Wu, Q., Suo, C., Brown, T., Wang, T., Teichmann, S. A.; Bassett, A. R. *Sci. Adv* (Vol. 7)[7]. Exclusive license American Association for the Advancement of Science. Distributed under a Creative Commons Attribution License 4.0 (CC BY).

1.2.5. HDA

In the HDA reaction, DNA helicase is employed to unwind the dsDNA and generates ssDNA for primer binding and the single-stranded binding protein (SSB) is coated with the ssDNA to prevent reassociation of the DNA templates (Figure 1.6). Then DNA polymerase will do primer extension to generate a million-fold amplification.[23] The HDA reaction needs incubation at 37°C or 65°C for 30 to 120 min. The commercial HDA kit is available through the New England BioLabs for research and Quidel for practical SARS-CoV-2 detection.

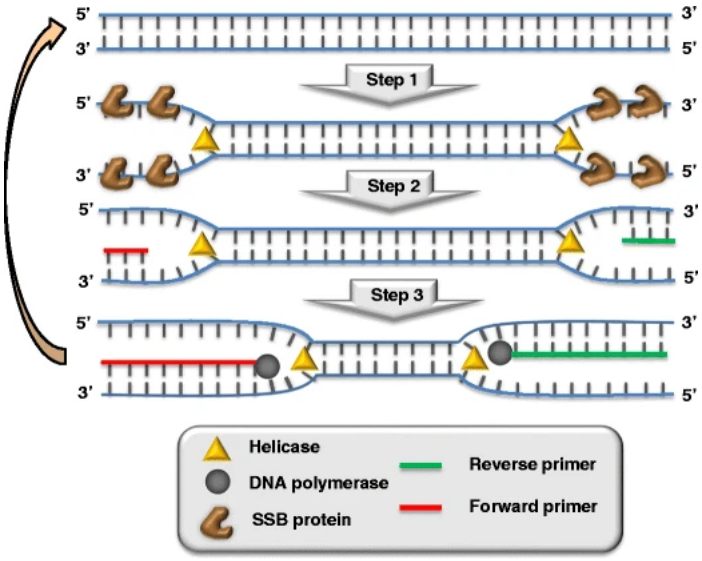

Figure 1.2.5. HDA overview. The figure was adapted from Barreda-García, S.; Miranda-Castro, R.; de-los-Santos-Álvarez, N.; Miranda-Ordieres, A. J.; Lobo-Castañón, M. J. *Analytical and Bioanalytical Chemistry*. Springer Verlag January 1, 2018, pp 679–693. [24]. Reprinted with permission from Springer Nature.

1.2.6. NEAR

NEAR was first described in a patent published in 2009. This idea was amended from the original linear mode exponential amplification reaction (EXPAR) where nicking enzyme that cleavage on only one strand of the dsDNA cleavage site and strand-displacing polymerase could continually do primer extension from the cleavage sites for linear amplification[25]. The NEAR (Figure 1.7) introduces nicking enzyme cleavage sites on both forward amplicon and reverse amplicon, making the nicking enzyme cleavage to be an exponential amplification for the same amplicon region[26]. One advantage is the short reaction time because the reaction is usually completed in 10 to 20 min. Whereas the drawback of the method is the potential false negatives caused by non-specific amplification[27]. Abbott's ID NOW device is a great example of using NEAR for COVID-19 detection.

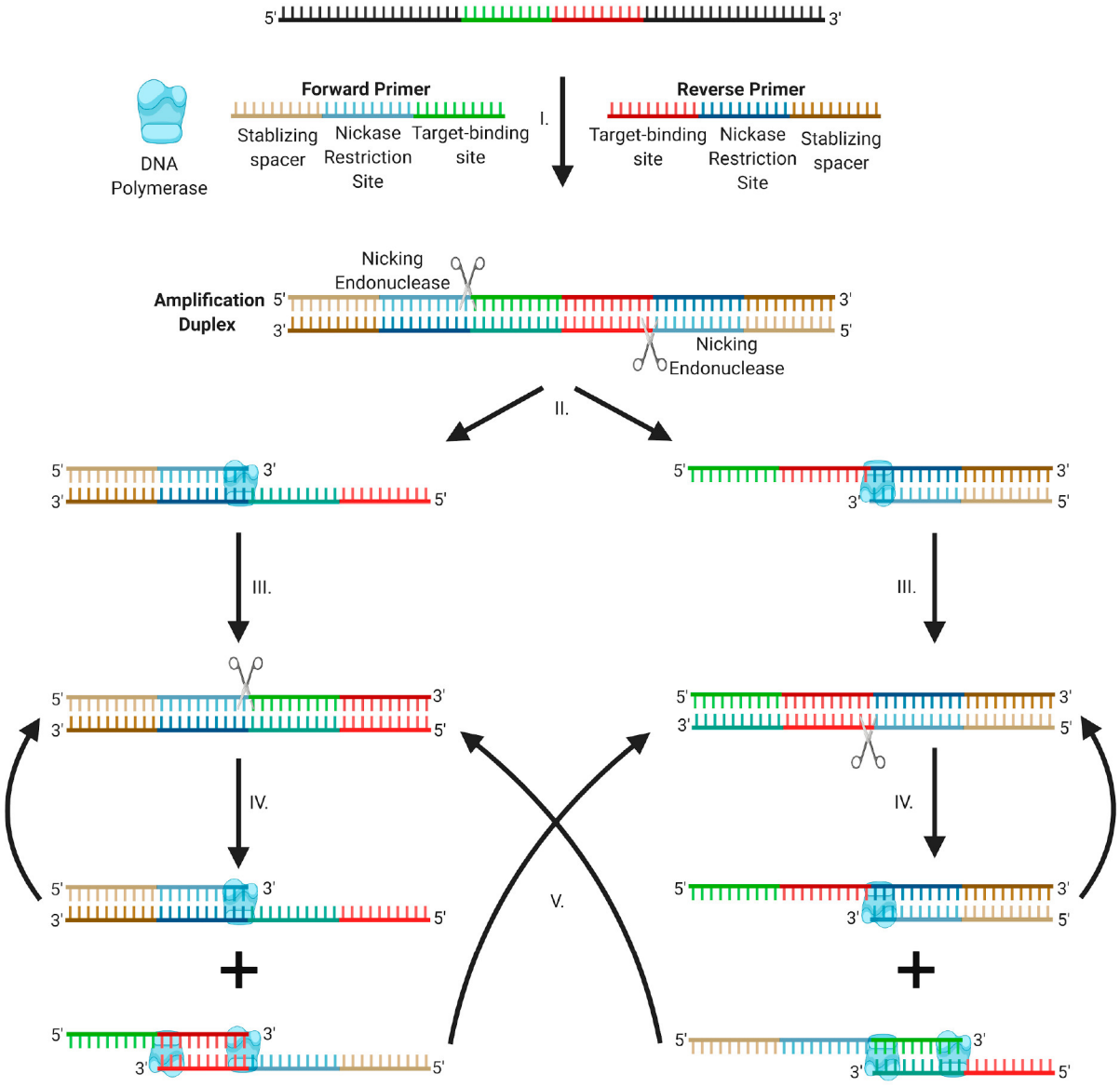

Figure 1.2.6. Nicking enzyme amplification reaction (NEAR). This figure was adapted from Khan, P., Aufdembrink, L. M.; Engelhart, A. E. *ACS Synthetic Biology*, 9(11), 2861–2880[14]. Reprinted with permission from the American Chemical Society.

1.3. Biosensor-based detection

Although the isothermal amplification-based methods show a lot of potentials, there exist trade-offs on these types of methods like sensitivity or specificity due to non-specific amplification, which limits their further applications for POCT or over-the-counter (OTC) devices. Thus, higher sensitivity and specificity methods are higher desired.

One potential solution for this issue is to couple a biosensor system with isothermal amplification to further enhance its sensitivity and specificity. Here we are going to describe two promising biosensors: CRISPR-Cas protein and multicomponent DNAzyme.

1.3.1. CRISPR-based methods

1.3.1.1. Derivation and Mechanism of CRISPR diagnostics

Since the discovery of the CRISPR-Cas9-based gene editing system in 2012[28], it has been widely used for gene therapy. The system was first applied to diagnose the discovery of collateral cleavage activity in 2016[29]. Since then, researchers further boosted the sensitivity by combining with NAAT, for example, LAMP, RPA, RCA, EXPAR, NASBA, etc, with the CRISPR-based biosensor. The two well-known assays are the specific high-sensitivity enzymatic reporter unlocking (SHERLOCK) system[30] and the DNA endonuclease targeted CRISPR trans reporter (DETECTR) system[31], which will be explained in detail later.

1.3.1.2. Summary of current NAAT assisted CRISPR based methods

There are three major categories (Cas9, Cas12, Cas13) distinguished by their protein families of CRISPR systems (Table 1.2). Cas9 targets dsDNA and cleaves on the dsDNA.

The detection system used deactivated Cas9 and could recognize the single nucleotide polymorphisms (SNP) by the different binding affinity between match or mismatch conditions. Whereas most Cas13 and Cas12-based detections rely on the collateral effect. Once the crRNA and CRISPR protein complex bind to the target analyte, the RNase activity (Cas13) or DNase (Cas12) activity will be triggered and do cleavage on the fluorescence-labeled reporter.[30]

The most popular NAAT methods that were used with CRISPR protein for COVID-19 detection are RT-LAMP and RT-RPA. The limit of detection (LoD) ranges usually in the low aM level, which is considered comparable with PCR-based assay. The addition of the CRISPR sensor to the NAAT reaction enhanced the sensitivity because of the additional signal amplification[32] and the combined system has the capability of recognizing a single mutation[30]. More importantly, it can minimize the drawback of isothermal amplification, the non-specific amplification.

The reaction time ranges from 40 min to 120 min, depending on the choice of NAAT, purification protocols, and signal readout methods. There are 3 major signal readouts: fluorescent readout, lateral flow readout, and naked-eye visualization. In general, the fluorescent readout gives the highest signal intensity and lateral flow readout[33], and naked eye visualization methods have better convenience towards POCT and OTC.

Based on the reaction liquid transferring steps, it could be separated as one pot reaction or two pot reaction. In general, two pot reaction has higher sensitivity but has a higher chance of getting contamination, needs well-trained researchers to operate, and requires extra liquid handling[34]. Whereas one-pot reaction is more convenient and tends to

be more suitable for practical POCT devices. There are several strategies to achieve one pot goal, for example, using special separation by adding CRISPR reagent to the wall or on cap[32,35], microfluidic device for liquid handling,[36] or utilizing the viscosity of glycerol[37]. Overall, the CRISPR system shows a huge potential for POCT or OTC of future precision medicine.

Table 1.2. NAAT assisted CRISPR based methods for COVID-19 detection

Classification	Assay name	NAAT method	LoD	Time (min)	Readout	1 / 2 pots	Ref
Cas13-based	CREST	RT-PCR	10 copies/reaction	120	Naked eye	2	[38]
	SHERLOCK	RT-RPA	42 copies/reaction	60	Fluorescent/LFA	2	[39]
	SHINE	RT-RPA	10 copies/ uL	50	Fluorescent/LFA	1	[40]
	DISCoVER	RT-LAMP	40 copies/ uL	60	Fluorescent	1	[36]
Cas12-based	STOPCovid.v2	RT-LAMP	100 copies/reaction	45	Fluorescent/LFA	2	[41]
	DETECTR	RT-LAMP	10 copies/reaction	40	LFA	2	[8,42]
	AIOD-CRISPR	RT-RPA	5 copies/reaction	40	Naked eye	1	[42]
	iSCAN	RT-LAMP	10 copies/reaction	40	Naked eye/LFA	2	[43]
	CASdetec	RT-RAA	10 copies/reaction	60	Fluorescent/Naked eye	1	[44]
Cas9-based	FELUDA	RT-RPA	10 copies/reaction	60	LFA	1	[40]

Note: LFA: lateral flow assay; RAA: recombinase-aided amplification.

1.3.1.3. SHERLOCK system

The specific high-sensitivity enzymatic reporter unlocking (SHERLOCK) system is the 1st mature CRISPR-based biosensing system established in 2017, which can achieve the attomolar (aM) level of DNA/RNA detection with single-based resolution (Figure 1.8). The nucleic acid targets are isothermally amplified by RPA, the dsDNA amplicon will then be converted to ssRNA by T7 transcription. Cas13 protein will then bind to the ssRNA with the assistance of crRNA and do collateral RNA cleavage on the fluorescent reporter and give distinguishable signals[45].

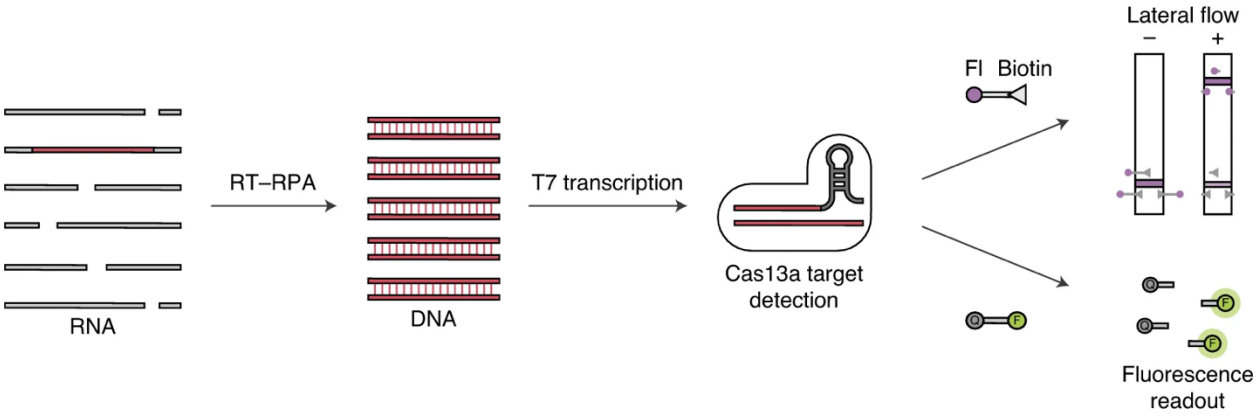

Figure 1.3.1.3. SHERLOCK nucleic acid detection platform. The figure was adapted from *Nat Biomed Eng* 2020, 4 (12), 1140–1149[39]. Reprinted with permission from Springer Nature. The SHERLOCK system was updated to the SHERLOCK v2 in 2018[46], which is a quantitative, multiplex, cascaded with Csm6 and lateral flow-based detection, making it more practical for POCT detection.

As the COVID-19 pandemic occurred in 2020, several clinical studies on rapid SARS-CoV-2 nucleic acid detection using the SHERLOCK system were performed. One clinical study in a Thailand hospital used 154 clinical samples using the original SHERLOCK system and achieved 100% positive perspective agreement (PPV) and 100% negative perspective agreement (NPV) with fluorescence readout. It shows the reliability of the assay for practical nucleic acid detection.

This assay is in process of being commercialized by SHERLOCK Bioscience and Proof Diagnostics. And SHERLOCK Bioscience received FDA emergency use authorization (EUA) approval on 02/18/2022. In the future, you could expect to get reliable nucleic acids test for infectious diseases like COVID-19 or sexually transmitted diseases (STDs) at home.

1.3.1.4. DETECTR system

The DETECTR system was first proposed by Jennifer Doudna and coworkers in 2018[31]. It discovered the non-specific ssDNA cleavage activity of Cas12 once binding to the dsDNA target (Figure 1.9). Since the Cas12 could do collateral cleavage after binding to

dsDNA amplificon, it simplified the T7 transcription step compared with the SHERLOCK system. Once combined with isothermal amplifications like RT-RPA or RT-LAMP, the whole system could detect low attomolar (aM) levels of DNA/RNA analyte.

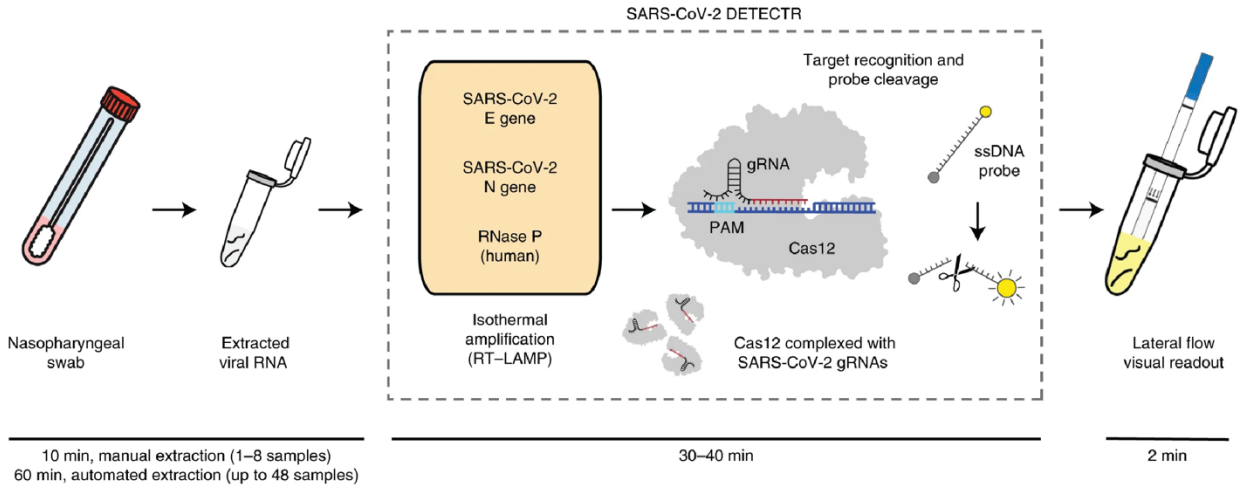

Figure 1.3.1. The DETECTR system for SARS-CoV-2 detection. The figure was adapted from Chen, J. S.; Ma, E.; Harrington, L. B.; da Costa, M.; Tian, X.; Palefsky, J. M.; Doudna, J. A. *Science* (1979) 2018, 360 (6387), 436–439[31]. Reprinted with permission from the American Association for the Advancement of Science.

To fight against the COVID-19 pandemic, researchers in Mammoth Bioscience evaluated the DETECTR assay for the SARS-CoV-2 virus with 78 patient samples and achieved 95% PPV and 100% NPV[8]. This assay received FDA EUA approval on 07/07/2021. Currently, they are in process of developing a system using automated liquid handling equipment. This new high throughput system could be able to detect thousands of samples per day.

1.3.2. Multicomponent RNA-cleaving DNAzyme-based methods

In addition to CRISPR-based biosensors, multicomponent RNA-cleaving DNAzyme is another promising biosensor to combine with NAAT for highly sensitive and specific amplification on COVID-19 detection. Here I will give a detailed description of the derivation of DNAzyme, the current state-of-art of multicomponent DNA enzyme, the SNP recognition capability examples, and the influences of chemical modifications.

1.3.2.1. Derivation and Mechanism of DNAzyme

The first RNA-cleaving DNAzyme was discovered by Gerald Joyce in 1997 through in vitro selection[47]. They found the 8-17 DNAzyme (the 17th clone from round 8) and 10-23 DNAzyme (the 23rd clone from round 10). The 10-23 DNAzyme is composed of a 15 nt catalytic core and two substrate binding arms that are reverse complementary to the target RNA (Figure 1.10). The preferred cleavage site is YR, where Y = U or C, and R = A or G and the UG site has the highest cleavage efficiency. The cleavage activity is dependent on the metal ion where magnesium (Mg^{2+}) is most frequently used and higher pH tends to accelerate the cleavage[48].

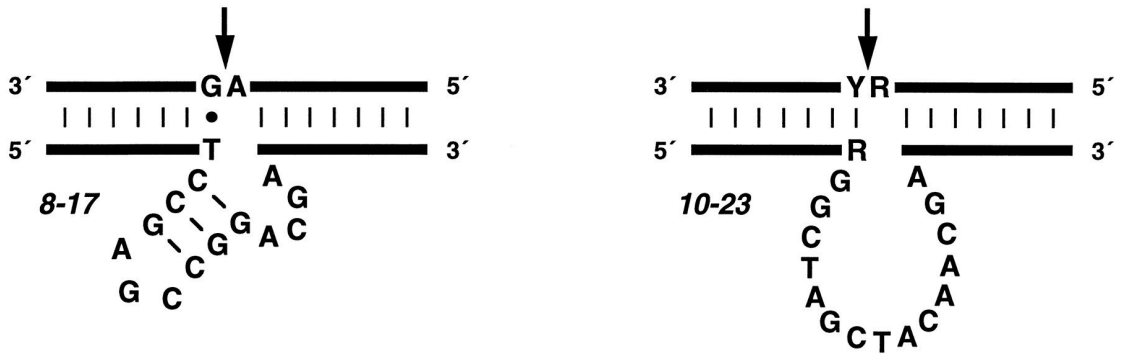

Figure 1.3.2 Composition of the DNAzyme catalytic motifs. This figure was adapted from Stephen W. Santoro and Gerald F. Joyce, *Biochemistry* 1997[47]. Reprinted with permission from the American Chemical Society.

Recently, researchers in Germany obtained the crystal structure of the 10-23 DNAzyme[49] where it forms a condensed core region with an additional turn around the RNA substrate (Figure 1.11a, b). The mechanism was illustrated through 3 major steps, substrate binding and metal ion binding, cleavage, and dissociation (Figure 1.11c). Based on Gerald F. Joyce's study and Manuel Etzkorn's study, the rate-limiting step might be the substrate binding or the release of Mg^{2+} shown as state B_2. These phenomena will be further studied in the following chapters.

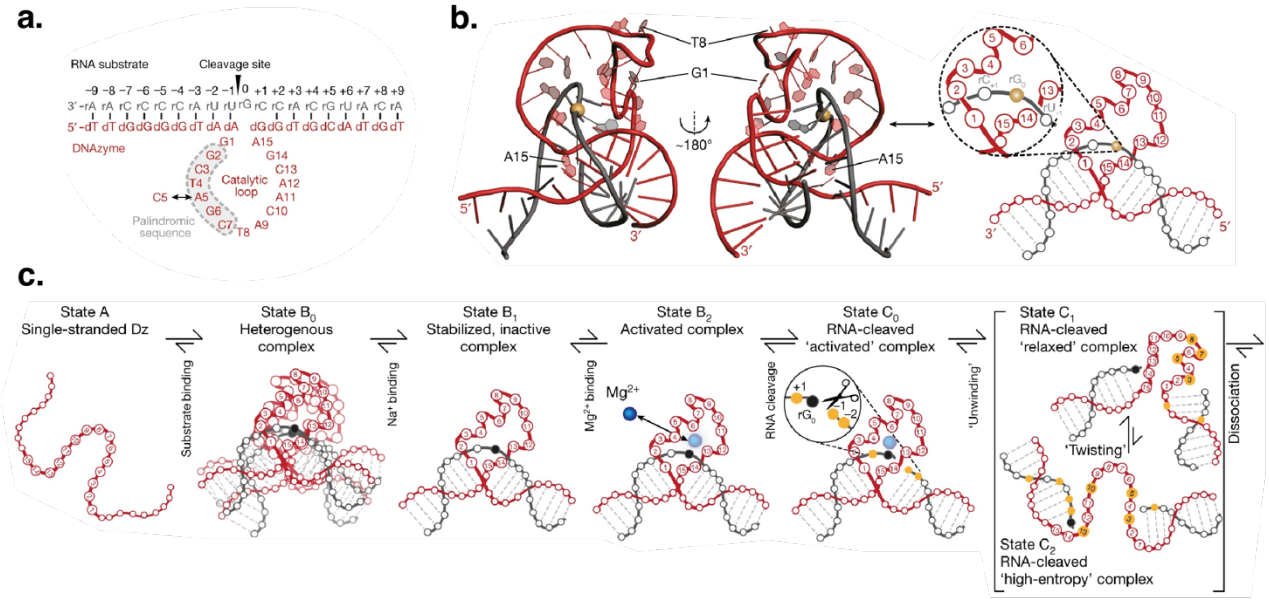

Figure 1.3.2. Crystal structure and states of cleavage transition of the 10-23 DNAzyme. a. overview of 10-23 DNAzyme with the catalytic core positive labeled. **b.** The crystal structure and its simplified version of the 10-23 DNAzyme. **c.** Overview of the cleavage transition states. This figure was adapted from *Nature* 2022, 601 (7891), 144–149[49]. Reprinted with permission from Springer Nature.

1.3.2.2. Derivation and development of Multicomponent DNAzyme

The split design was initially used as a binary DNA probe or a binary DNAzyme for analyte detection[50–52]. It was Alison V. Todd and her coworkers that first introduced the split design to 10-23 DNAzyme, which boosted the cleavage activity and made it more practical for analyte detection[53]. Over the last 10 years, the multicomponent deoxyribozyme (MNAzyme) has been well developed for multiple signal readouts and a better limit of detection for broader applications (Table 1.3).

The MNAzyme sensor for nucleic acid detection can be classified into 3 categories, MNAzyme only, MNAzyme with signal amplifications, and MNAzyme with NAAT. For MNAzyme only, researchers were further improving the performance of MNAzyme by using additional reagents like cationic copolymer[54], locked nucleic acid (LNA) modifications,[55] or using some special instrument like microwell[56]. To extend the application, researchers also

coupled with gold nanoparticles (GNPs)[57] for colorimetric readout or alkaline phosphatase (ALP)[58] for electrochemical readout.

For MNAzyme with signal amplifications, researchers introduced hybridizations-based amplification strategies like hybridization chain reaction (HCR)[59] or catalytic hairpin assembly reaction (CHA)[60] for signal transducers. Also, cascade designs were frequently to enhance the sensitivity or minimize the reaction time. MNAzyme were coupled with exonuclease[61], glucose oxidase,[62] or another DNAzyme[63,64] for explorational signal amplifications.

For MNAzyme with NAAT, the biosensors were coupled with NAAT methods like PCR[65] or RCA.[66] Alison V. Todd and her coworkers coupled MNAzyme with PCR, which served as an alternative for the TaqMan probe in real-time quantitively PCR (qRT-PCR). MNAzyme has also shown its capability of coupling with isothermal amplifications like RCA, which makes it a potential solution for the non-specific amplification issue of general isothermal amplification methods. We will further dig into this method category later.

Table 1.3. Summary of MNAzyme

Category	Year	Novelty	Detection limit	Signal Readout	Target	Time (min)	Ref.
MNAzyme only	2010	original MNAzyme	5 pM	optical	DNA	120	[67]
	2013	combined with gold nanoparticles (GNPs)	50 pM	colorimetric	DNA	60	[57]
	2015	cationic copolymer	2 pM	optical	DNA	60	[68]
	2016	alkaline phosphatase (ALP)	79 pM	electrochemical	DNA	150	[58]
	2020	microwell	7.8 pM (measured); 180 fM (calculated)	optical	DNA	60	[56]
	2020	cationic copolymer and LNA	2 pM (measured); 73 fM (calculated)	optical	miRNA	30	[55]
MNAzyme + Signal amplification	2011	HCR + MNAzyme	10 fM	optical	DNA	6480	[59]
	2015	exo III-assisted cascade target recycling	20 fM	optical	DNA	145	[61]
	2019	glucose oxidase + MNAzyme	65 pM	electrochemical	miRNA	120	[62]
	2019	CHA-HCR-MNAzyme	5 pM	optical	DNA/miRNA	240	[60]
	2019	subzyme	10 pM	optical	DNA	120	[64]
	2020	cross-catalytic subzymes	1 fM	optical	DNA	30	[63]
NAAT + MNAzyme	2012	PCR + MNAzyme	10 copies/reaction	optical	DNA/RNA	40 - 70	[65]
	2016	RCA + MNAzyme	1.66 fM	electrochemical	miRNA	420	[66]

1.3.2.3. SNP recognition of MNAzyme

In addition to nucleic acid detection, the MNAzyme also shows the capability of SNP detection[69]. The split design previously showed successful SNP detection with split G-quadruplex DNAzyme[70], split RNA-cleaving DNAzyme[52], split oligo probe with molecular beacon,[71] and split aptamer probe[72]. The split 10-23 DNAzyme, or MNAzyme also showed SNP detection capability by several studies[73,74].

Based on the studies above (Figure 1.12), there are several patterns for using split design for SNP detection. First, SNP detection is usually coupled with amplification methods like PCR because the sensors have LoD ranging from nM level to pM level, which is not enough for the practical test. Second, the SNP identification arm is usually shorter to be sensitive to single mismatch compared with the other half of the analyte binding arm. Third, the SNP detection positions in the middle region of the recognition arm tend to have the highest discrimination factor although the result is highly sequence dependent.

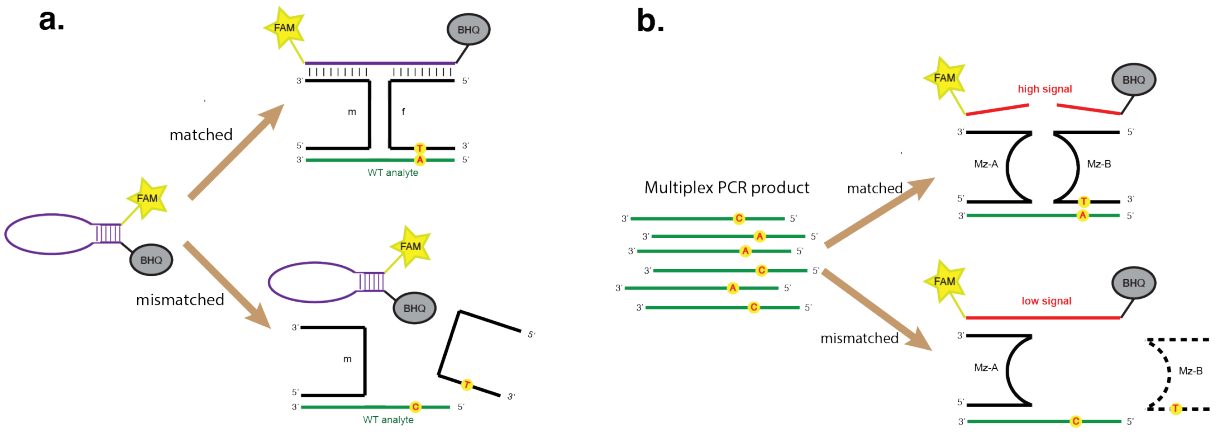

Figure 1.3.2. SNP detection with split design. (a) example of molecular beacon-based SNP detection with split design. (b) example of RNA-cleaving DNAzyme-based SNP detection with split design.

1.3.2.4. Chemical modifications of DNAzyme

As mentioned earlier, the rate-limiting step of the RNA cleaving DNAzyme is either the substrate binding or Mg^{2+} releasing. Deriving from that, researchers used a variety of chemical modifications, like 2′-deoxy-2′-fluoroarabino nucleic acid (FANA), LNA, 2'-o-methylribonucleic acid (OMe), phosphorothioate (PS) bond, etc. to further enhance the cleavage efficiency (Table 1.4).

Chemical modifications on substrate binding arms proved to be an efficient way to overcome the bottleneck of the substrate binding process. For example, LNA modification could lead to increase helical thermostability, better SNP recognition, and higher nuclease resistance. In 2002, Jesper Wengel and coworkers[75] proved that LNA modifications in the substrate binding arm could dramatically enhance the efficiency of RNA cleavage and better multiple turnover activity. After that Lun-Quan Sun and coworkers[76] showed that the substitution of deoxyguanine with deoxyinosine could also enhance the cleavage rate. Jens Kurreck and coworkers[77] proved that 2'OMe modifications could also enhance cleavage activity. More recently, John Chaput and coworkers[78] showed FANA modifications outcompete the DNA version of the substrate binding arm both in vitro and in vivo, making the substrate binding arm to be a key region for chemical modifications.

Modifications on the catalytic core could enhance the biostability of DNAzyme and potentially tune the catalytic cycle and enhance the cleavage activity. In 2003, Jens Kurreck and coworkers[77] proved that OMe modifications on the catalytic core could enhance the biostability against nucleases. In 2006, Wojciech J. Stec and coworkers[79] showed phosphorothioate modifications on catalytic core positions 1 or 8 enhanced the cleavage

activity by contributing to metal ion binding. John Chaput and coworkers[78] showed that FANA modifications on position 2 and 8 could enhance the cleavage rate. Most recently, Manuel Etzkorn and coworkers[49] rationally designed a 6-thio modification on position 14 and showed enhanced activity based on their discoveries on the first 10-23 DNAzyme crystal structure.

Last but not the least, chemical modifications on the trigger binding arm have also shown benefits when the arms are short. Atsushi Maruyama and coworkers[80] used LNA to enhance the binding efficiency for an 11-mer trigger binding arm and showed enhanced sensitivity.

Overall, chemical modifications could significantly influence cleavage activity. Thus, fully optimizing the 10-23 DNAzyme chemotypes would be very important to enhance the performance of the multicomponent DNAzyme biosensor.

Table 1.4. Chemical modifications on 10-23 DNAzyme

Modification position	Year	Modifications	Number of modifications	Ref
Substrate-binding arm only	2002	LNA	4 (arm)	75
	2003	deoxyinosine	1 (arm)	81
	2003	LNA	4 (arm)	82
	2004	LNA/2'OMe	6 (LNA) / 10 (OMe)	83
	2009	LNA	4 (arm)	84
Substrate-binding arm and catalytic core	2003	2'OMe	10 (arm) + 6 (core)	85
	2012	2'OMe	8 (arm) + 6 (core)	86
	2021	FANA	12 (arm) + 2 (core)	78
catalytic core only	2007	PS bond	1 (core)	79
	2013	2′-deoxyguanosine analogues	2 (core)	87
	2014	2'-C-methyl/2'Ome	3 (2'Ome) + 1 (2'S) + 2 (2'R)	88
	2016	3-Aminopropyl	1 (core)	89
	2022	6-thio modification	1 (core)	49
Trigger-binding arm	2020	LNA	8 (trigger arm)	55

CHAPTER 2

REVEALR: SARS CoV-2 nucleic acid detection platform

Publication Note

This chapter was originally published in the *Journal of the American Chemical Society*. Yang, Kefan, and John C. Chaput. "REVEALR: a multicomponent XNAzyme-based nucleic acid detection system for SARS-CoV-2." **Journal of the American Chemical Society** 143.24 (2021): 8957-8961.

Contribution Statement

KY and JC conceived the project and designed the experiments. KY performed the experiments. Both authors reviewed the data and wrote the manuscript.

2.1. Abstract of the Chapter

Isothermal amplification strategies capable of rapid, inexpensive, and accurate nucleic acid detection provide new options for large-scale pathogen detection, disease diagnosis, and genotyping. Here we report a highly sensitive multicomponent XNA-based nucleic acid detection platform that combines analyte preamplification with X10–23-mediated catalysis to detect the viral pathogen responsible for COVID-19. The platform, termed RNA-Encoded Viral Nucleic Acid Analyte Reporter (REVEALR), functions with a detection limit of $\leqslant$20 aM (~10 copies/μL) using conventional fluorescence and paper-based lateral flow readout modalities. With a total assay time of 1 h, REVEALR provides a

convenient nucleic acid alternative to equivalent CRISPR-based approaches, which have become popular methods for SARS-CoV-2 detection. The assay shows no cross-reactivity for other in vitro transcribed respiratory viral RNAs and functions with perfect accuracy against COVID-19 patient-derived clinical samples.

2.2. Introduction

The COVID-19 pandemic, caused by the spread of SARS-CoV-2 across the globe, represents the greatest challenge to U.S. health and prosperity since the Great Depression. With an estimated total cost of $16 trillion and more than 2.2 million deaths reported worldwide[90], routine large-scale testing capacity is urgently needed to control the spread of COVID-19 and facilitate safe environments for social and economic activities involving travel, school, and work[91]. Although quantitative reverse-transcription real-time PCR (qRT-PCR) is the gold standard analytical technique for SARS-CoV-2 detection in patients, long turnaround times (>24 h) have prompted a need for alternative public health screening tools[26]. The problem is exacerbated by the need for specialized equipment, reagents, and trained personnel, which may be unavailable in rural communities or developing countries. A more effective path to curbing the spread of the pandemic would involve the broad deployment of rapid and inexpensive point-of-care diagnostics for routine healthcare monitoring with positive cases subsequently confirmed by qRT-PCR-certified facilities.

Isothermal amplification strategies capable of rapid, inexpensive, and accurate viral detection offer a promising alternative to qRT-PCR as a public health tool for routine COVID-19 detection. The most common approaches include reverse-transcription loop-mediated isothermal amplification (RT-LAMP) and reverse-transcription recombinase polymerase

amplification (RT-RPA)[19,92]. Although inexpensive, rapid, and field-deployable, both techniques suffer from problems associated with nonspecific DNA amplification, leading to high rates of false positive diagnosis[93]. However, this problem can be overcome by using sequence-specific detection modalities that recognize unique nucleic acid signatures following an RT-LAMP or RT-RPA preamplification step. Common examples include the SHERLOCK and DETECTR systems based on CRISPR-Cas enzymology, which provide sensitive and highly accurate platforms for viral RNA detection[31,45].

Here we report the development and characterization of a simple nucleic acid detection platform called RNA-Encoded Viral Nucleic Acid Analyte Reporter (REVEALR) that can achieve viral RNA detection with attomolar (aM) sensitivity in 1 h using synthetic oligonucleotides that avoid the need for a recombinant Cas protein enzyme[94]. REVEALR is based on the newly discovered Xeno-nucleic acids enzyme (XNAzyme) 10–23, which was designed for enhanced gene silencing activity in cellular environments using finely tuned XNA chemotypes that balance RNA substrate binding with product release[78]. Conversion of X10–23 into a split enzyme, as originally described by Mokany and co-workers for the parent 10–23 DNAzyme[67], enables the production of a multicomponent optical sensor (Figure 2.1a) that can generate an output signal in response to the presence of an input target sequence, here termed the trigger. Signal amplification via cleavage of a quenched RNA reporter occurs if the complex is bound to the target sequence, allowing for highly specific monitoring of single-stranded viral RNA (Figure S2.1).

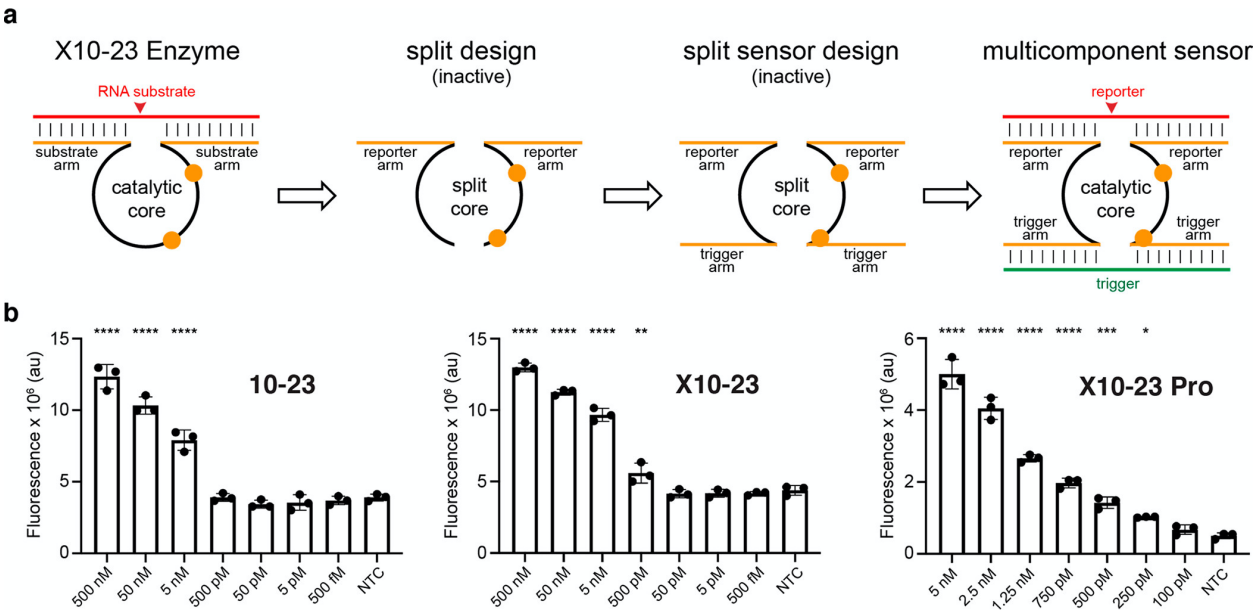

Figure 2.2. XNAzyme-mediated nucleic acid detection. (a) Overview of the nucleic acid sensor. Two catalytic cores (left and right) self-assemble in the presence of a viral RNA analyte (trigger) to produce a functionally active catalyst with a separate enzyme active site that is capable of site-specific cleavage of an RNA reporter. RNA (red), DNA (black), FANA (orange), input trigger (green). The red arrow indicates the G–U dinucleotide cleavage site. (b) Limits of detection for the 10–23, X10–23, and X10–23 Pro multicomponent sensors measured by fluorescence detection across a range of analyte concentrations after incubation for 30 min. n = 3; error bars represent the standard error of the mean (SEM). Two-tailed Student's t test: *, $P < 0.05$; **, $P < 0.01$; ***, $P < 0.001$; ****, $P < 0.0001$. Reactions were performed in buffer containing 50 mM $MgCl_2$ at pH 8.5 (24 °C). Abbreviations: au, arbitrary units; S, full-length 5′-labeled RNA substrate; P, 5′ cleavage product.

2.1. Results

To evaluate the nucleic acid strategy, we compared the limit of detection (LoD) for the classic 10–23 DNA design to the newly discovered X10–23 enzyme in a multicomponent format in which the catalytic core of both nucleic acid enzymes was divided into two separate parts that self-assemble into an active sensor in the presence of the viral RNA trigger (Figure 1a)[47]. In addition, we also evaluated a modified version of X10–23, termed X10–23 Pro, in which both DNA trigger arms were replaced with the unnatural nucleic acid analogue 2′-fluoroarabino nucleic acid (FANA) (Table S2.1)[95]. In the presence of in vitro transcribed (IVT) RNA analyte encoding a region of the S-gene from the SARS-CoV-2 genome (Figure S2.2),

the 10 – 23, X10 – 23, and X10 – 23 Pro sensors (Figure 2.1b) function with analytic LoDs of 5 nM, 500 pM, and 250 pM, respectively, when assayed after 30 min in buffer containing 50 mM magnesium chloride ($MgCl_2$) at pH 8.5 (24 °C). A kinetic analysis (Figure S2.3) revealed that X10–23 Pro functions with a first-order rate constant of 5.5 ± 0.89 min^{-1}.

To achieve the attomolar-level sensitivity necessary for SARS-CoV-2 detection in human samples, the multicomponent X10–23 Pro system was combined with a preamplification step like the one used for CRISPR-based SARS-CoV-2 detection[8,39]. Accordingly, IVT RNA diluted to attomolar levels was isothermally amplified by RT-RPA and forward-transcribed by T7 RNA polymerase to generate the single-stranded RNA trigger required for X10–23 Pro detection. We refer to the combined process of viral preamplification and specific nucleic acid detection by X10–23 Pro-mediated hydrolysis of a quenched RNA reporter as REVEALR (Figure 2.2a). The process requires a total of 60 min to complete, with 30 min of preamplification.

REVEALR was initially used to compare the kinetics of fluorescence signal generation for the multicomponent enzymes of 10–23, X10–23, and X10–23 Pro. The assays were performed in T7 RNA polymerase buffer containing 6 mM $MgCl_2$ at pH 7.9 (37 °C) across a dilution series of quantified IVT RNA targeting a portion of the viral genome that encodes a region of the spike (S) protein (Figure S2.2). Kinetic measurements performed in triplicate indicate that X10–23 Pro has the greatest potential for establishing a highly sensitive viral RNA detection assay with an initial LoD of 50 aM (Figure S2.4). Subsequent optimization of the reaction conditions by adjusting such factors as the magnesium acetate concentration and reverse transcriptase enzyme used in the RT-RPA

reaction reduced the analytical LoD to 2 aM after 90 min of detection (Figures 2.2b, S2.5, and S2.6).

Under optimal reaction conditions, the analytic LoD was determined to be ⩽20 aM after 30 min of preamplification and 30 min of analyte detection, which corresponds to ~10 copies of RNA/µL (Figure 2.2c). This value is below the average viral load observed in COVID-19 patients, which ranges from 80 to 752 copies/µL[96]. The LoD was independently validated using a paper-based lateral flow readout modality (Figure 2.2d), which confirmed an analytical LoD of at least 20 aM. The results from the two LoD assays are quantitatively like those from the CRISPR-based systems SHERLOCK and DETECTR, demonstrating that nucleic acid enzymes can compete with protein enzymes in a diagnostic assay format[8,39].

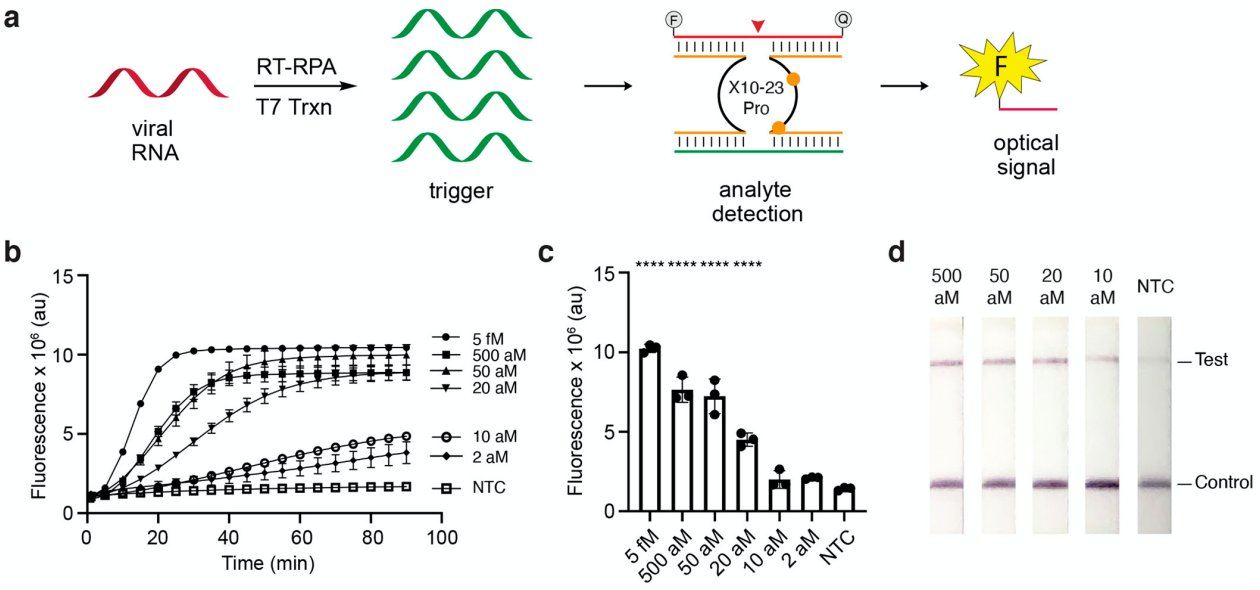

Figure 2.1. REVEALR detection of SARS-CoV-2. (a) Overview of the detection assay. The SARS-CoV-2 region of interest is isothermally amplified by RT-RPA and then transcribed with T7 RNA polymerase to produce multiple copies of the RNA trigger. X10–23 Pro assembly on the RNA trigger leads to the cleavage of a quenched fluorescent reporter for fluorescence detection or a biotin-labeled fluorescent RNA for lateral flow detection. Cleavage site (red arrow). (b) Kinetics of fluorescent signal generation over 90 min across a range of RNA dilutions. au, arbitrary units. (c) Limit of detection for fluorescence-based quantification at designated RNA concentrations. Measurements are mean ± SEM, $n = 3$ for (b) and (c). Two-tailed Student's t test: *, $P < 0.05$; **, $P < 0.01$; ***, $P < 0.001$; ****, $P < 0.0001$. (d) Limit of detection using lateral flow readout containing

control and test bands. (c) and (d) show data collected after 30 and 60 min of detection, respectively. au, arbitrary units; NTC, no-template control.

Next, we evaluated REVEALR in a partially blinded study comprising 24 IVT RNA samples. Twelve of the samples contained the SARS-CoV-2 RNA poised at concentrations of 20, 50, 100, and 500 aM, while the remaining samples contained SARS-CoV-1, middle east respiratory syndrome (MERS), rhinovirus, or influenza An RNA poised at a concentration of 500 aM. The samples were prepared and organized by a team member not affiliated with the study, and REVEALR was used to identify the SARS-CoV-2 samples. Fluorescence analysis (Figure 2.3c, Figure S2.7) showed that REVEALR was able to identify all 12 positive samples and 11 of the negative samples, indicating that the assay functions with 100% positive predictive agreement and 92% negative predictive agreement on IVT RNA. The one false negative result was thought to be due to contamination caused by human error.

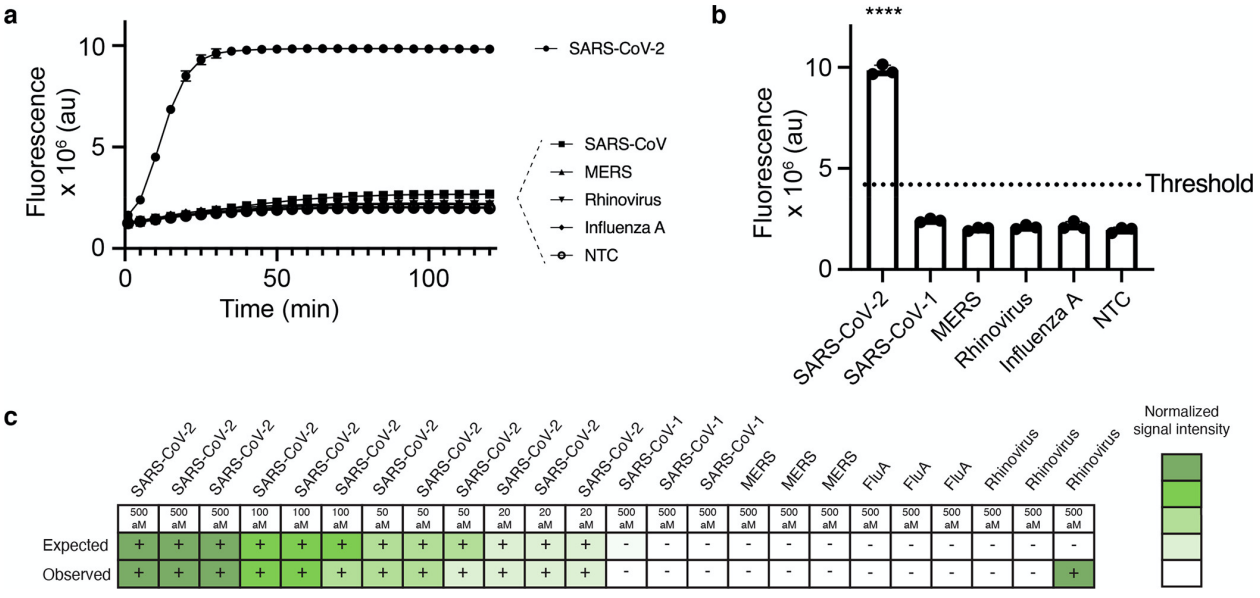

Figure 2.1. Specificity of SARS-CoV-2 detection. (a) Kinetics of fluorescence signal generation for a SARS-CoV-2-specific REVEALR assay performed on a range of viral RNA samples. (b) Fluorescence signal generated for a SARS-CoV-2-specific REVEALR assay after 30 min of detection. Two-tailed Student's t test: *, $P < 0.05$; **, $P < 0.01$; ***, $P < 0.001$; ****, $P < 0.0001$. Threshold is defined as twice the signal-to-noise (S/N)

ratio of the NTC fluorescence intensity. Samples were poised at 50 fM concentration. (c) Blinded viral RNA assay. REVEALR was used to identify SARS-CoV-2 samples in a randomized study. au, arbitrary units; NTC, no-template control containing nuclease-free water.

Last, we evaluated the power of REVEALR on clinically relevant samples. Consistent with our IVT RNA analysis, we observed an LoD of 9 aM on heat-inactivated virus obtained from Vero cells (Figure S2.8). We then tested the REVEALR system on extracted RNA from nasopharyngeal swaps collected from 10 PCR-positive and 2 PCR-negative COVID-19 patients (Table S2.2). REVEALR was 100% accurate using fluorescence and lateral flow readout modalities, identifying SARS-CoV-2 in all 10 PCR-positive samples, and yielding a negative result for both PCR-negative swaps (Figure 2.4).

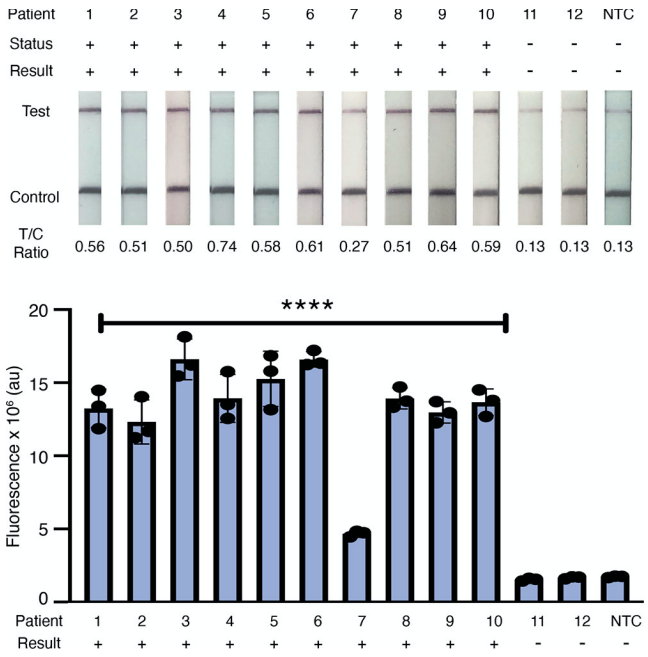

Figure 2.1 REVEALR detection of clinical samples. (top) Lateral flow readout containing control and test bands. (bottom) Fluorescence signal generated after 30 min of detection. Two-tailed Student's t test: *, $P < 0.05$; **, $P < 0.01$; ***, $P < 0001$; ****, $P < 0.0001$. au, arbitrary units; NTC, no-template control. The T/C ratio is the ratio of test to control band intensity.

We wished to investigate the specificity of REVEALR for SARS-CoV-2 RNA versus other RNA viruses that are known to cause respiratory infections. IVT RNA was constructed for SARS-CoV-1, MERS, rhinovirus, and influenza A. S-gene-specific SARS-CoV-2 REVEALR assays performed on all five RNA samples demonstrated that the SARS-CoV-2 assay is rapid (1 h) and highly specific for SARS-CoV-2 (Figure 2.3a, b). No cross-reactivity was observed for the other four viral samples, including SARS-CoV-1, which is 80% identical to SARS-CoV-2[97]. Real-time and single-end-point detection assays show that the off-target viral samples are indistinguishable from the no-template control (NTC) containing nuclease-free water, all of which have a signal-to-noise (S/N) ratio of less than 2.

2.2. Conclusion and discussion

In summary, we have demonstrated that REVEALR provides a new strategy to improve the speed, sensitivity, and specificity of COVID-19 detection. Sequence-specific target recognition is achieved using a chemically synthesized multicomponent nucleic acid enzyme that is capable of highly sensitive analyte detection ($\leqslant$20 aM) using an optical or visual readout system that relies on efficient cleavage of an RNA reporter. Relative to related CRISPR-base systems, REVEALR has several advantages, including (1) broader sequence targetability due to the absence of constraints imposed by the protospacer adjacent motif (PAM) motif, (2) increased simplicity by avoiding the need for protein expression and purification, and (3) reduced cost of detection because the sensor is based entirely on synthetic oligonucleotides. These features, along with a programmable platform and a nucleic acid enzyme that can compete with a protein enzyme in a diagnostic assay, make REVEALR an attractive system for pathogen detection. We suggest that broad-based

deployment of this and other related point-of-care diagnostics could help control the spread of COVID-19 in the U.S. and across the globe.

2.3. Experimental details

Materials

DNA and RNA oligonucleotides were purchased from Integrated DNA Technologies (Coralville, IA). DNA and FANA phosphonamidites were purchased from Glen Research Corporation (Sterling, VA). TwistAmp® Basic Kit and TwistAmp® Liquid Basic Kit was purchased from TwistDx (Maidenhead, UK). Solutions of dNTPs (100 mM) and SuperScript IV Reverse transcriptase were purchased from ThermoFisher (Waltham, MA). T7 RNA polymerase and buffer was purchased from Lucigen Corporation (Middleton, WI). HiScribe T7 High Yield RNA Synthesis Kit, RNase H, and Moloney murine leukemia virus (M-MuLV) Reverse transcriptase was purchased from New England Biolabs (Ipswich, MA). HybriDetect lateral flow strips were purchased from Milenia Biotec (Giessen, DE). 2019-nCoV N Positive Control was purchased from Integrated DNA Technologies (Coralville, IA).

In vitro transcribed RNA samples

DNA versions of the SARS-CoV-2 (S region), SARS-CoV-1, MERS, Rhinovirus, and Influenza A gene fragments were obtained from IDT. All genes were PCR amplified with forward primers containing the T7 promoter. Pseudoviral RNA was then prepared by in vitro transcription using HiScribe T7 High Yield RNA Synthesis Kit. The reaction mixtures contained 10 mM of each ribonucleoside triphosphate (NTP), 1X reaction buffer, 3 µL PCR product, 2 µL T7 RNA polymerase mixture and 5 µL of nuclease free water, which were

incubated at 37°C overnight. The crude RNA was purified by 15% denaturing urea polyacrylamide gel electrophoresis (PAGE) and electroeluted at 180 V for 3 hours. Purified RNA stocks were quantified by Nanodrop and diluted in nuclease-free water to desired concentrations.

Oligonucleotide synthesis

Synthetic oligonucleotides containing FANA residues were synthesized in-house using an automated solid-phase DNA synthesizer (Applied Biosystems 3400) on Glen UnySupport CPG columns (1 µmole, Glen Research, Sterling, VA). The standard DNA protocol was modified by increasing the coupling time to 360 seconds for FANA phosphonamidites. Cleavage from the solid support and final deprotection of each oligonucleotide was achieved by heating for 18 h at 55°C in 33% NH_4OH. Oligonucleotides were purified by denaturing PAGE, electroeluted, desalted using a YM-3 Centricon centrifugal filter (Millipore, Burlington, MA), and quantified by UV absorbance using a Nanodrop spectrophotometer. FANA containing oligonucleotides were validated by MALDI-TOF mass spectrometry (microflex MALDI-TOF MS, Bruker, Billerica, MA).

In vitro kinetic analysis of RNA cleavage

Kinetic cleavage reactions were performed at 25°C in 20 µL volumes containing 50 mM Tris-HCl (pH 8.5), 150 mM sodium chloride (NaCl), 50 mM $MgCl_2$, 500 nM Cy5-labeled RNA substrate, 500 nM RNA trigger strand, and 500 nM of each strand of the multicomponent enzyme (Mz-A and Mz-B). The sensor was assembled by heating a solution containing all the reagents except $MgCl_2$ for 5 min at 95°C and cooling for 5 min on ice.

Reactions were initiated by the addition of $MgCl_2$ and left incubating at 25°C for up to 60 min. Individual time points were collected by diluting 1.5 µL of reaction into 16.5 µL of formamide stop buffer (95% formamide, 25 mM EDTA) and cooling on ice. Samples were denatured for 10 min at 95°C and analyzed by 15% denaturing urea PAGE. Gels were visualized by the LI-COR Odyssey CLx. k_{obs} values were calculated by fitting cleavage percentage and reaction time (in min) to the first-order decay equation (1) using Prism 8 (GraphPad, San Diego, CA).

$$P_t = P_\infty(1 - e^{-k_{obs}t}) \quad (1)$$

Where P_t is the percentage of cleaved substrate at time t, P_∞ is the apparent reaction plateau and k_{obs} is the observed first-order rate constant.

Sensitivity of the 10-23, X10-23, and X10-23 Pro split catalysts

Sensitivity assays were performed at 25°C in 20 µL volumes containing 50 mM Tris-HCl (pH 8.5), 150 mM NaCl, 50 mM $MgCl_2$, 500 nM FQ RNA substrate, 500 nM Mz-A, 500 nM Mz-B, and RNA trigger strand. The trigger strand was poised at a range of concentrations to determine the limit of detection. Nuclease-free water was used in the case of the no template control. Mz-A, Mz-B, RNA trigger strand, and FQ RNA substrate were annealed in Tris-HCl and NaCl by heating for 5 min at 95°C and cooling on ice for 5 min. Reactions were initiated by the addition of $MgCl_2$ and the reaction was monitored by quantitative real-time PCR at 1 min intervals over a period of 2 hours.

RT-RPA preamplification

A lyophilized RPA pellet was resuspended with 29.5 µL rehydration buffer, 1 µL RNase H (5 U/µL), 0.5 µL SuperScript IV RT (200 U/µL), 0.5 µL of forward primer (50 µM), and 0.5 µL of reverse primer (50 µM). A portion (12.8 µL) of the master mix was transferred to each PCR tube. To initiate the assay, 2 µL of magnesium acetate and 6.4 µL of IVT RNA fragment were added to each tube. After brief agitation and centrifugation, the reactions were incubated for 25 min at 42°C. The strip was removed after the first 5 min, briefly vortexed, and returned to the heating device. After 25 min, the reaction was inactivated by heating for 5 min at 95°C. RT-RPA tube were then placed on ice before transferring to an X10-23 Pro driven fluorescence or lateral-flow detection assay.

Fluorescence-based detection assay

Split X10-23 Pro detection assays were performed at 37°C in a 20 µL volume containing 1X T7 RNA polymerase buffer (40 mM Tris-HCl, 6 mM $MgCl_2$, 10 mM DTT, 2 mM spermidine, pH 7.9), 0.5 mM of each NTP, 5 mM DTT, 1.5 U T7 RNA polymerase, 500 nM Mz-A, 500 nM Mz-B, and 500 nM FQ RNA substrate. A portion of the RT-RPA product (2 µL) was transferred to the reaction mixture (18 µL). Reactions were monitored by quantitative real-time PCR at 1 min intervals over a period of 2 hours at 37°C.

Lateral-flow strip detection assay

Split X10-23 Pro detection assays were performed at 25°C in a 20 µL volume containing 1X T7 RNA polymerase buffer (see above), 0.5 mM of each NTP, 5 mM DTT, 1.5 U T7 RNA polymerase, 500 nM Mz-A, 500 nM Mz-B, and 500 nM F-Biotin RNA substrate.

A portion of the RT-RPA product (2 µL) was transferred to the reaction mixture (18 µL). The tubes were then incubated for 1 h at 37°C before diluting the product in 80 µL HybriDetect assay buffer. After a brief agitation and centrifugation, the HybriDetect lateral flow strips were dipped in the reactions and incubated for 2 min at 25°C. The strips were then imaged, and the bands were quantified using ImageJ (NIH, Bethesda, MD).

Blinded test

24-IVT RNA samples were prepared with random order by a team member not affiliated with the study. Twelve of the samples contained the SARS-CoV-2 virus poised at concentrations of 20, 50, 100 and 500 aM with 3 replicates, while the remaining samples contain SARS-CoV-1, MERS, rhinovirus, or influenza A, each poised at a concentration of 500 aM with 3 replicates. The REVEALR system was used to identify the SARS-CoV-2. Samples with signal to noise(S/N) ratio > 2 were considered positive for SARS-CoV-2, while samples with a S/N < 2 were considered negative for SARS-CoV-2.

Evaluation of patient-derived clinical samples

Twelve patient-derived nasopharyngeal swabs were obtained from the University of California Irvine COVID-19 Research Biobank. All samples were collected by trained medical professionals at the University of California Irvine. The samples consisted of 10 PCR positive and 2 PCR negative samples for SARS-CoV-2. The samples were heat inactivated for 1 hour at 80°C by trained professionals at the UCI Biobank prior to receipt by our lab. SARS-CoV 2 viral RNA was extracted following the centers for disease control and prevention (CDC) recommended Qiagen DSP Viral RNA Mini kit protocol. The REVEALR

system was used to detect the extracted RNA using both fluorescence and lateral flow readout modalities as described above.

Sensitivity test of REVEALR with heat-inactivated SARS-CoV-2

Heat-inactivated SARS-CoV-2 (ATCC VR-1986HK) was diluted into nuclease-free water and quantified using CDC recommended Promega GoTaq® Probe 1-Step RT-qPCR System (A6120). The REVEALR system was used to test the limit of detection to the dilutions of heat-inactivated SARS-CoV-2 virus. Fluorescent signal was evaluated using student's t test to assess the statistical significance of the measurement.

Chapter 3:

REVEALR-genotyping: SARS CoV-2 nucleic acid variant identification platform

Publication Note

This chapter was originally published in the *Journal of the American Chemical Society*. Yang, Kefan, et al. "REVEALR-Based Genotyping of SARS-CoV-2 Variants of Concern in Clinical Samples." **Journal of the American Chemical Society** 144.26 (2022): 11685-11692.

Contribution Statement

Kefan Yang and John Chaput conceived the project and designed the experiments. Kefan Yang, Daniel Schuder, and Arlene Ngor performed the experiments. John Chaput wrote the manuscript with input from all the authors.

3.1. Abstract of the Chapter

The SARS-CoV-2 virus has evolved into new strains that increase viral transmissibility and reduce vaccine protection. The rapid circulation of these more harmful strains across the globe has created a pressing need for alternative public health screening tools. REVEALR (RNA-encoded viral nucleic acid analytic reporter), a rapid and highly sensitive DNAzyme-based detection system, functions with perfect accuracy against patient-derived clinical samples. Here, we design REVEALR into a novel genotyping assay

that detects single-base mismatches corresponding to each of the major SARS-CoV-2 strains found in the United States. Of 34 sequence-verified patient samples collected in early, mid, and late 2021 at the UCI Medical Center in Orange, California, REVEALR identified the correct variant [Wuhan-Hu-1, alpha (B.1.1.7), gamma (P.1), epsilon (B.1.427/9), delta (B.1.617.2), and omicron (B.1.1.529)] with 100% accuracy. The assay, which is programmable and amenable to multiplexing, offers an important new approach to personalized diagnostics.

3.2. Introduction

The coronavirus induced disease 19 (COVID-19) pandemic, caused by spread of the severe acute respiratory syndrome coronavirus 2 (SARS-CoV-2) across the globe, is responsible for nearly 6 million deaths worldwide and far-reaching socioeconomic disruptions[90]. Although the mutation rate of SARS-CoV-2 is relatively low due to the presence of an exonuclease enzyme that reduces the replication error rate by ~15–20-fold[98], evolution of the virus has led to the emergence of novel viral lineages, including variants of concern (VOC) that threaten pandemic recovery by increasing viral transmissibility and reducing vaccine protection[99]. Following rapid fixation of the D614G substitution in early 2020[100], new strains emerged that include the B.1.1.7 (alpha), B.1.351 (beta), P.1 (gamma), B.1.427/9 (epsilon), B.1.617.2 (delta), and B.1.1.529 (omicron) variants[101]. These new variants harbor mutations in the spike (S) glycoprotein that stabilize the receptor binding domain (RBD) in the up conformation, which supports increased binding of angiotensin-converting enzyme 2 (ACE2) on the host cell[102–104]. An increased risk of infection or reinfection[105], coupled with reduced protection afforded by vaccines or neutralizing

antibodies[106], has created a pressing need for additional diagnostic tools that can facilitate COVID-19 detection in conjunction with strain identification[107].

The COVID-19 pandemic has exposed critical gaps in point-of-care (POC) diagnostics that are needed to facilitate safe environments for social and economic activities[91]. Currently, whole genome sequencing is widely applied as a broad public health screening tool for monitoring epidemiological changes in the population, and more importantly, the early detection and prevalence of emerging SARS-CoV-2 variants (Figure 3.1a)[108]. However, the diagnosis of individual patients for a specific VOC is best performed by sequencing the S-gene of viral samples collected from nasopharyngeal swabs, which is a slow and costly process that does not scale to the population. Other approaches, such as S-gene target failure[109], TaqMan[110], and LAMP[111], suffer from limitations in their reliability, sensitivity, and specificity, making them suboptimal techniques for VOC genotyping[112]. Even CRISPR-based systems, though effective, have a narrow range of target sites due to constraints imposed by the PAM region[113]. This method also requires an extra base pair mismatch in the CRISPR RNA sequence that can lead to genotyping errors[45]. As such, new POC diagnostics are needed to rapidly detect nucleic acid sequences with high sensitivity and single-based specificity[107].

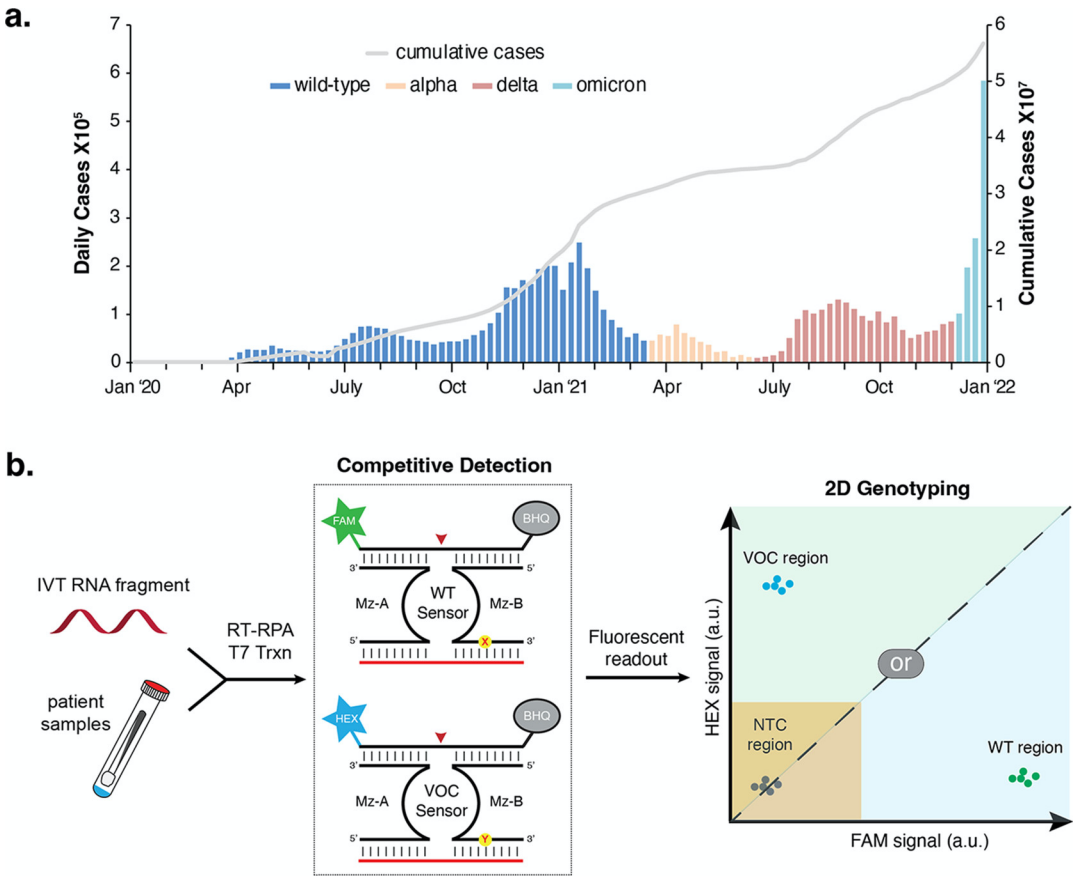

Figure 3.2 REVEALR-based detection of SARS-CoV-2 variants of concern. (a) Progression of COVID-19 cases in the United States from January 2020 to January 2022. Colors signify the dominant VOC observed at the collection date. Data points are based on a 7-day average. (b) Schematic view of competitive REVEALR genotyping. The SARS-CoV-2 region of interest is isothermally amplified by RT-RPA and T7 RNA polymerase to produce multiple copies of the RNA analyte. Competitive XNAzyme assembly on the viral RNA produces a fluorescent signal specific to the sample genotype via site-specific cleavage of a quenched fluorescent reporter. 2-D analysis shows WT or VOC detection based on the measured fluorescence observed for the FAM and HEX signal, respectively. Abbreviations: WT (wild type); VOC (variant of concern); X, Y (SNP position); and au (arbitrary units). Red arrow indicates substrate cleavage site. Colors: RNA (red); DNA (black); green (WT, Fam signal); and blue (VOC, Hex signal).

Here, we report the design and clinical validation of a two-step REVEALR-based (RNA-encoded viral nucleic acid analytic reporter) nucleic acid detection system for SARS-CoV-2 genotyping. The REVEALR strategy is based on a multicomponent DNA enzyme (DNAzyme) that assembles in vitro to produce an output signal in response to the presence of a specific nucleic acid sequence[47,114]. Signal amplification, via cleavage of a quenched

fluorescent reporter, occurs if the DNAzyme is bound to the target sequence[67], which allows for highly sensitive COVID-19 detection in patient-derived clinical samples[1]. To facilitate VOC genotyping, we converted REVEALR into a competitive binding assay that detects single-base mismatches associated with each of the major SARS-CoV-2 variants. We then validated the assay against sequence-verified patient samples collected in early, mid, and late 2021 at the UCI Medical Center in Orange, California. REVEALR identified the correct VOC associated with each patient sample with 100% accuracy. The assay, which is programmable and amenable to multiplexing, has the potential to serve as a rapid, low cost, and scalable public health screening tool for symptomatic and asymptomatic detection of specific SARS-CoV-2 variants.

3.3. Results

Transforming REVEALR into a Genotyping Assay

REVEALR is based on a split DNAzyme design strategy in which two halves of a catalytic core (Figure 3.1b) self-assemble in the presence of a viral RNA analyte to produce a functionally active catalyst that can cleave a quenched-fluorescent RNA oligonucleotide strand hybridized to the substrate binding arms of the DNA scaffold[67]. Signal amplification occurs via the multiple turnover activity of the enzyme, if the DNAzyme is bound to the viral RNA analyte and ceases when the complex dissociates into its individual pieces[67]. Previous studies have shown that REVEALR functions with an analytical limit of detection (LoD) of ~20 aM (~10 copies/μL), which is equivalent to the CRISPR-based methods of SHERLOCK[45] and DETECTR[31] and below the average viral load of COVID-19 patients[96].

Transforming REVEALR into a genotyping assay requires balancing differences in the energetics of hybridization between a perfectly matched viral RNA analyte and a viral analyte carrying a single-nucleotide mutation (*i.e.*, SNP). Since binding to a perfectly matched RNA strand is energetically more favorable than a mismatched strand, properly engineered sensors can be designed to detect a single mutation (transition or transversion) in a nucleic acid sequence[115]. To further enhance the sensitivity of detection, we designed a two-color competitive binding assay that challenges a wild-type and VOC-specific DNAzyme to recognize a genetic mutation within a small region of the viral RNA genome (Figure 3.1b). RNA substrates used in the competitive binding assay are equipped with fluorescent dyes (i.e., fluorescein (FAM) and hexachlorofluorescein (HEX)) that have non-overlapping spectral features and nucleic acid sequences that are complementary to their cognate DNAzyme (*e.g.*, wild-type and VOC). Data produced from the competitive assay is visualized in a two-dimensional (2-D) plot (Figure 3.1b) with the wild-type analyte producing a strong signal in the lower right quadrant and the VOC analyte generating an equivalently strong signal in the upper left quadrant depending on the identity of the viral RNA analyte present in the sample. By performing the assay against a panel of DNAzymes, each tailored to recognize a specific VOC, we reasoned that it should be possible to unambiguously identify the specific SARS-CoV-2 variant infecting a given patient-derived clinical sample.

Realizing that chemically modified nucleotides can increase the selectivity of SNP discrimination, we explored the use of locked nucleic acids (LNA) as a chemical tool for improving the activity of our DNAzymes[116]. LNA is a conformationally restricted nucleic acid analog that forces the ribose sugar to adopt a 3′-*endo* conformation by containing a methylene bridge between the *C*2′ and *C*4′ atoms[117]. Thermodynamic studies reveal that

LNA increases the melting temperature of DNA oligonucleotides by 4–8 °C per residue when base paired with complementary strands of RNA[118]. Critically, LNA residues are known to enhance the SNP discrimination power of oligonucleotide probes by stabilizing the matched complex to a greater extent than the mismatched complex[119]. In our analysis, we positioned the SNP recognition site in the center of the right substrate binding arm, which was thought to be an optimal position based on prior work in the field[52]. We also evaluated the inclusion of LNA residues in both substrate binding arms, as LNA residues at these positions are known to increase the catalytic efficiency of the parent 10-23 DNAzyme[75]. We discovered that DNAzymes carrying LNA residues at both the SNP position and 5′ and 3′ and terminal positions of the substrate binding arms (Figure 3.2) function with higher sensitivity than an unmodified version of the DNAzyme or a DNAzyme carrying a single LNA residue at the SNP position. Titration assays reveal that all three sensors exhibit a linear downward correlation between fluorescence and analytic concentration (Figure S3.1) with the DNAzyme carrying LNA residues at the SNP position and substrate binding arms yielding the highest change in fluorescence between the matched and mismatched substrates across a concentration range of 5 to 100 nM analyte (Figure 3.2). This design configuration was therefore used as the molecular basis of our REVEALR genotyping technology.

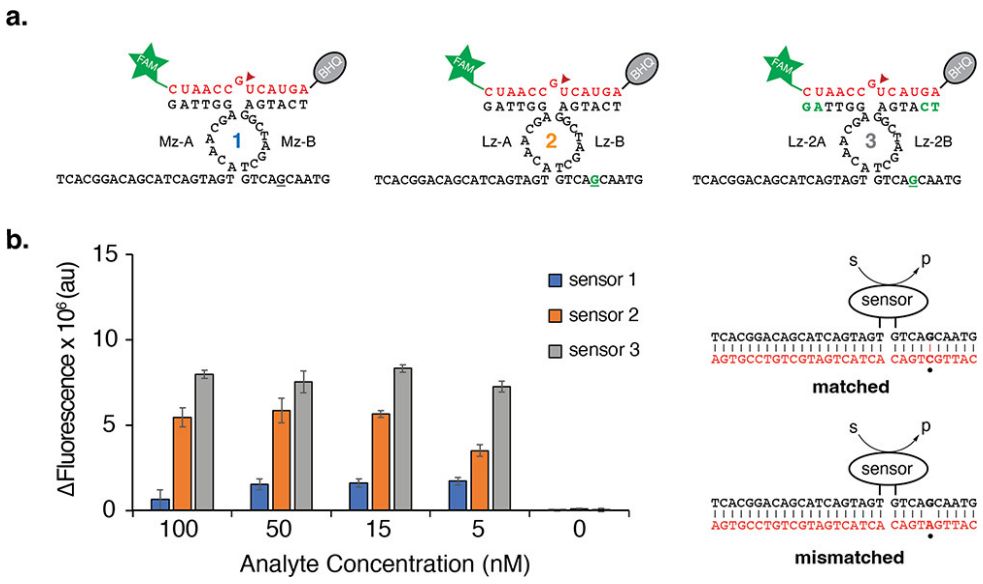

Figure 3.3. Sensor optimization. (a) Overview of multicomponent nucleic acid sensor. Two catalytic cores (Mz-A and Mz-B) self-assemble in the presence of a viral RNA analyte (not shown) to produce a functionally active catalyst with a separate active site that is capable of site-specific cleavage of a quenched fluorescent RNA reporter. Sensor 1 is DNA, sensor 2 contains a single LNA residue at the SNP position, and sensor 3 contains LNA residues at the SNP position and the 5′- and 3′-terminal positions of the substrate binding arms. Red arrow indicates the cleavage site and green nucleotides denote LNA residues. (b) Sensor optimization. Change in fluorescence observed for sensors 1–3 against decreasing concentration of a matched and mismatched DNA analyte corresponding to the A570D mutation observed in the S1 protein of the SARS-CoV-2 genome. Error bars represent the standard error of the mean (SEM) with n = 3. Abbreviations: au, arbitrary units; S, quenched 5′-fluorescent substrates; P, 5′-fluorescent products. Black dot denotes the SNP position.

Non-competitive and Competitive REVEALR

In designing the REVEALR system, we were initially concerned about the potential for cross-reactivity between our DNAzymes. This drawback, which exists for all hybridization-based strategies, could make it difficult to accurately identify VOCs in clinical samples. To evaluate this problem, we compared the cross-reactivity of DNAzymes that were designed to discriminate the wild-type (Wuhan-Hu-1) and alpha (B.1.1.7) strains of SARS-CoV-2 by distinguishing a C → A transversion in the viral genome responsible for the A570D mutation in the S1 glycoprotein (Figure S3.2, Table S3.1). We measured the fluorescent signal generated by the wild-type and alpha DNAzyme sensors targeting a perfectly matched DNA analyte or mismatched DNA analyte. SNP detection assays were

performed under non-competitive (individual DNAzymes) and competitive (both wild-type and VOC DNAzymes) binding conditions to compare the resolving power of nucleotide discrimination between the two assay formats (Figure S3.3). Fluorescence values collected across a range (5–500 nM) of analyte concentrations (Figure 3.3a, b) indicate that non-competitive binding conditions allow for accurate SNP detection at low analyte concentrations (5–15 nM range). However, the resolving power of this system is diminished when the analyte concentration reaches a higher level that is more reminiscent of viral RNA samples obtained after isothermal amplification by RT-RPA or LAMP (Figure 3.3a, b)[26]. This problem is less severe in the competitive binding assay, which exhibits lower background fluorescence due to competition between DNAzymes for the same viral analyte. As an example, the wild-type sensor distinguishes the wild-type analyte (at 100 nM) from the alpha variant by a factor of 10:1 under competitive conditions but only 2:1 under non-competitive conditions. This result suggests that it should be possible to genotype patient samples across a broader range of analyte concentrations, as illustrated in the 2-D plot shown in Figure 3.3c.

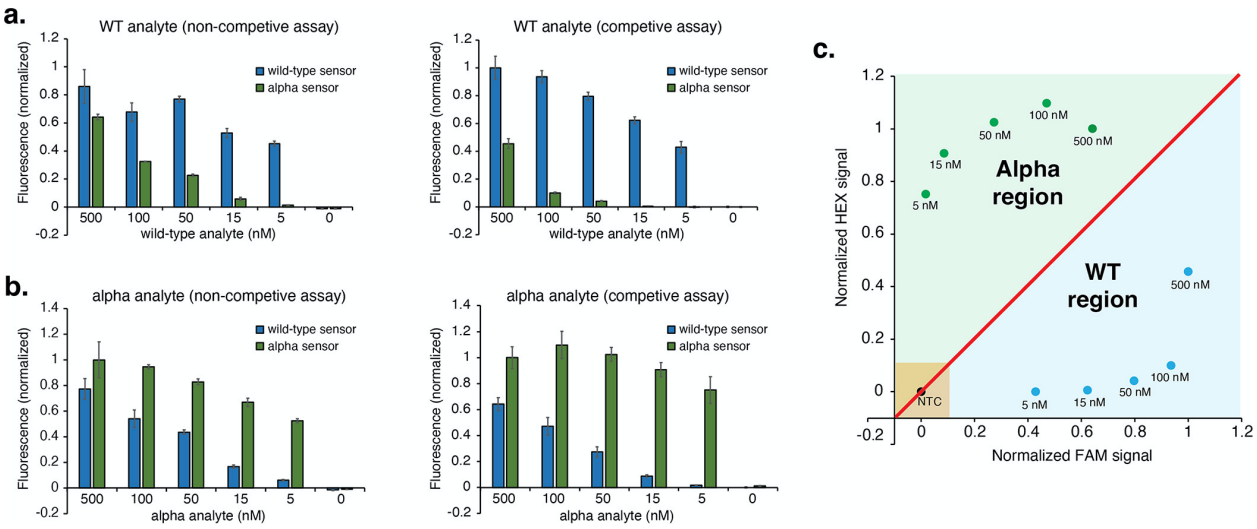

Figure 3.3. Nucleic acid detection assay. (a) Fluorescence signal generated by the wild-type and alpha sensors initialized by a segment of the wild-type analyte under non-competitive (left) and competitive (right) reaction conditions. (b) Fluorescence signal generated by the wild-type and alpha sensors initialized by a segment of the alpha variant under non-competitive (left) and competitive (right) reaction conditions. Error bars represent the standard error of the mean (SEM) with $n = 3$. (c) 2-D analysis showing wild-type and alpha variant detection under competitive reaction conditions. Each data point is the average of 3 replicates. NTC, no template control.

Multicomponent DNAzyme Sensors for SARS-CoV-2 Variants of Concern

We evaluated 18 single-nucleotide mutations across all regions of the SARS-CoV-2 genome (Table S3.2) to establish a panel of multicomponent DNAzymes that could identify each of the major VOCs observed in the population over the last 24 months. To ensure high sensitivity for each VOC, we focused our analysis on genomic mutations that were prevalent in >90% of each genotypic lineage[120]. The screen identified 11 DNAzymes that functioned with high discriminating power against the wild-type strain in genotyping assays using in vitro transcribed (IVT) RNA analytes. The five most promising sensors (Figure 3.4a) are capable of distinguishing the A570D mutation observed in the alpha (B.1.1.7) variant, the K417N mutation observed in the beta (B.1.351) variant, the K417T mutation observed in the gamma (P.1) variant, the L452R mutation observed in the epsilon (B.1.427/9) and delta (B.1.617.2) variants, and the T547K mutation observed in the omicron (B.1.1.529) variant.

Another six DNAzymes (Figure S3.4) showed strong discrimination against mutations observed in the alpha, beta, gamma, delta, and omicron strains, indicating that these sensors offer an additional layer of sensitivity for future diagnostic assays. The remaining 7 DNAzymes were unable to differentiate the wild-type and mutant analytes (Figure S3.5) at this time but could potentially be improved using additional chemical modifications or further optimization of the SNP recognition site.

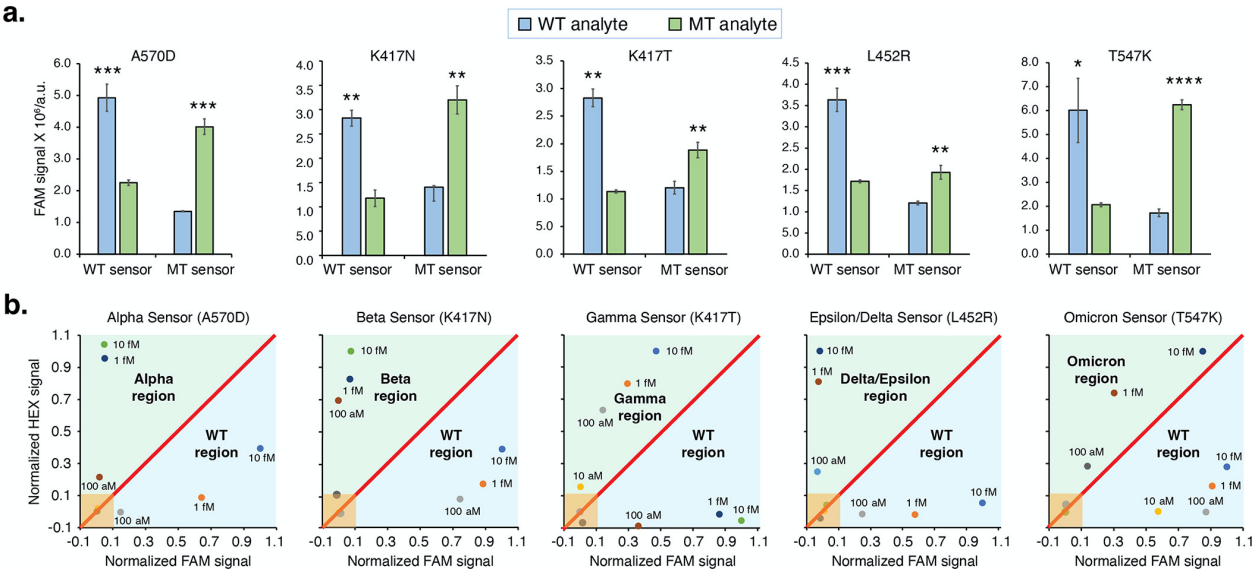

Figure 3.3. Sensitivity of REVEALR genotyping under competitive conditions. (a) Fluorescent signal generation for 15 nM of the A570D, K417N/K417T, L452R, and T547K DNA analyte after incubation for 30 min at 37 °C. Measurements are mean ± standard error (S.E.M), n = 3. Two tailed Student's t test; *P < 0.05, **P < 0.01, ***P < 0.001, ****P < 0.0001. (b) Data are presented in 2-D plots showing wild-type and VOC detection across a range of concentrations. Assays were performed by separately delivering either the wild-type or VOC analyte to the reaction mixture. Each data point is the average of 3 replicates.

In the context of a REVEALR-based detection assay, where IVT RNA is pre-amplified and detected in a two-step assay, the five most promising sensors were found to function with an analytic LoD of 10–100 aM (Figure 3.4). In each case, wild-type and VOC-specific DNAzymes were separately challenged with either the wild-type or mutant analyte in a

competitive binding format to assess the detection limit for a simulated viral target. When plotted in the 2-D format (Figure 3.4b), wild-type and VOC analytes show strong signal separation along the diagonal axis, illustrating the resolving power of the assay to clearly distinguish wild-type and VOC analytes.

Clinical Validation of REVEALR Genotyping for SARS-CoV-2 Surveillance

Surveillance testing in the United States, both nationally and locally, reveals the spread of SARS-CoV-2 variants of concern across the country. Beginning in January 2021, the country witnessed the chronological rise of five major VOCs, including the alpha (B.1.1.7), gamma (P.1), epsilon (B.1.427/9), delta (B.1.617.2), and omicron (B.1.1.529) strains, along with several other minor variants (Figure 3.5). The rapid circulation of these more harmful strains in the public created a need for rapid and accurate genotyping assays that could be deployed as an alternative to traditional sequencing methods, which are slow, costly, and difficult to scale to the population. As a possible solution to this problem, we evaluated our two-step REVEALR genotyping assay on heat-inactivated patient samples collected at the UCI Medical Center in Orange, California. RNA extracted from nasopharyngeal swaps obtained from 34 patients treated in early, mid, and late 2021 were individually assayed in the competitive binding format for the wild-type, alpha, beta, gamma, epsilon/delta, and omicron variants. The patient samples were each analyzed for activity against the set of five VOC sensors, with each VOC sensor competing against the wild-type sensor. In total, 170 diagnostic assays were performed against the set of 34 clinical samples, which reflect 31 COVID positive patients and 3 COVID negative patients (Table S3.3). All the samples were sequence verified, either at the UCI Medical Center or in our lab on the main campus.

REVEALR identified each VOC with perfect accuracy, including patients infected with the wild-type strain, and yielded a clear negative result for each of the three COVID negative swabs (Figure 3.5). Importantly, samples collected in early, mid, and late 2021 reflect the abundance of SARS-CoV-2 strains observed locally and nationally at that time, indicating that REVEALR offers a powerful new tool for population surveillance and patient diagnosis. This latter observation could have an important impact on options for therapeutic intervention, as emerging strains, such as delta and omicron, have different virulence levels that can affect patient treatment.

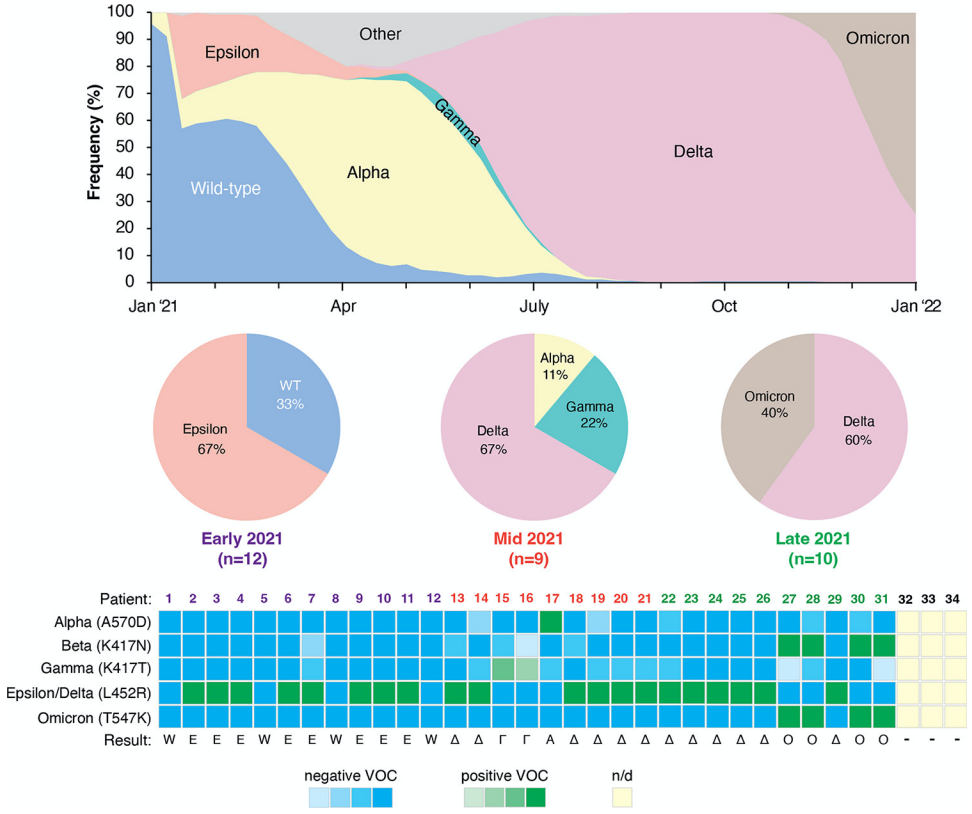

Figure 3.3. Surveillance testing of SARS-CoV-2 in the United States and Orange County, California. Surveillance of SARS-CoV-2 from GISAID shows the chronological frequency of variants of concern observed in the United States between January 2021 and January 2022 (top plot) using a subsampled dataset with time points documented at 7-day increments. Pie charts depict the distribution of sequence-verified SARS-CoV-2 variants observed in patients treated at the UCI Medical Center in Orange, California in early, mid, and late 2021. All 31 clinical samples were positively genotyped by competitive REVEALR. Although patient samples

27, 28, 30, and 31 yielded positive results for both the beta and omicron variants, due to a common K417N mutation shared between both strains, these samples were labeled omicron. This decision was based on a positive test for the T547K mutation, and the fact that the beta variant was not observed in the United States and its presence elsewhere in the world preceded the sample collection date. Each data point is the average of 3 replicates. Clinical samples 32–34 are negative controls obtained from healthy patients. Colors: blue, positive for wild-type; green, positive for VOC; yellow, clinical samples that are negative for COVID-19. Abbreviations: W, wild-type; A, alpha; E, epsilon; Γ, gamma; Δ, delta; and O, omicron; and n/d or -, not detected.

3.4. Discussion

The COVID-19 pandemic, caused by the spread of SARS-CoV-2 across the globe, represents the greatest threat to U.S. health and prosperity since the Great Depression. Controlling the spread of the disease will require the broad deployment of highly sensitive, low cost, and simple to use point-of-care diagnostics that are readily available for routine healthcare monitoring. Critical to this effort is the need to rapidly identify and triage patients infected with variants of concern that increase viral transmissibility and reduce vaccine protection. Current whole genome sequencing efforts designed to monitor epidemiological changes in the population are insufficient for this purpose, as this approach is used to provide a global picture of disease spread in local communities and across the nation. By contrast, the diagnosis of individual patients for a specific VOC is currently performed by Sanger sequencing, which is a slow and costly process that does not scale to the population.

Here, we describe the design, optimization, and clinical validation of a two-step genotyping system that is capable of precisely identifying the specific VOCs infecting COVID-19 patients. Our technology platform, called REVEALR, is based on a multicomponent DNAzyme strategy in which wild-type and VOC-specific DNAzymes compete to recognize single-nucleotide mutations in the viral RNA of patient-derived nasopharyngeal swaps. Assays performed in the competition format exhibit lower background fluorescence and higher discriminating power across a broader range of analyte

concentrations than assays performed in a conventional single-reagent format. We demonstrated the viability of REVEALR as a rapid and highly sensitive genotyping assay for detecting SARS-CoV-2 variants of concern by evaluating 34 samples collected from patients treated at the UCI Medical Center in Orange, CA. REVEALR identified the correct viral strain in all 31 of the COVID positive samples and yielded a clear negative result for each of the 3 COVID negative samples. In addition to strong positive and negative predictive capabilities, results obtained from the clinical validation study were consistent with local and national COVID-19 surveillance efforts.

We wish to note that the epsilon and delta variants analyzed in the current study were distinguished based on their sample collection dates (Figure 3.5, Table S3.3), as both strains share a common L452R mutation for which a sensor was available. In the future, it may be possible to distinguish these strains using the T19R and E156G backup sensors (Figure S3.4), which are specific to the delta strain. Likewise, it should also be possible to distinguish new omicron subvariants using a hierarchical system in which an initial positive result for omicron is followed by a second genotyping assay to elucidate the identity of the specific subvariant in a patient sample (Figure S3.6).

Although REVEALR is conceptually like known CRISPR-based approaches in terms of analyte detection and signal generation, the platform has several unique advantages that warrant consideration. These include (1) broader targetability due to the absence of sequence constraints imposed by the PAM motif, (2) lower background fluorescence as a result of the competitive binding assay, (3) lower risk of viral or bacterial contamination by avoiding the need for protein expression and purification, and (4) increased simplicity and

lower cost because the sensor is based entirely on the self-assembly of synthetic oligonucleotides and does not require recombinant protein or RNase inhibitors as reagents common to the CRISPR system. Together, these features make REVEALR an attractive system for SARS-CoV-2 genotyping.

Looking ahead to the future, REVEALR could benefit from further improvements that lead to higher sensitivity, high specificity, greater throughput, and increased user friendliness. Such advances could, for example, include the transition from a fluorescent-based detection system to a simpler lateral flow device as well as the creation of an amplification-free multiplex detection platform for routine healthcare monitoring. We have previously demonstrated the ability for REVEALR to function in a lateral flow system for COVID detection[1], suggesting that similar systems could be used as a diagnostic for patient genotyping. We could also optimize the chemistry and position of the SNP discrimination site in the sensor to allow for greater sensitivity of mismatch detection. Other less technical advances for improving signal detection may include changes to the virus inactivation protocol, which currently uses elevated temperatures that could damage the viral RNA analyte. More efficient lysis methods, such as glass bead-based ultrasonic power as applied to the Cepheid GeneXpert platform, could improve assay performance[121]. Finally, the incorporation of redundancy into the assay using multiple sensors per VOC would increase the confidence of SARS-CoV-2 genotyping. This last step could be done by utilizing backup sensors identified in this study, discovering new sensors, or by optimizing existing sensors for improved activity.

3.5. Conclusions

In summary, we have shown that REVEALR is a versatile and efficient method for genotyping SARS-CoV-2 strains in COVID-positive patients. This strategy offers a valuable new approach for improving the sensitivity and specificity of single-nucleotide detection assays in far reaching applications that include pathogen detection, antibiotic resistance, genetic diseases, and cancer. Future developments could enable routine testing in hospitals, clinical diagnostic laboratories, and possibly even local activities involving businesses and schools.

3.6. Experimental details

SARS-CoV-2 Metadata

SARS-CoV-2 data that track the frequencies of VOCs is available from the Global Initiative on Sharing All Influenza Data (GISAID) database (https://www.gisaid.org), which is a repository for COVID-19 genomic data. All GISAID data deposited through January 10, 2022, was used to examine active COVID-19 VOCs specifically in the United States and subsampled for the timespan of January 1, 2021, through January 1, 2022, with time points documented about every 7 days (n=51).

SARS-CoV-2 data that track new daily and cumulative COVID-19 cases in the United States originate from Worldometers (https://www.worldometers.info), which collects from government agencies and outlets for live reporting of statistics. Statistics for the daily new and growing total of COVID-19 cases were subset every 7 days from January 1, 2020, to January 1, 2022 (n=106).

Materials

DNA and LNA oligonucleotides were purchased from Integrated DNA Technologies (Coralville, IA). TwistAmp® Basic Kit was purchased from TwistDx (Maidenhead, UK). Solutions of dNTPs (100 mM) were purchased from ThermoFisher (Waltham, MA). T7 RNA polymerase and buffer, as well as M-MuLV Reverse transcriptase, were purchased from Lucigen Corporation (Middleton, WI). HiScribe T7 High Yield RNA Synthesis Kit was purchased from New England Biolabs (Ipswich, MA). GoTaq Probe 1-Step RT-qPCR System was purchased from Promega (Madison, WI).

Multicomponent enzyme screening against 20 genomic positions

Screening experiments were performed in reaction mixtures containing 50 mM Tris-HCl (pH 8.5), 150 mM NaCl, 200 mM $MgCl_2$, 500 nM of each Mz-A and Mz-B (split DNAzymes), 500 nM 7+8 FamQ RNA substrate, and 15 nM of DNA analyte comprising a short segment of either the wild-type or mutant variant. Reactions were performed using each wild-type and mutant DNAzymes targeting both the wild-type and mutant variant, respectively, at each position and monitored by real-time fluorescence using a qRT-PCR instrument at 1 min intervals over a period of 30 min at 37˚C (Figure S3.2).

LNA modifications experiments

DNA and LNA versions of the multicomponent DNAzyme (500 nM), named Sensor 1, Sensor 2 and Sensor 3 (Figure 3.2a) that target the wild-type region around the A570D mutation observed in the alpha variant, were added to a reaction containing 50 mM Tris-HCl (pH 8.5), 150 mM NaCl, 200 mM $MgCl_2$, 500 nM 6+6 FamQ RNA substrate, and defined

concentrations (0 – 100 nM) of DNA analyte comprising a short segment of either the wild-type or mutant A570D variant. Reactions were monitored by real-time fluorescence using a qRT-PCR instrument at 1 min intervals over a period of 30 min at 25°C for Sensor 1 and Sensor 2 and 37°C for Sensor 3.

Non-competitive genotyping experiments

Reaction mixtures were prepared containing 50 mM Tris-HCl (pH 8.5), 150 mM NaCl, 200 mM $MgCl_2$, 500 nM LNA modified split DNAzymes (Sensor 3), 500 nM 6+6 FamQ RNA substrate, and defined concentrations (0 – 500 nM) of DNA analyte comprising a short segment of either the wild-type or mutant A570D variant. Reactions were monitored by real-time fluorescence using a qRT-PCR instrument at 1 min intervals over a period of 30 min at 37°C.

Competitive genotyping experiments

The reactions were performed as described for the non-competitive genotyping experiments, with the exception of the solution containing LNA modified split DNAzymes (Sensor 3) that target both the wild-type and mutant analyte. To distinguish the signal generated from the wild-type and mutant analytes, the quenched RNA substrates were prepared with non-overlapping fluorescent dyes. Fluorescein (FAM) was used for the wild-type sensor and hexachlorofluorescein (HEX) was used for the mutant sensor. Additionally, the RNA substrates carried unique sequences that were complementary to their specific LNA modified split DNAzymes (Sensor 3). Reactions were monitored by real-time fluorescence using a qRT-PCR instrument at 1 min intervals over a period of 30 min at 37°C.

In vitro transcribed RNA

RNA analytes mimicking specific mutations (K417N/T, L452R, T547K, A570D) in the SARS-CoV-2 genome were prepared by in vitro transcription (IVT). IVT reactions were performed using the HiScribe T7 High Yield RNA Synthesis Kit. Each reaction contained 10 mM of each NTP, 1X reaction buffer, 3 µL PCR product, 2 µL T7 RNA polymerase mixture, and 5 µL nuclease free water. Reactions were incubated at 37°C overnight. Crude RNA was purified by 15% denaturing urea PAGE and electroeluted, either under 180 V for 3 h or 60 V overnight. Purified RNA was desalted with an Amicon Ultra 0.5 mL 30k centrifugal filter from EMD Millipore (Burlington, MA), quantified by Nanodrop, and diluted in nuclease-free water to desired concentrations.

REVEALR-based genotyping

A lyophilized RPA pellet was resuspended with 29.5 µL rehydration buffer, 1 µL M-MuLV-RT (200 U/µL), 0.5 µL forward primer (50 µM), 0.5 µL reverse primer (50 µM), and 1.25 uL ATP (100 mM). A portion (13.1 µL) of the master mix was transferred to the reaction tube. To initiate the assay, 2 µL magnesium acetate and 4.9 µL of IVT RNA or purified RNA from clinical samples were added to the side of each tube, without contacting the master mix. After briefly vertexing to mix the magnesium acetate initiator into the reaction, and subsequent centrifugation, the reactions were incubated for 25 min at 42°C. The reaction tube was removed after the first 5 min, briefly vortexed, and returned to the heating device. After incubation, the reaction was inactivated by heating the reaction tube for 5 min at 95°C. The RT-RPA reactions were then placed on ice before T7 transcription.

The dsDNA produced by RT-RPA was forward transcribed into ssRNA by in vitro transcription. T7 transcription reactions contained 1x T7 RNA Pol Buffer, 0.5 mM NTPs, 30 U T7 RNA polymerase, and 2 uL RT-RPA product for a 20 uL total volume. Reactions were incubated for 1 h at 37°C before being used for the competitive REVEALR genotyping assay.

The competitive genotyping assay was performed as described above, except for one step in which the reactions were seeded with 6 uL of in vitro transcribed RNA or purified RNA obtained from clinical samples that was amplified by RT-RPA/T7 isothermal amplification instead of DNA segments. Reactions were monitored by real-time fluorescence using a qRT-PCR instrument at 1 min intervals over a period of 1 h at 37°C.

Sensitivity test and data normalization

The sensitivity test was performed with 10 fM, 1 fM, 100 aM, and 10 aM of in vitro transcribed wild-type and mutant RNA following the competitive REVEALR genotyping assay described above. Data was normalized using the no template control (NTC) FAM/HEX signals as the negative value, 10 fM wild-type FAM signals as FAM positive value, and 10 fM mutant HEX signals as HEX positive value. The functions are listed as follows.

$$\text{Normalized FAM signal} = \frac{(\text{real FAM signal} - \text{negative FAM signal})}{(\text{positive FAM signal} - \text{negative FAM signal})}$$

$$\text{Normalized HEX signal} = \frac{(\text{real HEX signal} - \text{negative HEX signal})}{(\text{positive HEX signal} - \text{negative HEX signal})}$$

Evaluation of patient-derived clinical samples

Nasopharyngeal swabs from 34 patients were obtained from the COVID-19 Research Biobank of the Experimental Tissue Shared Resource Facility at University of California, Irvine. Each sample was collected, and heat inactivated for 1 h at 80°C by trained medical professionals at the University of California Medical Center in Orange, California. The samples were collected from patients treated in early, mid, and late 2021 at UCI Medical Center. The variant types of 9 samples were identified by the hospital and the other 25 samples were identified via Sanger sequencing. SARS-CoV 2 viral RNA samples were purified following the CDC recommended Qiagen DSP Viral RNA Mini kit protocol. The REVEALR genotyping system was used to detect the extracted RNA viral RNA using fluorescence readout as described above.

Sanger sequencing

Clinical samples were amplified using the GoTaq Probe 1-Step RT-qPCR System to target regions of interest. RT-PCR was performed following the manufacturers recommended protocol. dsDNA products were purified with an agarose gel purification step using 2% agarose gels. The DNA was extracted from the gel using the Monarch DNA Gel Extraction Kit from New England Biolabs (Ipswich, MA), and cleaned up using the DNA Clean and Concentrator Kit from Zymo Research (Irvine, CA). The primers used for amplifying each region of interest include the K417_RPA_FWD_S and RPA_L452R_RVS primer pair for the K417 and L452 regions and the RPA_T547K_FWD and RPA_A570D_RVS primer pair for the T547 and A570 regions (see Table S1). The samples

were then sent for Sanger sequencing, using the forward and reverse primers from the PCR for sequencing as well.

Chapter 4:

Droplet REVEALR: amplification-free nucleic acid detection platform

Publication Note

This chapter is part of a manuscript in preparation.

Contribution Statement

Kefan Yang and John Chaput conceived the project and designed the experiments. Kefan Yang performed the experiments. Eric Yik and Derek Vallejo assisted in the microfluidic droplet experiments. John Chaput wrote the manuscript with input from all the authors.

4.1. Abstract

The COVID-19 pandemic, caused by spread of the SARS-CoV-2 virus across the globe, exposed a pressing need for new public health screening tools for pathogen detection, disease diagnosis, and viral genotyping. REVEALR (RNA-encoded viral nucleic acid analyte reporter) is an isothermal DNAzyme-based point-of-care diagnostic that functions with a detection limit of ~10 copies/uL when coupled to a preamplification step and facilitates the viral genotyping of SARS-CoV-2 variants of concern in patient-derived clinical samples. Here we describe an improved REVEALR platform, termed digital droplet REVEALR (ddREVEALR), that can achieve direct viral detection and absolute quantitation utilizing a signal amplification strategy that relies on DNAzyme multiplexing and volume compression. Using an AI-assisted image-based readout, ddREVEALR was found to achieve 95% positive predictive agreement from a set of 20 nasal pharyngeal swabs collected at UCI Medical

Center in Orange, California. We suggest that the combination of amplification-free and protein-free analysis makes ddREVEALR a promising approach for direct viral RNA detection of clinical samples.

4.2. Introduction

The coronavirus disease 2019 (COVID-19) pandemic caused by the spread of the severe acute respiratory syndrome coronavirus 2 (SARS-CoV-2) across the globe fostered unprecedented growth in the development of novel methods for nucleic acid detection[122]. As of November 2022, 275 diagnostic tests have received emergency use authorization by the US Food and Drug Administration (FDA), the vast majority of which rely on reverse transcription polymerase chain reaction (RT-PCR) for analyte detection. A much smaller subset (~10%) utilize isothermal amplification strategies, such as loop-mediated isothermal amplification (LAMP)[292] and recombinase polymerase amplification (RPA)[19], to increase copy number by avoiding the thermocycling requirements of RT-PCR. However, despite their widespread use in FDA-approved diagnostics, amplification-based approaches developed for routine healthcare monitoring suffer from problems associated with non-specific DNA amplification, elevated costs due to the need for specialized enzymes, and bottlenecks in product development caused by poor supply chain resilience[123]. These difficulties raise an important challenge in the field of nucleic acid biochemistry of how to develop a nucleic acid detection assay that can accurately quantify pathogen levels in patient samples independent of sample amplification.

Recent advances in nucleic acid technologies have led to the development of a broad range of amplification-free approaches for pathogen detection[124]. Several of these methods

have been shown to function with analytical limits of detection (LoD) in the low attomolar range (10^{-18} M), corresponding to ~1000 copies of a viral genome/mL[125]. Among the various methods under development, CRISPR-based approaches have attracted significant attention due to their strong sequence-specific recognition modalities that allow for the precise detection of pathogen nucleic acid signatures. Such examples include a graphene field-effect transistor for targeted DNA detection[126,127] and a multiplex strategy that is compatible with mobile phone microscopy[128]. Given the success of CRISPR-based systems toward the problem of amplification-free detection, we wondered if this paradigm could be made even simpler by establishing a protein-free approach for direct pathogen detection.

REVEALR (RNA-encoded viral nucleic acid analyte reporter) is a rapid and highly sensitive DNAzyme-based point-of-care diagnostic developed for SARS-CoV-2 detection[1]. The technology is based on a multicomponent nucleic acid enzyme (Mz) that self-assembles in the presence of a target analyte to produce a functional DNAzyme capable of generating an output signal by cleaving a quenched fluorescent oligonucleotide reporter[67]. REVEALR maintains high sequence specificity through complementary Watson-Crick base pairing between the target binding arms of the multicomponent enzyme and viral RNA sequence, allowing for continuous signal amplification while the DNAzyme is bound to the single-stranded viral RNA. When coupled to an RPA-preamplification step, REVEALR can achieve an analytical LoD (≤20 aM, ~10 copies/μL), which comparable to the SHERLOCK and DETECTR systems based on CRISPR-Cas enzymology[31,45]. In a competitive binding assay format, REVEALR was shown to be capable of genotyping sequence-verified clinical

samples spanning the complete set of SARS-CoV-2 variants of concern circulating in the US in 2021[2].

Here we report the conversion of our standard REVEALR assay into a digital droplet format, termed digital droplet REVEALR (ddREVEALR), that can achieve absolute RNA quantitation through single-molecule viral RNA detection in uniform water-in-oil (w/o) droplets (Figure 4.1). Through a combination of chemical optimization, volume compression, and multiplexing, ddREVEALR was found to achieve 95% positive predictive agreement from a set of 20 PCR-verified patient-derived nasal pharyngeal swabs collected at UCI Medical Center in Orange, California. Based on the simplicity of the design and use of low-cost renewable reagents, we suggest that ddREVEALR offers a promising approach for personalized diagnostics.

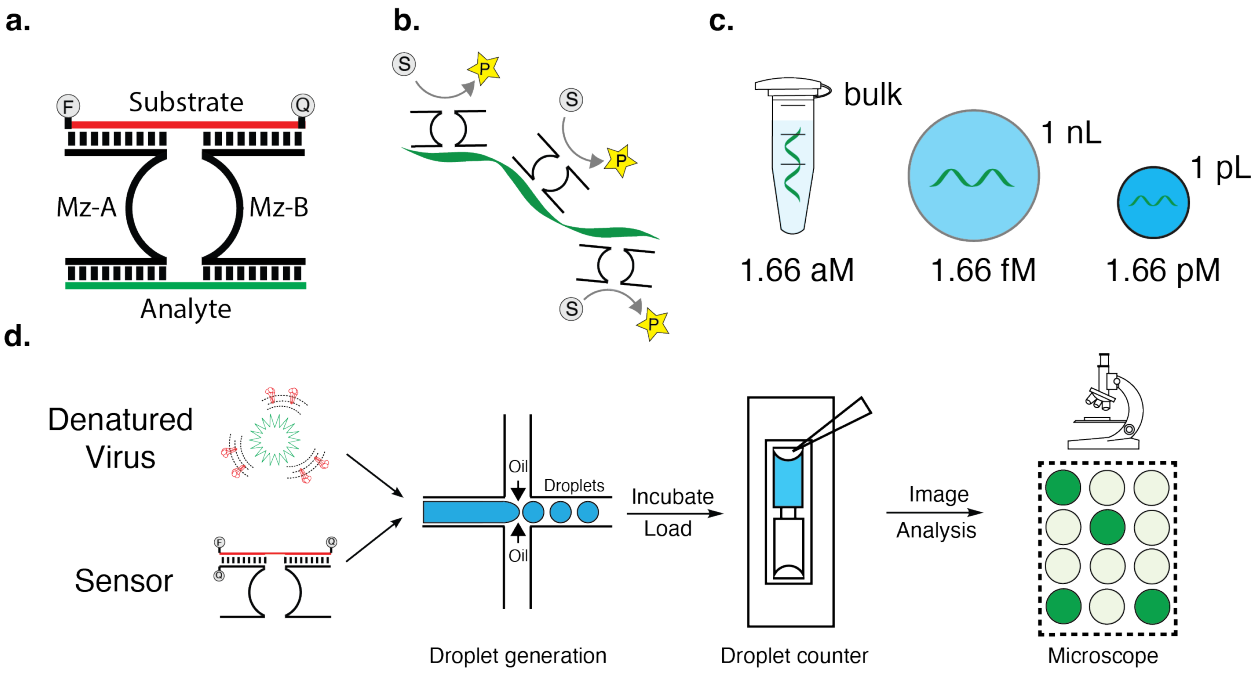

Figure 4.1. Amplification-free COVID-19 detection by digital droplet REVEALR. (a) Cartoon representation of a multicomponent DNAzyme sensor developed for SARS-CoV-2 detection. The catalytic core (black) self-assembles in the presence of a viral RNA analyte (green) to produce a functionally active enzyme that can generate an optical signal by cleaving a quenched fluorescent RNA reporter (red). (b-c) Signal

amplification. The optical signal produced by the DNAzyme can be increased by multiplexing (b) and volume compression (c). Multiplexing involves targeting the viral analyte with sets of DNAzymes that recognize different regions of the viral genome. Volume compression increases analyte concentration through microfluidic encapsulation in uniform water-in-oil droplets of defined size. (d) Workflow. Reaction mixture containing denatured virus and multiple DNAzymes is encapsulated in microdroplets, incubated, transferred to a droplet counter, and imaged. The droplet population is then digitally assessed and fit to a calibration curve. Abbreviations: S, substrate and P, product.

4.3. Result

Assay Design

We envisioned developing an amplification-free assay for COVID-19 detection that would enable absolute quantitation of the viral genome in a digital droplet format that is sensitive, rapid, and affordable. As outlined in Figure 1, a small aliquot of patient-derived sample, reaction buffer, and DNAzyme sensors targeting different regions of the viral genome are encapsulated in uniform w/o microcompartments. Since the average viral load of patients infected with SARS-CoV-2 ranges from 80 to 752 copies per μL,[96] Poisson distribution dictates that a large droplet population will consist of mostly unoccupied droplets, with a small fraction of occupied droplets containing only 1 copy of the viral genome. However, it should be noted that it is statistically possible for patients infected with a higher viral load to have a small number of droplets containing two copies of the RNA genome. Following incubation to facilitate target recognition and catalysis, the droplet population is transferred to a droplet counter and imaged by confocal microscopy. AI-assisted image analysis produces a droplet segmentation pattern that is used to determine positive and negative results based on the fluorescence signal of each droplet. Similar to digital droplet PCR, absolute quantitation is achieved by converting the percentage of positive droplet (PPD) into a precise analyte concentration based on Poisson statistics (Figure S4.1).[129]

Critical to the success of this workflow was the need to increase the LoD of our REVEALR assay. In bulk solution, direct detection of the SARS-CoV-2 genome requires an analytical LoD of 1.6 aM, which is 10^8-fold lower than the analytical LoD previously measured for a REVEALR assay performed using a modified DNAzyme sensor without sample preamplification.[1] Assay miniaturization can be used to reduce the magnitude of this problem; as analyte concentration increases through the effects of volume compression when analytical samples are compartmentalized in microfluidic droplets, with smaller size droplets poising the RNA analyte at higher concentrations. As an example, droplets produced with an average diameter length of 12 μm increase the viral RNA concentration by 10^6-fold relative to bulk solution (Figure 4.1). In compartments of this size, the analytical LoD required to achieve single viral RNA genome detection is 1.6 pM, which is only ~150-fold lower than the LoD observed for the REVEALR assay described above.[1] Based on previous experience,[1,67] we reasoned that it may be possible to increase the sensitivity of our assay through optimization of the DNAzyme sensor and reagent multiplexing. However, it was unclear if such steps would be sufficient to enable direct viral RNA detection of patient samples in a digital droplet format, as single-molecule nucleic acid detection by a DNA enzyme has not been achieved previously.

Assay Miniaturization and sensor optimization

To explore the benefit of performing REVEALR-based nucleic acid detection assays in a digital droplet format, we compared the analytical LoD of an all-DNA version of a DNAzyme sensor targeting in vitro transcribed RNA encoding a region of the S-gene from the SARS-CoV-2 genome in a bulk aqueous solution to reagents encapsulated in uniform microdroplets. For simplicity, this assay was performed using a commercial Bio-Rad digital droplet

generator and digital droplet reader designed to produce and analyze medium size droplets (1 nL volume, 124 μm diameter) that are stable and easy to generate from commercial reagents. After 1 hour of incubation at 25°C, DNAzyme 1 was observed to function with an analytical LoD of 5 nM in bulk solution as previously reported,[1] which improved to 50 pM when the assay was performed in a digital droplet format (Figure S4.2). Although this result demonstrated the ability for volume compression to increase the sensitivity of REVEALR-based RNA detection, it also revealed the challenges of achieving direct viral RNA detection as the analytical LoD of our assay was still above the limit required to permit direct pathogen detection.

Substrate binding is widely viewed as the rate-limiting step of DNAzyme-mediated RNA strand cleavage.[48] Based on our prior experience with chemically modified DNAzymes,[78] we postulated that the sensitivity of our assay could be increased by enhancing the catalytic turnover of the enzyme using chemical modifications introduced at key structural positions along the backbone architecture of the DNAzyme scaffold. Following a systematic analysis of diverse chemotypes, we discovered several DNAzyme sensors with improved activity (Figure 4.2a, Figure S4.3) under their optimized incubation temperature (Figure S4.4), buffer conditions (Figure S5), and substrate design (Figure S4.6). The most active sensor, Mz-13, contains a black hole quencher (BHQ) at the 3' terminus of Mz-A, a locked nucleic acid (LNA) residue at the 5' terminus of Mz-B, a phosphorothioate linkage between residues A_0 and G_1 of the catalytic loop, and a 2'-*O*-methoxyethylribonucleic acid (MOE) substitution for the standard 2'-deoxyguanosine residue at position 14 of the catalytic loop. The BHQ and LNA modifications enable improved contact quenching (Figure S4.7) and increased substrate hybridization, respectively, while modifications made to the catalytic loop are designed to

increase catalytic activity of the multicomponent enzyme. Compared to an all-DNA version of the sensor, the functionally enhanced sensor established for Mz-13 exhibits an increase (>4-fold) in catalytic activity (Figure 4.2b, Table S4.3), indicating that alternative chemotypes can significantly improve the performance of multicomponent DNA enzymes.

Next, we attempted to increase the sensitivity of our assay using a multiplexing strategy that involved the application of multiple DNAzyme sensors targeting different regions of the viral genome (Figure 4.1). Five DNAzyme sensors (N1-N5) were designed to recognize different regions of the N-gene, which is a highly conserved region of the SARS-CoV-2 genome.[130] To improve the overall activity of the assay, each DNAzyme was prepared using the optimal chemistry developed for Mz-13 (Figure 4.2) and reactions were performed and analyzed in 1 nL Bio-Rad droplets as described above. After 3 hours of incubation at 34°C, the multiplex assay afforded ~5-fold higher signal than the average signal obtained using each DNAzyme sensor individually (Figure 4.2c). However, despite improvements imbued through the multipronged approach of chemical optimization, multiplexing, and volume compression, the analytical LoD of 250 fM (Figure S4.8) remained above the 1.6 fM level required for single RNA detection in a 1 nL droplet. This observation suggested that an effective single-molecule DNAzyme strategy would require smaller volume compartments.

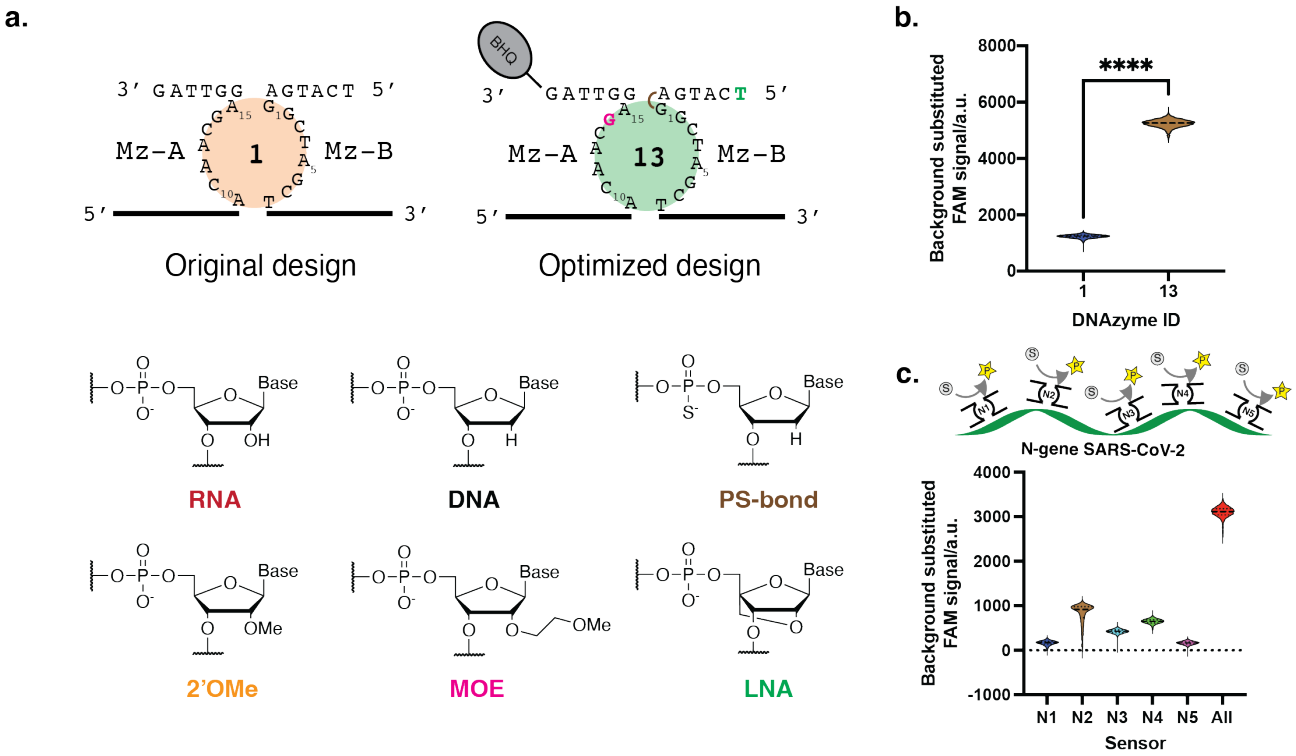

Figure 4.2. Sensor optimization. (a) Comparison of original DNAzyme 1 and chemical optimized DNAzyme 13. Chemical modifications are indicated by color and residue showed at the bottom. (b) Analyte detection. Quantitative analysis comparing the original all-DNA design (Dz sensor 1) to the most active design (Dz sensor 13) (c) SARS-CoV-2 detection using DNAzyme sensors individually and collectively in a multiplex format. Assays were performed in Bio-Rad droplets generated from buffer containing 200 mM MgCl2, 50 mM Tris (pH 8.5), 150 mM NaCl, 500 nM FAM-labeled RNA substrate and 500 nM DNAzyme, 100 pM of in vitro transcribed RNA analyte, 1X Bio-Rad ddPCR Supermix. Droplet populations were evaluated after a 1 hour incubation using a Bio-Rad ddPCR droplet reader. Abbreviations: 2'-O-methylribonucleic acid (2'-OMe), 2'-O-methoxyethylribonucleic acid (MOE), locked nucleic acid (LNA), phosphonothioate (PS), and black hole quencher (BHQ).

Digital Droplet REVEALR

In an effort to achieve direct viral RNA detection, we turned to microdroplets produced in-house using a custom fluorocarbon-coated polydimethylsiloxane (PDMS) microfluidic device previously developed for enzyme engineering applications.[131] By adjusting the flow rate of the aqueous component, we discovered that it was possible to generate populations of ~10^7 droplets in 6 minutes. The resulting confocal microscopy image indicates that these conditions allowed the PDMS device to produce uniform w/o droplets that were much smaller in size (average diameter: 12 μm, average volume: 1 pL) than the droplets produced using a commercial Bio-Rad instrument (Figure 4.3a). Simulation of analyte concentrations across

a range of droplet sizes (Figure 4.3b) indicates that droplets containing a single copy of the viral genome would have a concentration of 1.8 pM, which is ~10^3-fold higher than the concentration predicted for 1 nL size Bio-Rad droplets.

To explore the potential for smaller size droplets to achieve direct viral RNA detection, we performed a time course analysis with in vitro transcribed RNA encoding a region of the SARS-CoV-2 genome. Reactions were performed at a fixed analyte concentration of 10 fM over a time period of 6 hours at 34°C. This analyte concentration is the range expected for a patient-derived clinical sample.[96] At this analytic concentration, we would expect most of the occupied droplets to contain a single copy of the viral genome, with doubly occupied droplets present at a probability of only ~0.001% (Figure S4.9). The resulting images obtained by confocal microscopy reveal that the fluorescent signal plateaus after 3 hours (Figure 4.3c-e), indicating that 3 hours is sufficient to generate a fluorescence signal from a single-molecule DNAzyme-mediate detection assay. Analysis of the images by AI-assisted software reveals close concordance between the experimental and predicted values (~0.4% versus ~0.5%, respectively) for the fluorescent droplets (Table S4.2). This result implies that 12 μm compartments should be sufficient in size to enable direct viral RNA detection of SARS-CoV-2 from patient-derived samples.

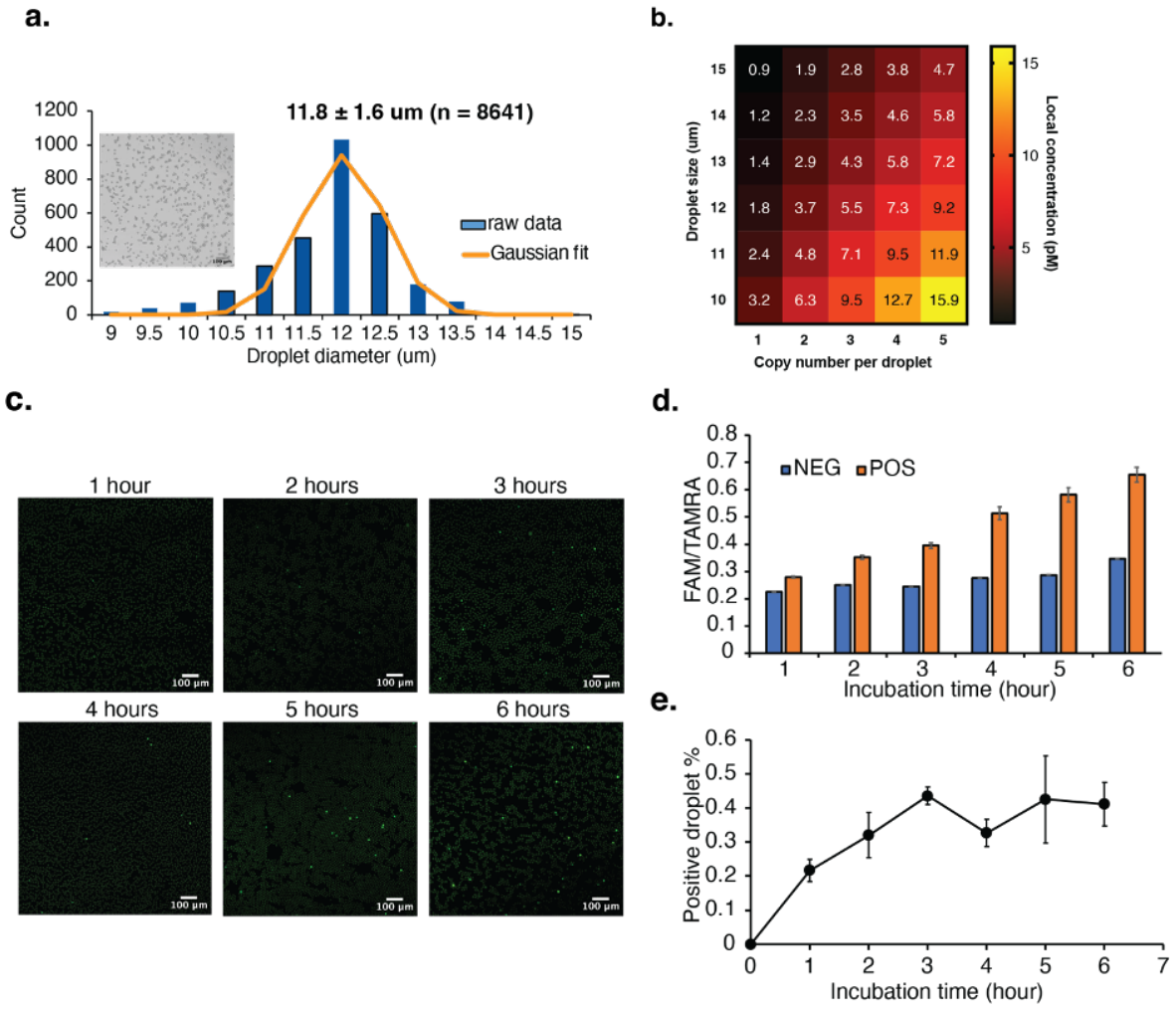

Figure 4.3. Digital droplet REVEALR in custom microfluidic droplets. (a) Droplet size distribution for custom in-house microfluidic droplet production. (b) Simulation of analyte concentration across a range of droplet sizes. (c) Digital time course analysis of SARS-CoV-2 signal generation produced from 10 fM in vitro transcribed RNA analyte. (d) Average positive and negative droplet signal observed after 1 to 6 hours of incubation at 34°C. (e) Positive drop percentage observed as a function of time. Error bars denote ± standard error of the mean for 3 independent replicates. Reactions were performed in droplets generated from buffer containing 200 mM $MgCl_2$, 50 mM Tris (pH 9.0), 150 mM NaCl, 1 uM FAM labeled RNA substrate, 500 nM TAMRA labeled reference oligo, 20 nM of each multicomponent DNAzyme, 10 fM in vitro transcribed RNA analyte and 1X Bio-Rad ddPCR Supermix. Droplet populations were imaged by confocal microscopy with data analysis performed using Biodock.

Sensitivity Test

We evaluated the sensitivity of ddREVEALR by measuring the fluorescence signal of individual droplets produced across a range of analyte concentrations. As illustrated in Figure 4.4a, in vitro transcribed RNA spanning a concentration gradient of 1 to 100 fM were individually encapsulated in 12 μm microdroplets. After 3 hours of incubation at 34°C,

analyte concentration was measured by digital detection (Figure 4.4b) and the resulting values compared to a linear regression plot of Ct values obtained by qRT-PCR. Comparison of the ddREVEALR data to qRT-PCR results provides a close correlation between the positive droplet percentage and authentic values (Figure 4.4c), indicating that droplet population analysis of DNAzyme-mediated fluorescence offers a viable path for quantifying biological samples. In this case, we evaluated 3 randomly selected fields of view, which allowed us to evaluate ~10,000 droplets per sample or ~0.05% of the droplet population. Analysis of the no template control revealed a false positive rate of ≤0.01% (Figure S4.10), which we attribute to either degradation of the RNA fluorophore or imperfect oligonucleotide synthesis. Using this approach, the current limit of detection is ~1 fM (Figure 4.4c), which corresponds to ~5 positive droplet observed within a 10,000-droplet population (Table S4.2).

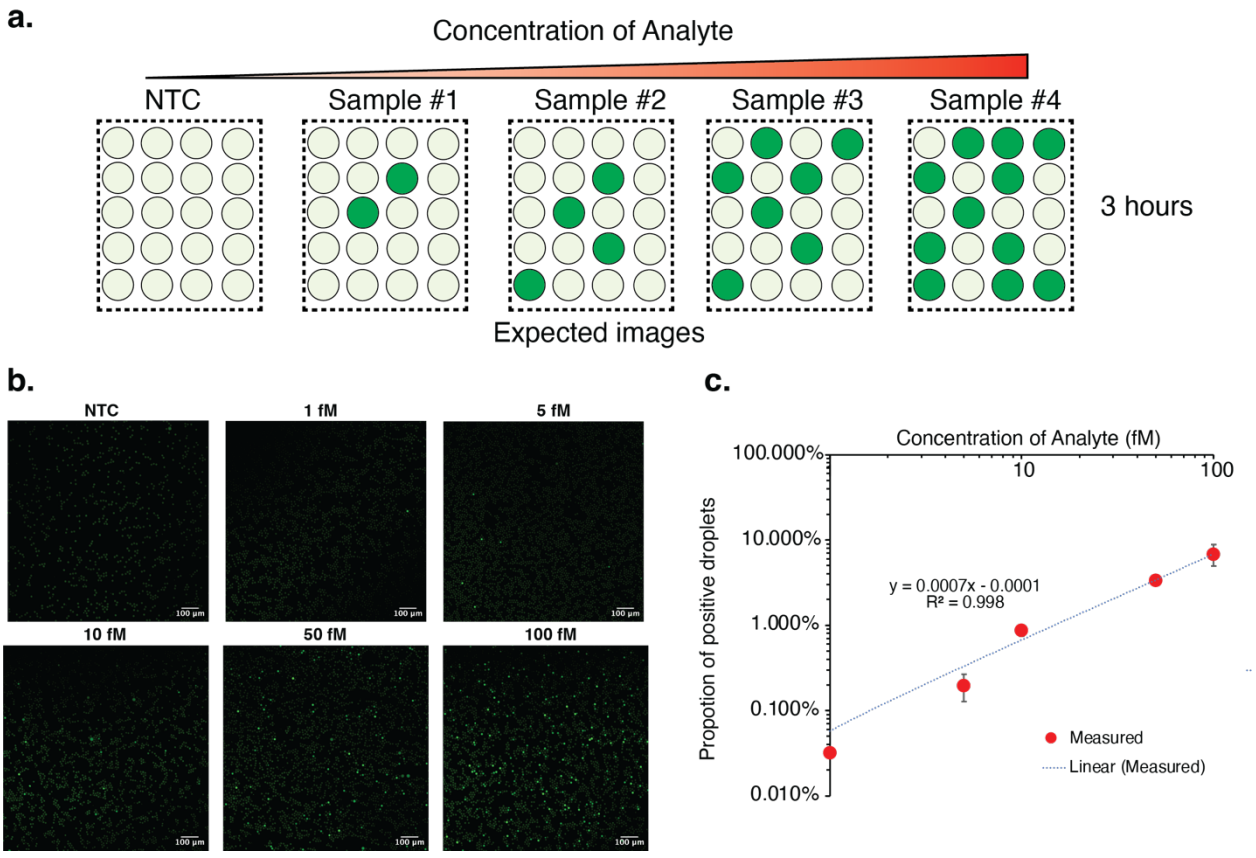

Figure 4.4. Sensitivity of digital droplet REVEALR. (a) Illustration of droplet signal across a gradient of analyte concentrations. (b) Images of digital droplets collected after 3 hours of incubation. (c) Calibration curve defining analyte concentration as a function of positive droplets. Red dots indicate positive percent values. The dashed line is a linear fit of experimental data. Error bars denote ± standard deviation of the mean for 2 independent replicates. Reactions were performed in droplets generated from buffer containing 200 mM $MgCl_2$, 50 mM Tris (pH 9.0), 150 mM NaCl, 1 uM FAM labeled RNA substrate, 500 nM TAMRA labeled reference oligo, 20 nM of each DNAzyme, in vitro transcribed RNA analyte and 1X Bio-Rad ddPCR Supermix. Droplet populations were evaluated after 3 hours of incubation at 34°C by confocal microscopy with data analysis performed using Biodock.

Clinical Validation

To establish ddREVEALR as an amplification-free diagnostic for COVID-19 detection, we evaluated 20 patient-derived nasal pharyngeal samples collected at UCI Medical Center in Orange, California. The samples consisted of 18 PCR positive patients and 2 PCR negative patients, which were placed in viral transfer media (VTM) and autoclaved to inactive the virus prior to receipt. After receipt, the RNA was purified and directly evaluated by ddREVEALR and qRT-PCR. The PCR positive samples were selected to display a range of

viral loads, as measured by qRT-PCR (Ct values of 17 - 35). ddREVEALR analysis positively confirmed 19 of the 20 samples following overnight incubation at 34°C. However, sample #18, with a Ct value of 35 (low aM concentration of SARS-CoV-2 RNA) was misread as a COVID negative sample due to the low concentration of the viral RNA present in this sample. Currently, our image-based readout system is evaluating ~0.05% of the droplets, which limits the testing capability for ultralow concentration of samples. It could be enhanced in future using a flow-based readout for higher droplet testing fraction. Nevertheless, this false positive value places the current limit of detection at 3.7 fM, which is equivalent to a Ct value of ~25.4 and within typical the range of clinical samples.

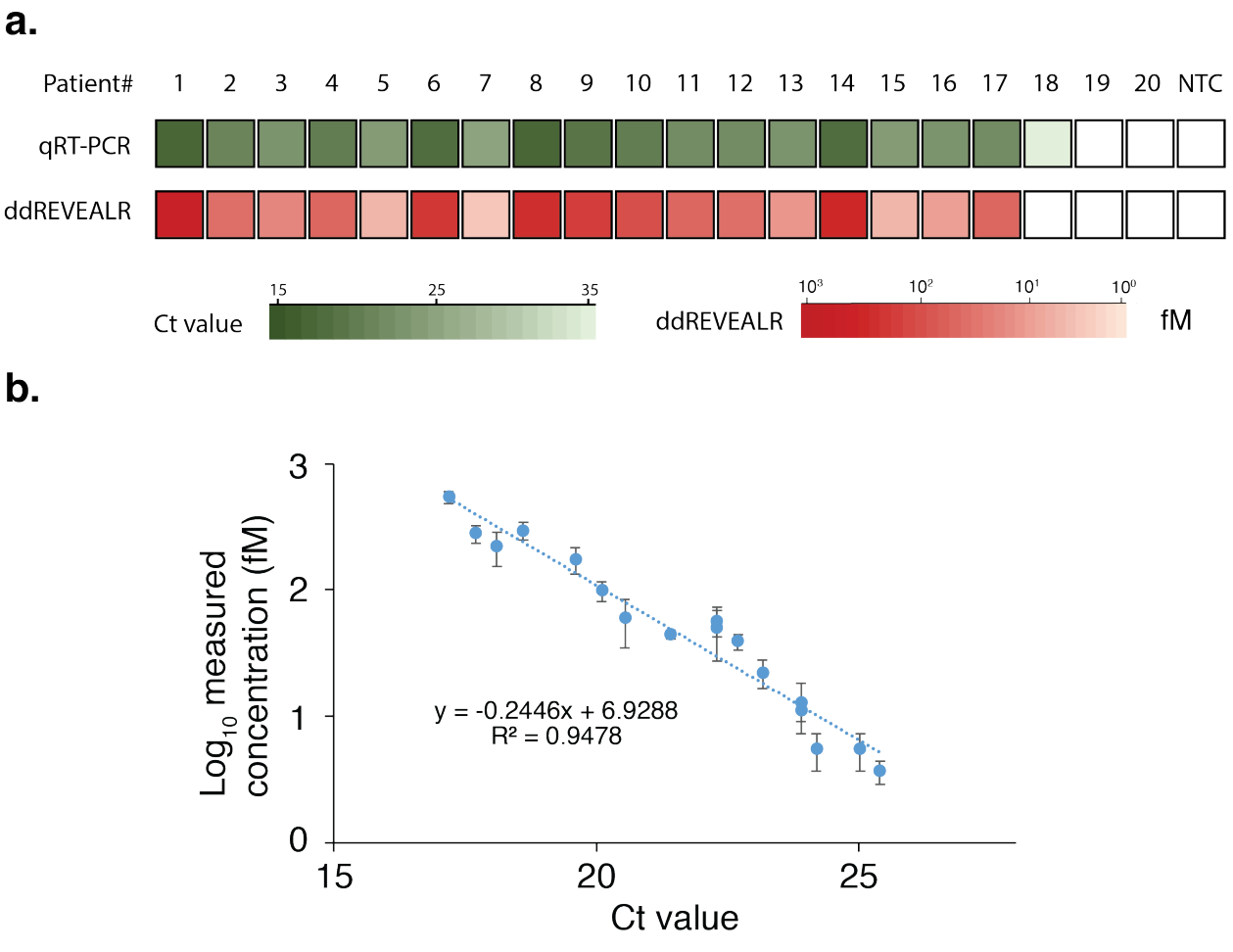

Figure 4.5. Clinical validation of patient derived samples. (a) Test results for 20 clinical samples of nasal pharyngeal swabs collected from COVID-19 patients treated at UCI Medical Center in Orange, California. (b) Linear relationship of Ct values obtained from qRT-PCR and viral RNA concentration measured by digital

droplet REVEALR. Error bars denote ± standard deviation of the mean for 2 independent replicates. Reactions were performed in droplets generated from buffer containing 200 mM $MgCl_2$, 50 mM Tris (pH 9.0), 150 mM NaCl, 1 uM FAM labeled RNA substrate, 500 nM TAMRA labeled reference oligo, 20 nM of each DNAzyme, 1 uL of purified clinical sample and 1X Bio-Rad ddPCR Supermix. Droplet populations were evaluated after 18 hours of incubation at 34°C by confocal microscopy with data analysis performed using Biodock.

4.4. Discussion and conclusion

The COVID-19 pandemic catalyzed unprecedented growth in the development of new analytical techniques for pathogen detection. In the area of nucleic acid detection, specifically, isothermal amplification strategies have emerged as rapid and inexpensive alternatives to quantitative RT-PCR, which remains the gold standard for SARS-CoV-2 detection. When coupled to sequence-specific detection modalities, such as those found in CRISPR-Cas enzymes, these systems offer sensitive and highly accurate platforms for viral RNA detection. Similar detections routes can also be achieved using DNAzyme constructs that have been engineered into point-of-care diagnostics by introducing an analyte recognition domain into the scaffold. However, despite their many benefits, amplification-based approaches are cumbersome due to the need for a sample pre-amplification step that places an additional burden of time and cost on the assay. They can also suffer from background problems due to nonspecific DNA amplification.

The current study demonstrates the feasibility of using DNAzymes to directly quantify viral RNA levels in patient-derived clinical samples. The resulting platform, termed digital droplet REVEALR (ddREVEALR), was found to achieve 95% positive predictive agreement from a set of 20 nasal pharyngeal swabs collected at UCI Medical Center in Orange, California. The sensitivity of the assay was greatly improved through a systematic optimization process that involved the use of chemical modifications that increased the catalytic activity of the DNAzyme, reagent multiplexing to improve signal amplification, and

volume compression to increase the local concentration of the viral analyte. Additionally, sample analysis was aided by the use of an AI-assisted image-based readout system that allowed for absolute quantitation of patient-derived clinical samples. The software assisted an efficient binary analysis of the droplet population, yielding a strong linear correlation to Ct values measured by qRT-PCR.

ddREVEALR has several advantages relative to other previously reported DNAzyme-based amplification-free nucleic acid strategies. In their original description, DNAzymes were shown to achieve picomolar level detection of a nucleic acid target.[67] Subsequent optimizations have improved the sensitivity of the assay to sub-picomolar levels using cascade designs,[132] cationic copolymers,[68] nucleic acids modifications,[80] and microwells.[56] However, to the best of our knowledge, this current study represents the first example of viral RNA quantification in a digital droplet formal using DNAzyme-based optical sensor. Since analyte quantification by digital droplet methods was previously established by protein enzymes through PCR amplification, this work demonstrates the ability for nucleic acid enzymes to compete with protein enzymes in similar biological assays.[129]

ddREVEALR compares favorably to related CRISPR-based approaches for amplification-free viral RNA detection. Unlike CRISPR, which relies on RNA and protein-based reagents that are temperature sensitive and must be stored and transported at low temperatures,[133] ddREVEALR is a DNA-based protein-free system (Figure S4.11) that is stable at room temperature, therefore avoiding the costly expense of the cold-chain problem. The DNA components of ddREVEALR are also easier and cheaper to produce as the they can be made by chemical synthesis rather than cellular protein expression and purification. This property allows for higher purity and greater scalability of the reagents, as cellular

processes are difficult to scale and can be prone to unwanted viral or bacterial contamination. Finally, the catalytic mechanism of the ddREVEALR system allows for greater targetability of the viral genome, as the targetability of CRISPR-based system is restricted by the protospacer adjacent motif (PAM) for Cas9 and Cas12 or protospacer flanking site (PFS) for Cas13.

Looking ahead to the future, the ddREVEALR system could benefit from a new generation of DNAzyme sensors, better signal readout methods, and possible cascade designs. The performance of the DNAzyme biosensor could be further improved through the use of new chemical modifications that allow for better substrate targeting or increased catalytic activity. More preferred substrate cleaving motif, or even new DNAzyme containing different catalytic domain that have higher cleavage rate could also enhance the performance. The ddREVEALR platform itself could be further improved by changing the system from its current image-based readout format to flow-based system that is more similar to ddPCR (Figure S4.12). It could increase the fraction of droplet tested to near 100%, which could lead to more accurate result for low concentration samples. Finally, the incorporation of other signal amplification strategies like hybridization chain reaction (HCR), catalytic hairpin assembly (CHA) into cascade detection could also potentially boost the detection efficiency and signal intensity.

4.5. Experimental details

Materials

All the oligonucleotides were purchased from Integrated DNA Technologies (Coralville, IA). ddPCR Supermix for Probes (No dUTP) was purchased from Bio-Rad (Hercules, CA). Poly(dimethyl) siloxane (PDMS) base and curing agent was purchased from Dow Corning (Midland, MI). Fluorinated oil HFE-7500 was purchased from 3M Novec (St Paul, MN), and Pico-SurfTM surfactant, Pico-GlideTM, and Pico-BreakTM were all purchased from Dolomite Microfluidics (UK). Proteinase K and HiScribe T7 High Yield RNA Synthesis Kit was purchased from New England Biolabs (Ipswich, MA). GoTaq Probe 1-Step RT-qPCR System was purchased from Promega (Madison, WI), the cell counting chamber slides were purchased from Invitrogen (Waltham, MA).

DNAzyme modifications experiments

Modified versions of the multicomponent DNAzyme (500 nM) were added to a reaction containing 2X ddPCR Supermix for probe, 50 mM Tris-HCl (pH 8.5), 150 mM NaCl, 200 mM $MgCl_2$, 500 nM 6+6 FamQ RNA substrate, and 100 pM of IVT RNA analyte. Reactions were monitored by end-point fluorescence using a Bio-Rad ddPCR instrument after incubation under the optimized temperature of the DNAzyme (Figure 2b) for 1 hour. The catalytic enhancement was calculated from the cleavage percentage and compared to the fold-change value.

$$\text{Cleavage(x)} = \frac{\text{FAM (x)} - \text{FAM (NTC)}}{\text{FAM (Pos)} - \text{FAM (NTC)}} \times 100\%$$

$$\text{Fold change} = \frac{\text{Cleavage(x)}}{\text{Cleavage(control)}}$$

Where FAM means FAM fluorescence signal, x means the tested DNAzyme, control means DNAzyme 1 that is composed of DNA only. Pos means the reaction with DNAzyme 1 and 500 nM and IVT RNA analyte, and NTC means the reaction with DNAzyme 1 and no IVT RNA analyte.

Comparison of singleplex reaction and multiplex reaction

The reactions were compared with 50 mM Tris-HCl (pH 9.0), 150 mM NaCl, 200 mM MgCl2, 1 uM 6+6 FamQ RNA substrate, 1X ddPCR Supermix for probe, and 10 pM IVT RNA analyte. All sensors (N1, N2, N3, N4, N5) were modified using design No.13 from Figure 2. IVT RNA was used as the input analyte. All data were collected through Bio-Rad ddPCR instrument, with 3 hours of incubation at 34°C. Background was subtracted to the average signal intensity of sample with 1 uL of water instead of analyte.

In vitro transcribed RNA

RNA analytes in the SARS-CoV-2 genome were prepared by in vitro transcription (IVT). IVT reactions were performed using the HiScribe T7 High Yield RNA Synthesis Kit. Each reaction contained 10 mM of each NTP, 1X reaction buffer, 3 µL PCR product, 2 µL T7 RNA polymerase mixture, and 5 µL nuclease-free water. Reactions were incubated at 37°C overnight. Crude RNA was purified by 15% denaturing urea PAGE and electroeluted, either under 180 V for 3 h or 60 V overnight. Purified RNA was desalted with an Amicon Ultra 0.5 mL 30k centrifugal filter from EMD Millipore (Burlington, MA), quantified by Nanodrop, and diluted in nuclease-free water to desired concentrations.

Droplet generation

Droplets were generated using custom PDMS chips described previously[131,134]. 20 uL of the reaction mixture (described below) was pushed into the microfluidic device via positive air pressure. The aqueous was sheared by a low-viscosity fluorinated oil (HFE-7500, 3M Movec) containing 1%(w/w) Pico-Surf surfactant (Dolomite Microfluidics, UK). Under constant inlet pressure, 10-15 um droplets were generated with production rates of 30-35 kHz. Each sample takes 6-7 min to complete. Droplets were collected under a layer of mineral oil in a 1.5 mL tube.

Droplet imaging

The prepared droplets were diluted and loaded onto a cell counting chamber slide (Invitrogen, Waltham, MA) and imaged using a confocal microscope (Stellaris 8, Leica) to record bright field and fluorescence signals (FAM and TAMRA). The TAMRA channel was used for adjusting the focus and normalizing the size of the droplets. A 10X magnification objective lens was used to image a 2048 X 2048 um2 area and 16 repeats for each scanning line.

Size distribution analysis

Three randomly chosen images were used for droplet size analysis. ImageJ software (https://imagej.nih.gov/ij/) was used to measure the area of each droplet with the TAMRA channel. Gaussian fitting was done through Excel to confirm the distribution of the droplet size.

Droplet quantification

The fluorescence signals of droplets were captured and analyzed using Biodock (https://www.biodock.ai/). AI cell segmentation pipeline was used where the TAMRA channel was set as the nuclear channel, 0 pixels to grow from the nucleus, and 5 average nuclear diameters (pixels). Then, the result was analyzed by setting the TAMRA signal as the X-axis, FAM signal as the Y-axis. After overlying the experimental groups with the NTC group, the negative droplets and positive droplets could be classified and counted based on their locations of the 2-D plot. Each droplet was represented by the FAM signal/TAMRA signal to normalize the influence of droplet size. The percentage of positive droplet (PPD) was calculated by the number of positive droplets over the total number of droplets.

Time course

The time course experiments were performed with 10 fM of IVT RNA, 50 mM Tris-HCl (pH 8.5), 150 mM NaCl, 200 mM MgCl2, 500 nM 6+6 FamQ RNA substrate, 2X ddPCR Supermix for probe, and 500 nM TAMRA reference. After droplet generation, the samples were incubated at 34°C for 6 hours, and a small portion of samples was taken out for imaging every 1 hour.

Calculation of the local concentration in droplets

Droplet volume (V) could be calculated based on the diameter (D),

$$V = \frac{1}{6}\pi \mathrm{D}^3$$

The local concentration of the analyte inside the droplet could be calculated by

$$c = -\frac{\ln\left(1 - PPD\right)}{V}$$

Where c is the average concentration with the unit of copy / uL and *PPD* is the percentage of positive droplet.

When the PPD is needed with known analyte concentration, the function is as follows:

$$PPD = (1 - \exp(-c \times V)) \times 100\%$$

Sensitivity test and calibration curve

The sensitivity test was performed with gradient concentration of in vitro transcribed RNA (1 fM, 5 fM, 10 fM, 50 fM and 100 fM), 50 mM Tris-HCl (pH 9.0), 150 mM NaCl, 200 mM $MgCl_2$, 500 nM 6+6 FamQ RNA substrate, 1X ddPCR Supermix for probe, 500 nM TAMRA reference and 20 nM of each modified multicomponent DNAzyme shown in Figure 2 following the droplet generation steps. The collected sample was incubated under 34°C for 3 hours before imaging. The proportion of positive droplets (PPD) was calculated and plotted against the concentration of IVT RNA. Error bars came from 3 replicates.

Evaluation of patient-derived clinical samples

Nasopharyngeal swabs from 20 patients were obtained from the COVID-19 Research Biobank of the Experimental Tissue Shared Resource Facility at the University of California, Irvine. Each sample was collected and heat-inactivated for 1 h at 80°C by trained medical professionals at the University of California Medical Center in Orange, California. SARS-CoV-2 viral RNA samples were purified following the CDC-recommended Qiagen DSP Viral RNA Mini kit protocol. The Ct value of each clinical sample was double-checked with 1 uL of the purified sample using the GoTaq Probe 1-Step RT-qPCR kit (Promega, WA). Then 1

uL of the purified sample was loaded in the ddREVEALR system for detection and quantification. The protocol is the same as described above except incubating at 30°C for overnight for better quantification.

Proteinase K validation

The proteinase K validation experiment was performed with 100 fM of IVT RNA, 50 mM Tris-HCl (pH 9.0), 150 mM NaCl, 200 mM $MgCl_2$, 500 nM 6+6 FamQ RNA substrate, 1X ddPCR Supermix for probe, 500 nM TAMRA and 20 nM of each modified multicomponent DNAzyme shown in Figure 2c. Also, 0.8 U of Proteinase K was added to the test group. The control group added 1 uL DI water instead. Then incubate at 34°C for 3 hours before imaging.

False-positive rate screening

The background screening experiment was performed with 50 mM Tris-HCl (pH 9.0), 150 mM NaCl, 200 mM $MgCl_2$, 500 nM 6+6 FamQ RNA substrate, 1X ddPCR Supermix for probe, 500 nM TAMRA and 20 nM of each modified multicomponent DNAzyme shown in Figure 2c. For No Mz group, no multicomponent DNAzyme was added. Then incubate at 34°C for 4 hours before imaging. 10 images were randomly taken for each sample. Data was analyzed using the Biodock platform.

Poisson distribution

When encapsulating analytes into microfluidic droplets, the probability of a droplet containing given amount of analyte (e.g., 0, 1, 2 …) can be estimated using a Poisson distribution

$$P(X = k) = \frac{l^k}{k!} e^{-l}$$

Where **k** is the number of analytes in each droplet, and λ is the average number of analytes per droplet.

CHAPTER 5:

Conclusion and discussion

Here we described the assay development process for the multicomponent DNAzyme biosensor-based nucleic acid detection for SARS-CoV-2. Through a series of publications, we have advanced this work from a simple COVID detection assay to a genotyping strategy and eventually to a digital droplet amplification-free system using a microscope. In this chapter, I will continue to discuss other potentials of the REVEALR system, make a comparison with its key competitor, CRISPR diagnostic systems, and give some insights into the future directions of the multicomponent DNAzyme biosensor.

5.1. Alternatives for the REVEALR platform

LAMP-based REVEALR system

The REVEALR system was originally established with RPA, which is rapid, ultrasensitive, and durable to couple with the MNAzyme system. As an alternative, Loop-mediated isothermal amplification (LAMP) is another popular isothermal amplification that can amplify DNA/RNA rapidly with high sensitivity and specificity. The target is amplified with a constant temperature of ~65°C using 4 or 6 primers and the Bst polymerase which has high strand displacement activity. The final products of LAMP are a mixture of cauliflower-like structures with multiple loops and concatemers of the DNA with various stem lengths. The products of LAMP may be classified into four categories: single-loop (SL) amplicon, terminated (T) amplicon, single-stranded (SS) amplicon, and partially double-

stranded (PDS) amplicons (Figure 5.1).[135] Among all of them, SS and PDS products contain the single-strand domain that could trigger our multicomponent DNAzyme system for signal amplification.

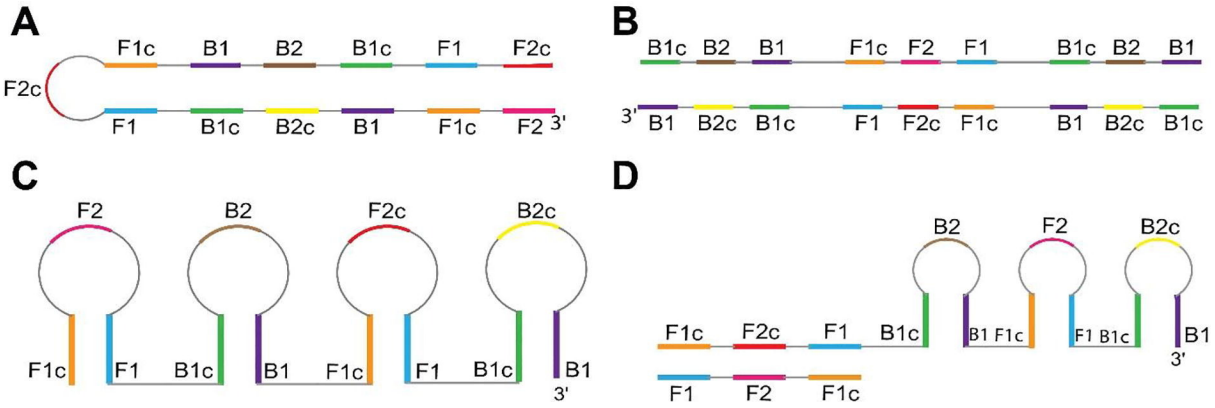

Figure 5.1. Classification of LAMP amplicons into four categories. (A) Single loop amplicon (SL), (B) Terminated amplicon (T), (C) Single-stranded amplicon (SS), and (D) Partially double-stranded amplicon (PDS). This figure was adapted from Kaur, N.; Thota, N.; Toley, B. J. *Comput Struct Biotechnol J* 2020, 18, 2336–2346[135]. This is an open-access article distributed under the terms of the Creative Commons CC-BY license from Elsevier.

The amplified LAMP products could be detected by several methods,[136] including intercalating dsDNA binding dyes, turbidity measurement, gel electrophoresis, lateral flow assays, CRISPR-based assays, etc. Among all these methods, most methods (intercalating dyes, turbidity, gel electrophoresis, lateral flow assays) are non-sequence specific. Because one of the biggest challenges of LAMP is non-specific amplification[137], these methods take the risk of false positive results. To solve this issue, there are a few sequences specific assays including DARQ probe-based detection[138] and CRISPR-based detection[8]. DARQ has sequence-specific detection for one of the forward inner primers (FIP), still containing the risk of primer-dimer non-specific amplification. CRISPR-based sequence-specific methods showed great potential in utilizing the dsDNA recognition property of the Cas12 enzyme.

Here we proposed the second version of RNA-encoded viral nucleic acid analyte reporter (REVEALR v2) detection that could achieve viral RNA detection with attomolar sensitivity utilizing LAMP and multicomponent DNAzyme detection system (Figure 5.2).

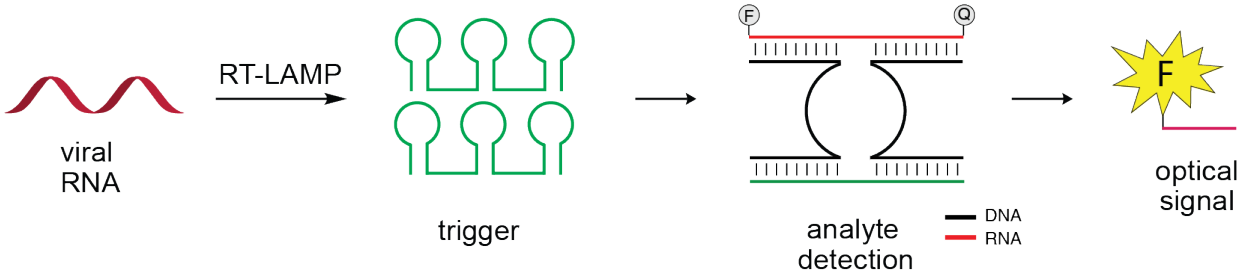

Figure 5.2. Overview of LAMP-based REVEALR v2 detection system. Schematic overview of the detection assay. The SARS-CoV-2 region of interest is isothermally amplified by RT-LAMP. Then multicomponent X10-23 Pro assembly on the ssDNA portion of LAMP products, leading to the cleavage of a quenched fluorescent reporter for fluorescence detection or a biotin-labeled fluorescent RNA for lateral flow detection.

The REVEALR v2 is the 2nd version of the REVEALR system and has the following improvements. First, REVEALR v2 uses fewer enzymes thus resulting in lower cost for each test.[139] Second, this system is going to explore a one-pot approach that could simplify the operation process and prevent cross contaminations. Third, by using a one-pot approach, REVEALR v2 can potentially minimize the whole detection step from ~1 hour to ~30 min, which is very important to rapid nucleic acid detection.

Also, REVEALR v2 has the following novelties. As far as I am aware, it's the first proposed approach to combine a multicomponent DNAzyme system with LAMP for sequence-specific detection. Overall, REVEALR v2 would be able to set up a great example for rapid, sensitive nucleic acid detection.

As a proof-of-concept, the LAMP reaction is combined with a multicomponent DNAzyme (MNAzyme) detection system for the first time. To utilize the ssDNA region of the

LAMP product, MNAzyme was designed complementary to the ssDNA region between B1 to F1c. After 30 min RT-LAMP reaction, 1 uL of the product was transferred into the MNAzyme detection system and the fluorescent signal was recorded using a plate reader under 25°C (Figure 5.3). The result showed that the sample containing the LAMP template could give a distinguishable signal compared with the NTC group. Thus, REVEALR v2 system is validated to be possible for sequence-specific nucleic acid detection.

Using synthetic in vitro-transcribed (IVT) SARS-CoV-2 RNA gene targets in nuclease-free water, we demonstrated that the LAMP-based multicomponent XNAzyme detection system has the attomolar level of sensitivity. This detection is targeting on S gene fragment and RT-LAMP step at 65°C for 30 min and multicomponent XNAzyme detection is initiated by adding DNAzyme oligos and extra salts into each tube and signals would be distinguishable after incubating at 25°C for 10 min. The SARS-CoV 2 REVEALR v2 assay is considered positive if there is a significantly higher fluorescent signal compared with the NTC group or if it shows a fluorescent signal under UV light by naked eye visualization. RT-LAMP could also be visualized by gel electrophoresis which showed consistent results with the REVEALR v2 system (Figure 5.3).

One of the biggest challenges for LAMP reaction is non-specific amplification. The potential reasons include multimerization[140] and ab initio DNA synthesis.[137] Once this happened, it will give false positive signals if using intercalating dye or turbidity-based LAMP detection. since REVEALR v2 is a sequence-specific nucleic acid detection method, even if the non-specific amplification happened, REVEALR v2 detection system could still

recognize the true positive samples and give a distinguishable fluorescent signal.

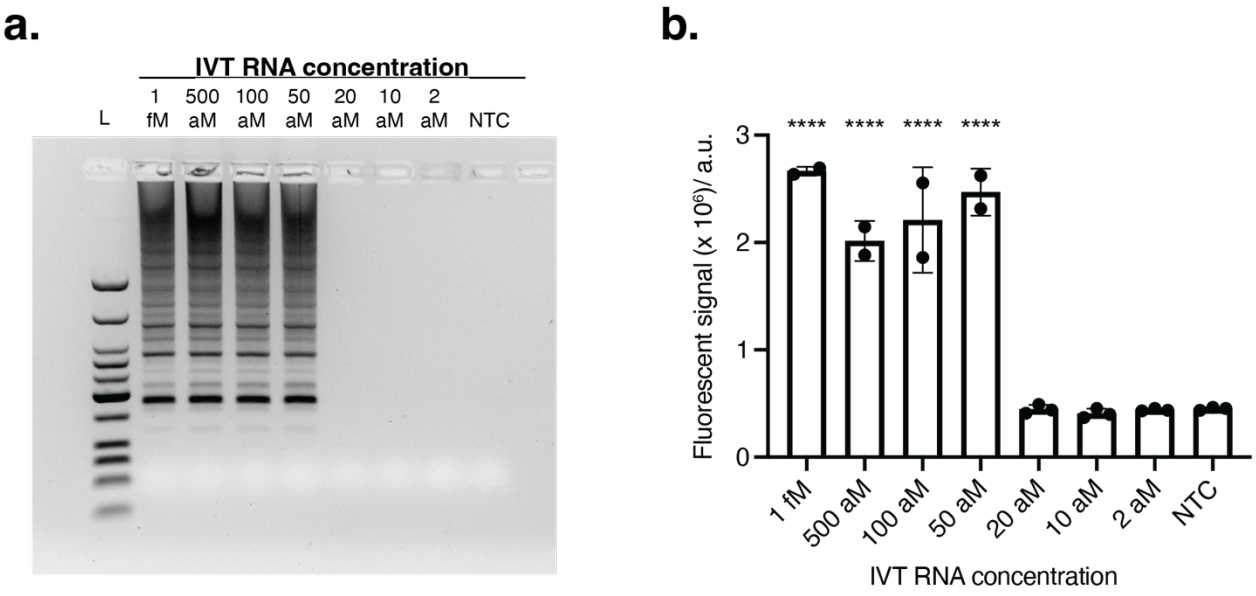

Figure 5.3. Preliminary data for LAMP-based REVEALR detection system. (a) Agarose gel electrophoresis data of sensitivity test with WarmStart LAMP kit with 30 min incubation time. LAMP reaction was set up with 1x NEB WarmStart LAMP mastermix, 1x LAMP primer mix for SARS-CoV-2 N gene, and 10 uL gradient concentration of in vitro transcribed RNA. The reaction mixture was incubated at 65°C for 30 min and 95°C for 5 min. (b) Florescent signal of MNAzyme detection with LAMP product. Reactions were performed in buffer containing 50 mM $MgCl_2$, 50 mM Tris (pH 8.5), 150 mM NaCl, 500 nM FAM-labeled RNA substrate, and 500 nM DNAzyme, 2 uL of LAMP product, n = 3. After incubation at 25°C for 30 min, signals were obtained through the QuantStudio™ 6 Flex Real-Time PCR System. Error bars represent the standard error of the mean (SEM). Two-tailed Student's t test: *, $P < 0.05$; **, $P < 0.01$; ***, $P < 0.001$; ****, $P < 0.0001$.

5.2. Comparison of REVEALR and CRISPR diagnostic systems

In comparison with the CRISPR diagnostic systems, like SHERLOCK, DNA endonuclease targeted CRISPR trans reporter (DETECTR), etc, our REVEALR system has the following similarities. Both MNAzyme biosensor systems and the CRISPR diagnostic systems could be coupled with major amplification methods like PCR, LAMP, and RPA to achieve a low aM level of RNA detection. Both systems could cleave a fluorescent-labeled reporter and give an optical signal or lateral flow signal.

On the other hand, there exist several differences. First, our biosensor is composed of RNA-cleaving deoxyribozyme (DNAzyme) oligos whereas the CRISPR diagnostic systems utilize Cas proteins. The proteins need to be expressed, harvested, and purified whereas the DNAzyme oligos are usually made by solid phase synthesis. In this regard, the DNAzyme sensor could be cheaper, more stable, and more approachable.

Second, the mechanism of these two biosensor systems is different. The major CRISPR diagnostic systems are based on the collateral effect of Cas 12 or Cas 13 proteins whereas the multicomponent DNAzyme is based on the general acid-based mechanism[141]. Deriving from this, the optimizations of the CRISPR system may come from protein screening or engineering to obtain better variants whereas the optimizations of the MNAzyme system could come from the nucleic acid modifications of the DNAzyme binding arms and catalytic core.

Third, the analyte recognition mechanism and role are also different. On the one hand, the CRISPR system needs the assistance of crRNA and is restricted by specific sequences

like PAM for Cas9 and Cas12 or protospacer flanking site (PFS) for Cas13 whereas the analyte recognition for the MNAzyme system is based on Watson–Crick base pairing which does not have too many restrictions. Thus, MNAzyme has more targetable regions. On the other hand, the CRISPR system could target both ssRNA and dsDNA whereas MNAzyme could only recognize ssDNA or ssRNA, which makes it require an extra conversion step for signal readout. Some tools like peptide nucleic acid (PNA) clamp[142] might be able to fill this gap and recognize dsDNA amplicon with an MNAzyme sensor.

Last but not the least, since the CRISPR diagnostic systems are much more well-studied, many features could potentially be applied to MNAzyme-based detection systems. First, the CRISPR systems achieved a one-pot reaction by using special separation[32,35], microfluidic device,[36] or additional reagent like glycerol [37] which could be potentially applied to the REVEALR system for more practical POCT or OTC applications. Second, some readout methods like naked eye visualization under blue light-emitting diode (LED) light are durable for the REVEALR system for portable detection in the future.

Table 5.1. Comparison of REVEALR with CRISPR diagnostic systems.

Categories		CRISPR diagnostic			MNAzyme (REVEALR)
		Cas13	Cas12	Cas9	
Biosensor compound		protein	protein	protein	oligo
Assistant compound		crRNA	crRNA	crRNA	/
Mechanism		collateral effect	collateral effect	nuclease	RNA-cleaving DNAzyme
Major NAATs		RPA/LAMP	RPA/LAMP	PCR/RPA	RPA/LAMP
Target		ssRNA	ssDNA/dsDNA	dsDNA	ssDNA/ssRNA
Sensitivity	Biosensor only	high fM	nM to pM	fM	nM to pM
	Biosensor with NAAT	low aM	low aM	aM	low aM
Target restriction		PFS	PAM	PAM	/
one-pot vs. two-pots		1 or 2	1 or 2	2	2
Signal readout		F/L	F/L/NE	F/L/E	F/L

Note: F: Fluorescence, L: Lateral flow, NE: naked eye visualization, E: electrochemical.

5.3. Future directions

For NAAT based REVEALR system, there are three potential directions. The first direction is to simplify the liquid handling steps from a 1-pot reaction to a 2-pots reaction. Professor Alison V. Todd and her SpeeDx company coupled MNAzyme with PCR and give a great example of how to use it as a sequence-specific probe in a one-pot format with an automatic liquid handling instrument for high-throughput testing. Our current REVEALR system used isothermal amplifications like RPA and LAMP showing the possibility of using MNAzyme for POCT or OTC purposes. However, the current system used a 2-pots protocol. Optimizing the REVEALR system towards a 1-pot is critical to minimize the potential contaminations through liquid handling and make it more convenient for the customer. More importantly, it could show the capability of MNAzyme as a general sequence-specific probe for isothermal amplification methods, like the relationship between the TaqMan probe and qPCR. The 2nd direction would be potentially combined with some strategies like PNA clamp for dsDNA recognition. As indicated in Chapter 2, the RPA-based REVEALR system requires the conversion of dsDNA amplicon into ssRNA analyte through T7 transcription. With the PNA clamp, we could potentially get rid of this step and apply this probe to broader isothermal amplification methods where most of their amplicons are dsDNA. The 3rd direction would be extending the readout methods from florescence and lateral flow to the electrochemical readout. Just like Lucira Health and Cue Health, they worked on LAMP-based assay and simultaneously moved towards electrochemical-based product because it could be used multiple times, had high consistency, and was sensitive.

The ddREVEALR system described in Chapter 4 gives a great example of using MNAzyme for single molecule detection and shows the advantages of using chemical modifications to boost the sensitivity of the DNAzyme biosensor. However, there are several limitations: 1) current ddREVEALR system requires at least 3 hours to achieve digital detection, which doesn't fulfill the requirement of practical nucleic acid detection. 2) The signal-to-noise ratio of the system is not high enough which might lead to a false positive. 3) The current image-based readout methods could only scan 0.05% of the droplets for each sample, which gives a low fM to sub fM level of sensitivity. To address issues 1 and 2, we could 1) further enhance the cleavage activity by using better chemical modifications. 2) Couple with some signal amplifications like CHA, HCR, or cascade biosensor designs. 3) Couple with some NAAT like RPA, and LAMP for more rapid and practical tests. To address issue 3, flow-based readout has the potential to screen 100% droplets within a short time, which is like the Bio-Rad ddPCR system.

For the MNAzyme as a biosensor (Figure 5.4), it serves as a promising biorecognition element[143]. Compared with direct probe capturing-based nucleic acid detection methods, MNAzyme gives another layer of signal amplification thus could lead to better sensitivity and specificity. On the other hand, the sensitivity of the diagnostic detection platform not only depends on the bio transducer portions but also depends on the signal readout methods.

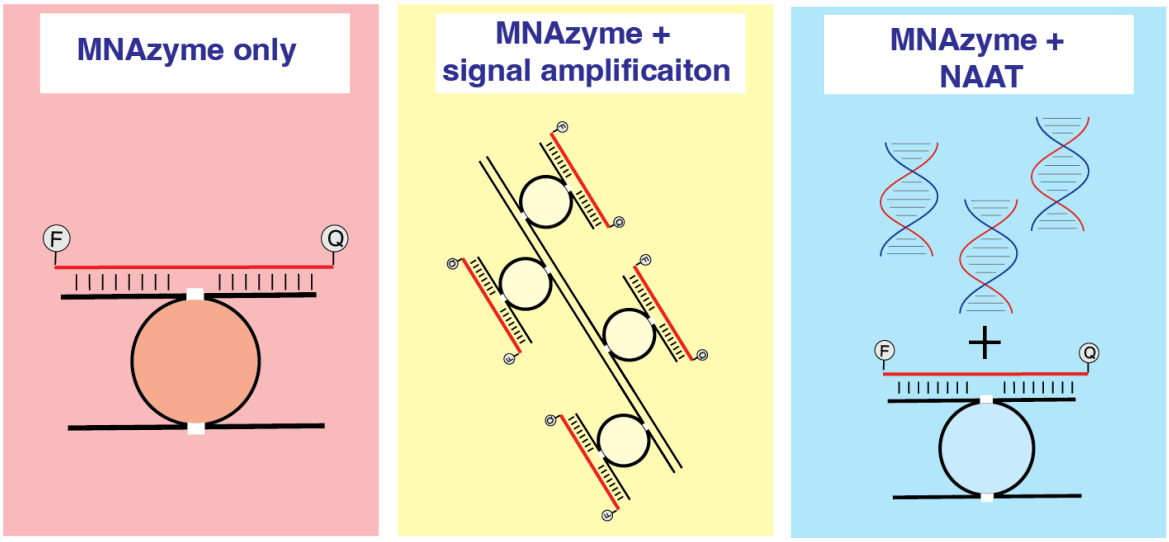

Figure 5.3. Categories of MNAzyme biosensors.

APPENDIX A: Supplementary Tables

Supplementary Table 2.1. List of Oligonucleotides

Name	Sequence 5'-3'
FluA_fragment	GGCCATGGTGTCTAGGGCCCGGATTGATGCCAGAATTGACTTCGAG TCTGGAAGGATTAAGAAGGAAGAGTTCTCTGAGATCATGAAGATCTG TTCCACCATTGAAGAACTCAGACGGCAAAAATA
MERS_fragment	ATTGTTACACAATTCGCGCCCGGTACTAAGCTTCCTAAAAACTTCCA CATTGAGGGGACTGGAGGCAATAGTCAATCATCTTCAAGAGCCTCTA GCTTAA
Rhinovirus_fragment	GTGTGCTCACTTTGAGTCCTCCGGCCCCTGAATGCGGCTAACCTTA AACCTGCAGCCATGGCTCATAAGCCAATGAGTTTATGGTCGTAACGA GTAATTGCGGGATGGGACC
SARS-CoV-1_fragment	CCAGCTGGTGGTGCGCTTATAGCTAGGTGTTGGTACCTTCATGAAG GCTCAACCAAACTGCTGCATTTAGAGACGTACTTGTTGTTTTAAATAA
SARS-CoV-2_fragment	AGGTTTCAAACTTTACTTGCTTTACATAGAAGTTATTTGACTCCTGGT GATTCTTCTTCAGGTTGGACAGCTGGTGCTGCAGCTTATTATGTGGG TTATCTTCAACCTAGGA
Rhinovirus_RPA_FWD	GAAATTAATACGACTCACTATAGGGGTGTGCTCACTTTGAGTCCTCC GGCCCCTG
Rhinovirus_RPA_RVS	GGTCCCATCCCGCAATTACTCGTTACGACC
MERS_FWD	GAAATTAATACGACTCACTATAGGGATTGTTACACAATTCGCGCCCG GTACTAAG
MERS_RVS	TTAAGCTAGAGGCTCTTGAAGATGATTGAC
SARS_FWD	GAAATTAATACGACTCACTATAGGGCCAGCTGGTGGTGCGCTTATAG CTAGGTGT
SARS_RVS	TTATTTAAAACAACAAGTACGTCTCTAAAT
FluA_FWD	GAAATTAATACGACTCACTATAGGGGGCCATGGTGTCTAGGGCCCG GATTGATGC
FluA_RVS	TATTTTTGCCGTCTGAGTTCTTCAATGGTG
SARS-CoV-2-S-RPA-Forward	GAAATTAATACGACTCACTATAGGGAGGTTTCAAACTTTACTTGCTTT ACATAGA
SARS-CoV-2-S-RPA-Reverse	TCCTAGGTTGAAGATAACCCACATAATAAG
SARS-CoV_2_Sgene_mid	AGTTATTTGACTCCTGGTGATTCTTCTTCAGGTTGGACAGCTGGTGC TGCAG
S-RPA-Mz_A_66sub_20	CACCAGCTGTCCAACCTGAAACAACGAGGTTAG
S-RPA-Mz_B_66sub_20	TCATGAGGCTAGCTGAAGAATCACCAGGAGTCAA
S-RPA-Mz_A_X10-23	CACCAGCTGTCCAACCTGAAACAACGAfGfGfUfUfAfG
S-RPA-Mz_B_X10-23	fUfCfAfUfGfAGfGCTAGCfUGAAGAATCACCAGGAGTCAA
S-RPA-Mz_A_X10-23_Pro	fCfAfCfCfAfGfCfUfGfUfCfCfAfAfCfCfUfGfAfAACAACGAfGfGfUfUfAfG
S-RPA-Mz_B_X10-23_Pro	fUfCfAfUfGfAGfGCTAGCfUfGfAfAfGfAfAfUfCfAfCfCfAfGfGfAfGfUfCfAfA
FBiotin_RNA_substrate	/56FAM/rCrUrArArCrCrGrUrCrArUrGrA/Bio/
FQ RNA substrate	/56FAM/rCrUrArArCrCrGrUrCrArUrGrA/3IBkFQ/
Cy5 RNA substrate	/5Cy5/rCrUrArArCrCrGrUrCrArUrGrA

Supplementary Table 3.1. List of oligonucleotides

Name	Sequence 5'-3'
RNA Substrates	
FamQ-RNA-sub_6+6	/56-FAM/CUAACCGUCAUGA/3IABkFQ/
HexQ-RNA-sub-6+6	/5HEX/UUCCUCGUCCCUG/3BHQ_1/
FamQ-RNA-sub-7+8	/56FAM/CUUUCCUCGUCCCUGG/3IABkFQ/
T19R	
T19R_WT_analyte	TCTTA**C**AACCAGAACTCAATTACCCCCTGC
T19R_MT_analyte	TCTTA**G**AACCAGAACTCAATTACCCCCTGC
Mz-A_T19R-7+8sub	GCAGGGGGTAATTGAGTTCTacaacgaGAGGAAAG
Mz-B_T19R-WT-7+8sub	CCAGGGAggctagctGGTT**G**TAAGA
Mz-B_T19R-MT-7+8sub	CCAGGGAggctagctGGTT**C**TAAGA
S26L	
S26L_WT_analyte	TCCTT**C**AGATTTTGTTCGCGCTACTGCAAC
S26L_MT_analyte	TCCTT**T**AGATTTTGTTCGCGCTACTGCAAC
Mz-A_S26L-7+8sub	GTTGCAGTAGCGCGAACAAAacaacgaGAGGAAAG
Mz-B_S26L-WT-7+8sub	CCAGGGAggctagctATCT**G**AAGGA
Mz-B_S26L-MT-7+8sub	CCAGGGAggctagctATCT**A**AAGGA
P71L	
P71L_WT_analyt	AGTTC**C**TGATCTTCTGGTCTAAACGAACTA
P71L_MT_analyt	AGTTC**T**TGATCTTCTGGTCTAAACGAACTA
Mz-A_P71L-7+8su	TAGTTCGTTTAGACCAGAAGacaacgaGAGGAAAG
Mz-B_P71L-WT-7+8sub	CCAGGGAggctagctATCA**G**GAACT
Mz-B_P71L-MT-7+8sub	CCAGGGAggctagctATCA**A**GAACT
D80A	
D80A_WT_analyte	GTTTG**A**TAACCCTGTCCTACCATTTAATGA
D80A_MT_analyte	GTTTG**C**TAACCCTGTCCTACCATTTAATGA
Mz-A_D80A-7+8sub	TCATTAAATGGTAGGACAGGacaacgaGAGGAAAG
Mz-B_D80A-WT-7+8sub	CCAGGGAggctagctGTTA**T**CAAAC
Mz-B_D80A-MT-7+8sub	CCAGGGAggctagctGTTA**G**CAAAC
I82T	
I82T_WT_analyte	TGCTA**T**CGCAATGGCTTGTCTTGTAGGCTT
I82T_MT_analyte	TGCTA**C**CGCAATGGCTTGTCTTGTAGGCTT
Mz-A_I82T-7+8sub	AAGCCTACAAGACAAGCCATacaacgaGAGGAAAG
Mz-B_I82T-WT-7+8sub	CCAGGGAggctagctTGCG**A**TAGCA
Mz-B_I82T-MT-7+8sub	CCAGGGAggctagctTGCG**G**TAGCA
E156G	
E156G_WT_analyte	AAGTG**A**GTTCAGAGTTTATTCTAGTGCGAA
E156G_MT_analyte	AAGTG**G**GTTCAGAGTTTATTCTAGTGCGAA
Mz-A_E156G-7+8sub	TTCGCACTAGAATAAACTCTacaacgaGAGGAAAG

Mz-B_E156G-WT-7+8sub	CCAGGGAggctagctGAACTCACTT
Mz-B_E156G-MT-7+8sub	CCAGGGAggctagctGAACCCACTT
S235F	
S235F_WT_analyte	AATGTCTGGTAAAGGCCAACAACAACAAGG
S235F_MT_analyte	AATGTTTGGTAAAGGCCAACAACAACAAGG
Mz-A_S235F-7+8sub	CCTTGTTGTTGTTGGCCTTTacaacgaGAGGAAAG
Mz-B_S235F-WT-7+8sub	CCAGGGAggctagctACCAGACATT
Mz-B_S235F-MT-7+8sub	CCAGGGAggctagctACCAAACATT
S253P	
S253P_WT_analyte	GTTCATCCGGAGTTGTTAATCCAGTAATGG
S253P_MT_analyte	GTTCACCCGGAGTTGTTAATCCAGTAATGG
Mz-A_S253P-7+8sub	CCATTACTGGATTAACAACTacaacgaGAGGAAAG
Mz-B_S253P-WT-7+8sub	CCAGGGAggctagctCCGGATGAAC
Mz-B_S253P-MT-7+8sub	CCAGGGAggctagctCCGGGTGAAC
K417N/T	
K417_WT_analyte	GGAAAGATTGCTGATTATAATTATAAATTA
K417N_MT_analyte	GGAAATATTGCTGATTATAATTATAAATTA
K417T_MT_analyte	GGAACGATTGCTGATTATAATTATAAATTA
K417_WT_RPA_template	GAAGTCAGACAAATCGCTCCAGGGCAAACTGGAAAGATTG CTGATTATAATTATAAATTACCAGATGATTTTACAGGCTGCG TTATAGCT
K417N_MT_RPA_template	GAAGTCAGACAAATCGCTCCAGGGCAAACTGGAAATATTG CTGATTATAATTATAAATTACCAGATGATTTTACAGGCTGCG TTATAGCT
K417T_MT_RPA_template	GAAGTCAGACAAATCGCTCCAGGGCAAACTGGAACGATTG CTGATTATAATTATAAATTACCAGATGATTTTACAGGCTGCG TTATAGCT
K417_RPA_FWD	GAAATTAATACGACTCACTATAGGGGTGATGAAGTCAGACA AATCGCTCCAGGGC
K417_RPA_RVS	TTCCAAGCTATAACGCAGCCTGTAAAATCA
Mz-A_K417-7+8sub	TAATTTATAATTATAATCAGacaacgaGAGGAAAG
Mz-B_K417N-WT-7+8sub	CCAGGGAggctagctCAATCTTTCC
Mz-B_K417N-MT-7+8sub	CCAGGGAggctagctCAATATTTCC
Mz-B_K417T-MT-7+8sub	CCAGGGAggctagctCAATCGTTCC
Lz-B_K417N-MT-6+6sub_FAM	TCATGAggctagctCAATATTTCC
Lz-B_K417T-MT-6+6sub_FAM	TCATGAggctagctCAATCGTTCC
Lz-A_K417-6+6sub_FAM	TAATTTATAATTATAATCAGacaacgaGGTTAG
Lz-A_K417-6+6sub_HEX	TAATTTATAATTATAATCAGacaacgaGAGGAA
Lz-B_K417N-MT-6+6sub_HEX	CAGGGAggctagctCAATATTTCC
Lz-B_K417T-MT-6+6sub_HEX	CAGGGAggctagctCAATCGTTCC
Lz-B_K417N-MT-6+6sub_HEX	CAGGGAggctagctCAATATTTCC
Lz-B_K417T-MT-6+6sub_HEX	CAGGGAggctagctCAATCGTTCC

Lz-B_K417-WT-FAM	TCATGAggctagctCAATCTTTCC
Lz-B_K417-MT-HEX	CAGGGAggctagctCAATATTTCC
L452R	
L452R_WT_analyte	TTACCTGTATAGATTGTTTAGGAAGTCTAA
L452R_MT_analyte	TTACCGGTATAGATTGTTTAGGAAGTCTAA
L452R_WT_template	AATTCTAACAATCTTGATTCTAAGGTTGGTGGTAATTATAAT TACCTGTATAGATTGTTTAGGAAGTCTAATCTCAAACCTTTT GAGAGA
L452R_MT_template	AATTCTAACAATCTTGATTCTAAGGTTGGTGGTAATTATAAT TACCGGTATAGATTGTTTAGGAAGTCTAATCTCAAACCTTTT GAGAGA
RPA_L452R_RVS	ATATCTCTCTCAAAAGGTTTGAGATTAGAC
RPA_L452R_FWD	GAAATTAATACGACTCACTATAGGGCTTGGAATTCTAACAA TCTTGATTCTAAGG
Mz-A_L452R-7+8sub	TTAGACTTCCTAAACAATCTacaacgaGAGGAAAG
Mz-B_L452R-WT-7+8sub	CCAGGGAggctagctATACAGGTAA
Mz-B_L452R-MT-7+8sub	CCAGGGAggctagctATACCGGTAA
Lz-A_L452R-HEX	TTAGACTTCCTAAACAATCTacaacgaGAGGAA
Lz-B_L452R-WT-HEX	CAGGGAggctagctATACAGGTAA
Lz-B_L452R-MT-HEX	CAGGGAggctagctATACCGGTAA
Lz-A_L452R-FAM	TTAGACTTCCTAAACAATCTacaacgaGGTTAG
Lz-B_L452R-WT-FAM	TCATGAggctagctATACAGGTAA
Lz-B_L452R-MT-FAM	TCATGAggctagctATACCGGTAA
T547K	
T547K_WT_template	AATTTGGTTAAAAACAAATGTGTCAATTTCAACTTCAATGGT TTAACAGGCACAGGTGTTCTTACTGAGTCTAACAAAAAGTT TCTGCCT
T547K_MT_template	AATTTGGTTAAAAACAAATGTGTCAATTTCAACTTCAATGGT TTAAAAGGCACAGGTGTTCTTACTGAGTCTAACAAAAAGTT TCTGCCT
RPA_T547K_FWD	GAAATTAATACGACTCACTATAGGGCTACTAATTTGGTTAAA AACAAATGTGTCA
RPA_T547K_RVS	TGGAAAGGCAGAAACTTTTTGTTAGACTCA
Mz-A_T547K-7+8sub	GACTCAGTAAGAACACCTGTacaacgaGAGGAAAG
Mz-B_T547K-WT-7+8sub	CCAGGGAggctagctGCCTGTTAAA
Mz-B_T547K-MT-7+8sub	CCAGGGAggctagctGCCTTTTAAA
Lz-A_T547K-FAM	GACTCAGTAAGAACACCTGTacaacgaGGTTAG
Lz-B_T547K-WT-FAM	TCATGAggctagctGCCTGTTAAA
Lz-B_T547K-MT-FAM	TCATGAggctagctGCCTTTTAAA
Lz-A_T547K-HEX	GACTCAGTAAGAACACCTGTacaacgaGAGGAA
Lz-B_T547K-WT-HEX	CAGGGAggctagctGCCTGTTAAA
Lz-B_T547K-MT-HEX	CAGGGAggctagctGCCTTTTAAA
A570D	

A570D_WT_analyte_S	CATTGCTGACACTACTGATGCTGTCCGTGA
A570D_MT_analyte_S	CATTGATGACACTACTGATGCTGTCCGTGA
A570D_WT_template	TCTAACAAAAAGTTTCTGCCTTTCCAACAATTTGGCAGAGA CATTGCTGACACTACTGATGCTGTCCGTGATCCACAGACAC TTGAGATT
A570D_MT_template	TCTAACAAAAAGTTTCTGCCTTTCCAACAATTTGGCAGAGA CATTGATGACACTACTGATGCTGTCCGTGATCCACAGACAC TTGAGATT
RPA_A570D_RVS	TCAAGAATCTCAAGTGTCTGTGGATCACGG
RPA_A570D_FWD	GAAATTAATACGACTCACTATAGGGCTGAGTCTAACAAAAA GTTTCTGCCTTTCC
Mz-A_A570D-7+8sub	TCACGGACAGCATCAGTAGTacaacgaGAGGAAAG
Mz-B_A570D-WT-7+8sub	CCAGGGAggctagctGTCAGCAATG
Mz-B_A570D-MT-7+8sub	CCAGGGAggctagctGTCATCAATG
Mz-66_A_A570D-FAM	TCACGGACAGCATCAGTAGTacaacgaGGTTAG
Mz-66_B_A570D-WT-FAM	TCATGAggctagctGTCAGCAATG
Mz-66_B_A570D-MT-FAM	TCATGAggctagctGTCATCAATG
Lz-A_A570D-HEX	TCACGGACAGCATCAGTAGTacaacgaGAGGAA
Lz-B_A570D-WT-HEX	CAGGGAggctagctGTCAGCAATG
Lz-B_A570D-MT-HEX	CAGGGAggctagctGTCATCAATG
Lz-A_A570D-FAM	TCACGGACAGCATCAGTAGTacaacgaGGTTAG
Lz-B_A570D-WT-FAM	TCATGAggctagctGTCAGCAATG
Lz-B_A570D-MT-FAM	TCATGAggctagctGTCATCAATG
Lz-B_A570D-WT-FAM_SNP	TCATGAggctagctGTCAGCAATG
Lz-B_A570D-MT-FAM_SNP	TCATGAggctagctGTCATCAATG
P681H	
P681_WT_analyte	TTCTCCTCGGCGGGCACGTAGTGTAGCTAG
P681H_MT_analyte	TTCTCATCGGCGGGCACGTAGTGTAGCTAG
Mz-A_P681H-7+8sub	CTAGCTACACTACGTGCCCGacaacgaGAGGAAAG
Mz-B_P681H-WT-7+8sub	CCAGGGAggctagctCCGAGGAGAA
Mz-B_P681H-MT-7+8sub	CCAGGGAggctagctCCGATGAGAA
D796Y	
D796Y_WT_analyte	TTAAAGATTTTGGTGGTTTTAATTTTTCAC
D796Y_MT_analyte	TTAAATATTTTGGTGGTTTTAATTTTTCAC
Mz-A_D796Y-7+8sub	GTGAAAAATTAAAACCACCAacaacgaGAGGAAAG
Mz-B_D796Y-WT-7+8sub	CCAGGGAggctagctAAATCTTTAA
Mz-B_D796Y-MT-7+8sub	CCAGGGAggctagctAAATATTTAA
D950N	
D950N_WT_analyte	TTCAAGATGTGGTCAACCAAAATGCACAAG
D950N_MT_analyte	TTCAAAATGTGGTCAACCAAAATGCACAAG
Mz-A_D950N-7+8sub	CTTGTGCATTTTGGTTGACCacaacgaGAGGAAAG
Mz-B_D950N-WT-7+8sub	CCAGGGAggctagctACATCTTGAA

Mz-B_D950N-MT-7+8sub	CCAGGGAggctagctACATTTTGAA
T1027I	
T1027I_WT_analyte	TGCTACTAAAATGTCAGAGTGTGTACTTGG
T1027I_MT_analyte	TGCTATTAAAATGTCAGAGTGTGTACTTGG
Mz-A_T1027I-7+8sub	CCAAGTACACACTCTGACATacaacgaGAGGAAAG
Mz-B_T1027I-WT-7+8sub	CCAGGGAggctagctTTTAGTAGCA
Mz-B_T1027I-MT-7+8sub	CCAGGGAggctagctTTTAATAGCA
D1118H	
D1118H_WT_analyte	CTACAGACAACACATTTGTGTCTGGTAACT
D1118H_MT_analyte	CTACACACAACACATTTGTGTCTGGTAACT
Mz-A_D1118H-7+8sub	AGTTACCAGACACAAATGTGacaacgaGAGGAAAG
Mz-B_D1118H-WT-7+8sub	CCAGGGAggctagctTTGTCTGTAG
Mz-B_D1118H-MT-7+8sub	CCAGGGAggctagctTTGTGTGTAG

Note: Black stands for DNA nucleotides. red for RNA nucleotides, and green for LNA nucleotides. Lower case stands for the catalytic core of DNAzyme. Yellow highlight reflects the SNP site on the sensor. Blue highlight reflects the SNP site on the analyte. Pink highlight signifies the T7 promoter region. Underline represents the substrate binding arm. MT stands for mutant type. WT stands for wild type.

Table S3.2. Single-nucleotide mutations evaluated in the SARS-CoV-2 genome

Region	Position	Amino Acid	Alpha (B.1.1.7)	Beta (B.1.351)	Gamma (P.1)	Delta (B.1.617.2)	Omicron (B.1.1.529)	SNP discrimination*
S gene	19	T				R		✓
	80	D		A				✓
	156	E				G		✓
	417	K		N			N	✓
	417	K			T			✓
	452	L				R		✓
	547	T					K	✓
	570	A	D					✓
	681	P	H			R	H	✓
	796	D					Y	✓
	950	D				N		×
	1027	T			I			×
	1118	D	H					×
ORF3a gene	26	S				L		×
	253	S			P			✓
E gene	71	P		L				×
M gene	82	I				T		×
N gene	235	S	F					×

* Denotes the ability of the sensor to discriminate VOC-specific SNPs at the indicated position. Checkmarks confirm the ability to discriminate the desired SNP and X refers to inability to discriminate the SNP. Red colored checkmarks indicate the mutations that were targeted for REVEALR-based genotyping of clinical samples.

Table S3.3. Summary of patient-derived clinical samples

Patient No.	Sex	Age	Date Collected	Timeframe	Media	CT Value	Variant	Variant Identification Source*
1	M	55	12/2/20	Early	HARDY	12.80	Wild type	2
2	F	58	12/2/20	Early	REMEL	17.20	Epsilon	1
3	M	69	12/9/20	Early	HARDY	3.38	Epsilon	1
4	M	70	12/13/20	Early	HARDY	13.1	Epsilon	2
5	M	46	12/21/20	Early	Remel	17.7	Wild type	2
6	F	30	12/30/20	Early	HARDY	8.86	Epsilon	2
7	F	68	1/5/21	Early	HARDY	11.34	Epsilon	1
8	F	30	1/6/21	Early	Remel	12.45	Wild type	2
9	M	23	1/6/21	Early	HARDY	4.5	Epsilon	2
10	F	64	1/9/21	Early	Remel	16.8	Epsilon	2
11	F	36	1/12/21	Early	Remel	14.89	Epsilon	2
12	F	26	3/10/21	Early	Remel	17.8	Wild type	2
13	M	39	7/8/21	Mid	XPERT	14.83	Delta	2
14	M	24	7/8/21	Mid	XPERT	16.12	Delta	2
15	F	37	7/15/21	Mid	XPERT	-	Gamma	1
16	F	14	7/22/21	Mid	XPERT	-	Gamma	1
17	F	60	7/23/21	Mid	XPERT	12.02	Alpha	1
18	M	26	7/23/21	Mid	XPERT	14.67	Delta	1
19	M	46	7/26/21	Mid	XPERT	-	Delta	1
20	F	30	7/27/21	Mid	XPERT	17.25	Delta	2
21	F	53	7/28/21	Mid	XPERT	16.98	Delta	1
22	F	35	11/29/21	Late	BD	15.15	Delta	2
23	F	97	12/8/21	Late	BD	8.63	Delta	2
24	M	68	12/8/21	Late	BD	13.30	Delta	2
25	M	31	12/9/21	Late	BD	17.80	Delta	2
26	F	27	12/15/21	Late	BD	9.30	Delta	2
27	M	37	12/20/21	Late	BD	19.70	Omicron	2
28	F	21	12/22/21	Late	BD	17.50	Omicron	2
29	M	62	12/22/21	Late	BD	17.85	Delta	2
30	M	69	12/23/21	Late	BD	19.05	Omicron	2
31	F	59	12/31/21	Late	-	17.95	Omicron	2

*Denotes the source of sequence verification of the patient-derived nasopharyngeal samples. Sequence verification of clinical samples was either done by Experimental Tissue Shared Resource Facility team at UCI Medical Center (source 1) or by study researchers via Sanger sequencing (source 2).

Supplementary Table 4.1. List of oligonucleotides

Name	Sequence 5'-3'
RNA Substrates and reference oligo	
FamQ-whole RNA-sub	/56-FAM/CUAACCGUCAUGA/3IABkFQ/
FQ-rGrU-sub	/56-FAM/CTAACCGUCATGA/3BHQ_1/
Ref_oligo_TAMRA	/56-TAMN/TTCTATGAAGACTTTTTAGAGTATTAAAAAGT CTTCATAGAAACTTTG
DNAzyme modification study	
No.1_Mz-A	CACCAGCTGTCCAACCTGAAACAACGAggttag
No.1,5_Mz-B	tcatgaGGCTAGCTGAAGAATCACCAGGAGTCAA
No.2_Mz-A	CACCAGCTGTCCAACCTGAAACAACGAggttag
No.2,6,8,9,10_Mz-B	tcatgaGGCTAGCTGAAGAATCACCAGGAGTCAA
No.3_Mz-A	CACCAGCTGTCCAACCTGAAACAACGAggttag
No.3,7_Mz-B	tcatgaGGCTAGCTGAAGAATCACCAGGAGTCAA
No.4_Mz-A	CACCAGCTGTCCAACCTGAAACAACGAggttag
No.4_Mz-B	tcatgaGGCTAGCTGAAGAATCACCAGGAGTCAA
No.5,6,7,11_Mz-A	CACCAGCTGTCCAACCTGAAACAACGAggttag/3BHQ_1/
No.8_Mz-A	CACCAGCTGTCCAACCTGAAACAACGAggttag/3BHQ_1/
No.9,12_Mz-A	CACCAGCTGTCCAACCTGAAACAACGAggttag/3BHQ_1/
No.10,13_Mz-A	CACCAGCTGTCCAACCTGAAACAAC*GAggttag/3BHQ_1/
No.11,12,13_Mz-B	tcatga*GGCTAGCTGAAGAATCACCAGGAGTCAA
No.14_Mz-A	CACCAGCTGTCCAACCTGAAACAACGAggttag
No.14_Mz-B	tcatgaGGCTAGCTGAAGAATCACCAGGAGTCAA
No.15_Mz-A	CACCAGCTGTCCAACCTGAAACAACGAggttag
No.15_Mz-B	tcatgaGGCTAGCTGAAGAATCACCAGGAGTCAA
No.16_Mz-A	CACCAGCTGTCCAACCTGAAACAACGAggttag
No.16_Mz-B	tcatgaGGCTAGCTGAAGAATCACCAGGAGTCAA
No.17_Mz-A	CACCAGCTGTCCAACCTGAAACAACGAggttag
No.17_Mz-B	tcatgaGGCTAGCTGAAGAATCACCAGGAGTCAA
No.18_Mz-A	CACCAGCTGTCCAACCTGAAACAACGAggttag
No.18_Mz-B	tcatgaGGCTAGCTGAAGAATCACCAGGAGTCAA
Sgene_mid-RPA	AGTTATTTGACTCCTGGTGATTCTTCTTCAGGTTGGACAG CTGGTGCTGCAG
DNAzyme used in Droplet REVEALR	
Q-MOE-A-N1_66sub	CAGTTGAATCTGAGGGTCCACACAACGAggttag/3BHQ_1/
Q-MOE-A-N2_66sub	ACATTCCGAAGAACGCTGAAACAACGAggttag/3BHQ_1/
Q-MOE-A-N3_66sub	GTTGTAGCACGATTGCAGCAACAACGAggttag/3BHQ_1/

Q-MOE-A-N4_66sub	CCCTTCTGCGTAGAAGCCTTACAACGAggttag/3BHQ_1/
Q-MOE-A-N5_66sub	TGTTGCGACTACGTGATGAGACAACGAggttag/3BHQ_1/
Lz-L1-B-N1_66sub_PS	tcatga*GGCTAGCTCAAACGTAATGCGGGGTGC
Lz-L1-B-N2_66sub_PS	tcatga*GGCTAGCTGCGCTGGGGGCAAATTGTGC
Lz_L1-B-N3_66sub_PS	tcatga*GGCTAGCTTTGTTAGCAGGATTGCGGGT
Lz_L1-B-N4_66sub_PS	tcatga*GGCTAGCTTTGGCAATGTTGTTCCTTGA
Lz-L1-B-N5_66sub_PS	tcatga*GGCTAGCTGAACGAGAAGAGGCTTGACT
Template for IVT	
T1_5sets_N1N2N3N4N5	GAAATTAATACGACTCACTATAGGGGCACCCCGCATTACGTTTGGTGGACCCTCAGATTCAACTGGCACAATTTGCCCCCAGCGCTTCAG
T2_5sets_ N1N2N3N4N5	ATTTGCCCCCAGCGCTTCAGCGTTCTTCGGAATGTACCCGCAATCCTGCTAACAATGCTGCAATCGTGCTACAACTCAAGGAACAACATT
T3_5sets_ N1N2N3N4N5	TGTTGCGACTACGTGATGAGGAACGAGAAGAGGCTTGACTCCCTTCTGCGTAGAAGCCTTTTGGCAATGTTGTTCCTTGAGTTGTAGCAC

Note: Black stands for DNA nucleotides. red for RNA nucleotides, orange for 2'OMe nucleotides, purple for MOE nucleotides, and green for LNA nucleotides. * Stands for PS bond. Underline represents the catalytic core. The lower case stands for the substrate binding arm of DNAzyme. Pink highlight signifies the T7 promoter region.

Table S4.2. Proportion of positive droplet (PPD) calculation

Diameter of droplet um	Vol pL	Sample concentration					
		10 aM	100 aM	1 fM	10 fM	100 fM	1 pM
15	1.77	0.001%	0.011%	0.106%	1.059%	10.095%	65.499%
14	1.44	0.001%	0.009%	0.086%	0.861%	8.288%	57.904%
13	1.15	0.001%	0.007%	0.069%	0.690%	6.693%	49.980%
12	0.90	0.001%	0.005%	0.054%	0.543%	5.303%	42.008%
11	0.70	0.000%	0.004%	0.042%	0.419%	4.110%	34.274%
10	0.52	0.000%	0.003%	0.032%	0.315%	3.104%	27.044%

Table S4.3. Multicomponent DNAzyme optimizations

ID	Average FAM signal	Standard deviation	cleavage %	Cleavage-STD%	$k_{obs}(min^{-1})$	temperature (°C)	Fold-change
1	1699.9	62.2	12.2%	0.7%	10.2	25	1.00
2	2278.6	69.0	16.3%	0.6%	13.6	30	1.34
3	3645.5	168.0	29.8%	1.7%	24.8	37	2.44
4	2914.3	96.7	22.5%	1.0%	18.7	37	1.84
5	3168.2	90.7	24.5%	0.8%	20.4	30	2.01
6	2955.5	137.5	22.5%	1.3%	18.8	30	1.85
7	3377.4	98.0	26.4%	0.9%	22.0	30	2.17
8	1529.2	66.6	8.6%	0.7%	7.2	37	0.71
9	4843.3	121.2	39.8%	1.1%	33.2	30	3.27
10	4606.9	162.1	41.0%	1.6%	34.2	34	3.37
11	3488.0	145.3	30.1%	1.4%	25.1	34	2.47
12	3830.0	148.9	33.5%	1.4%	27.9	34	2.75
13	5636.7	144.0	51.1%	1.4%	42.6	34	4.19
14	1537.4	54.2	11.5%	0.6%	9.6	25	0.95
15	383.9	53.2	-0.9%	0.6%	-0.7	25	-0.07
16	1567.4	73.5	9.8%	0.7%	8.2	30	0.80
17	1618.2	65.6	10.3%	0.6%	8.6	30	0.84
18	2198.4	77.1	15.6%	0.7%	13.0	30	1.28

APPENDIX B: Supplementary Figures

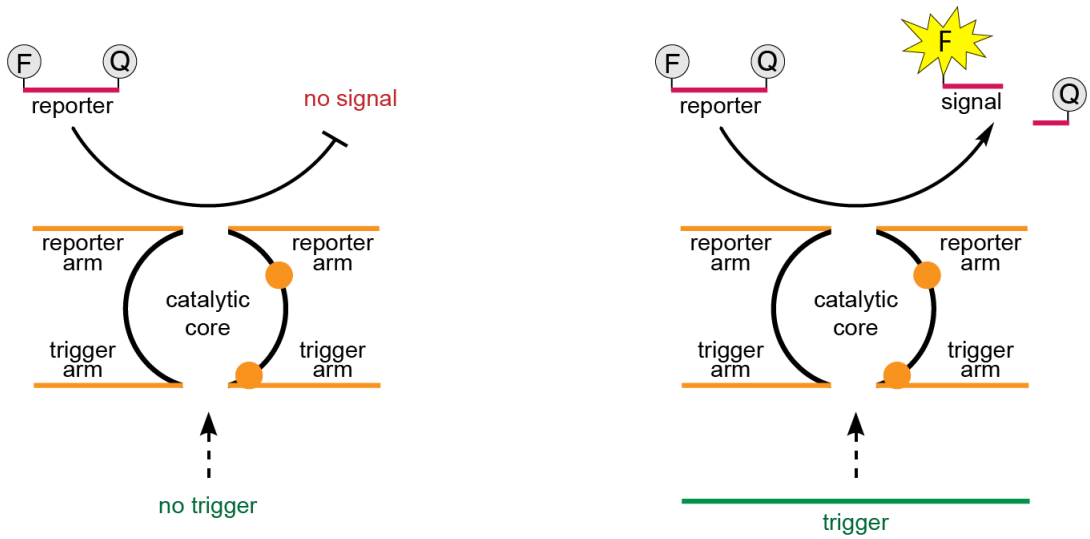

Figure S2.1. Multicomponent nucleic acid sensor for viral RNA detection. The multicomponent enzyme consists of a split XNA enzyme in which the catalytic core is separated into two halves (left and right), each carrying partial arms that are complementary in sequence the reporter and trigger. In the presence of a trigger (e.g., viral RNA), the split enzyme self-assembles into an active catalyst with site-specific endonuclease activity that can generate an optical signal by cleaving a quenched fluorescent RNA reporter. Signal amplification occurs only in the presence of the trigger and continues as long as the trigger is bound to the complex.

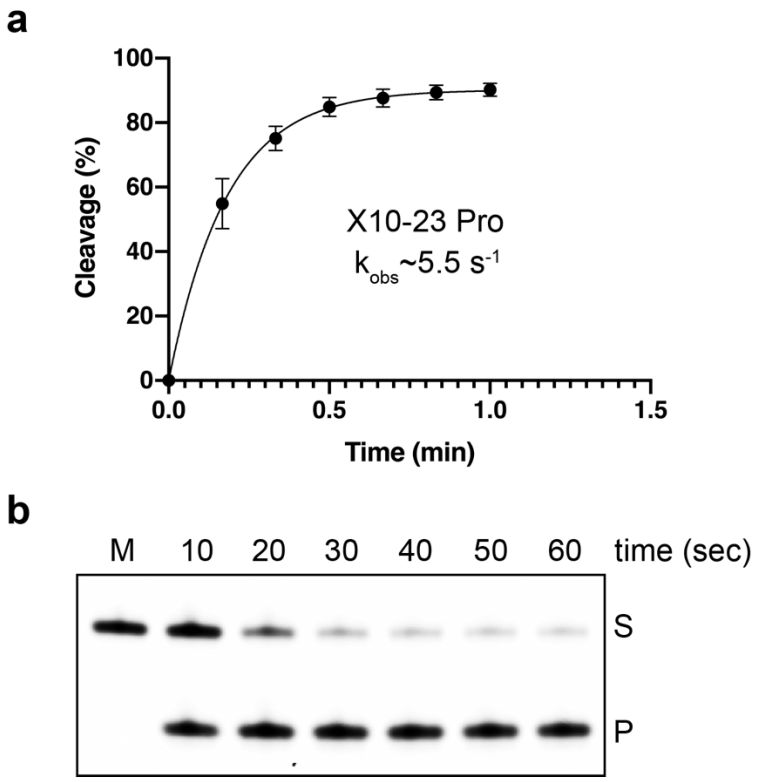

Figure S2.2. Kinetic analysis of the split X10-23 Pro multicomponent enzyme. (a) Steady state kinetic analysis of RNA cleavage by split X10-23 Pro. Reactions were performed in buffer containing 50 mM Tris-HCl (pH 8.5), 50 mM $MgCl_2$, 150 mM NaCl, and 0.5 µM of each nucleic acid component (5' labeled RNA reporter, both halves of the enzyme, and the S-gene trigger). n = 3, error bars denote standard error of the mean (SEM). (b) Representative denaturing polyacrylamide gel used to calculate the rate of RNA cleavage by X10-23 Pro. S: full-length substrate, P: 5' cleavage product.

Figure S2.3. Annotated genome map of SARS-CoV-2. Region of the S-gene selected for detection is denoted (red rectangle) with the nucleotide positions labelled. Abbreviations: UTR, untranslated region; ORF, open reading frame; S, spike; E, envelope; M, membrane; and N, nucleocapsid.

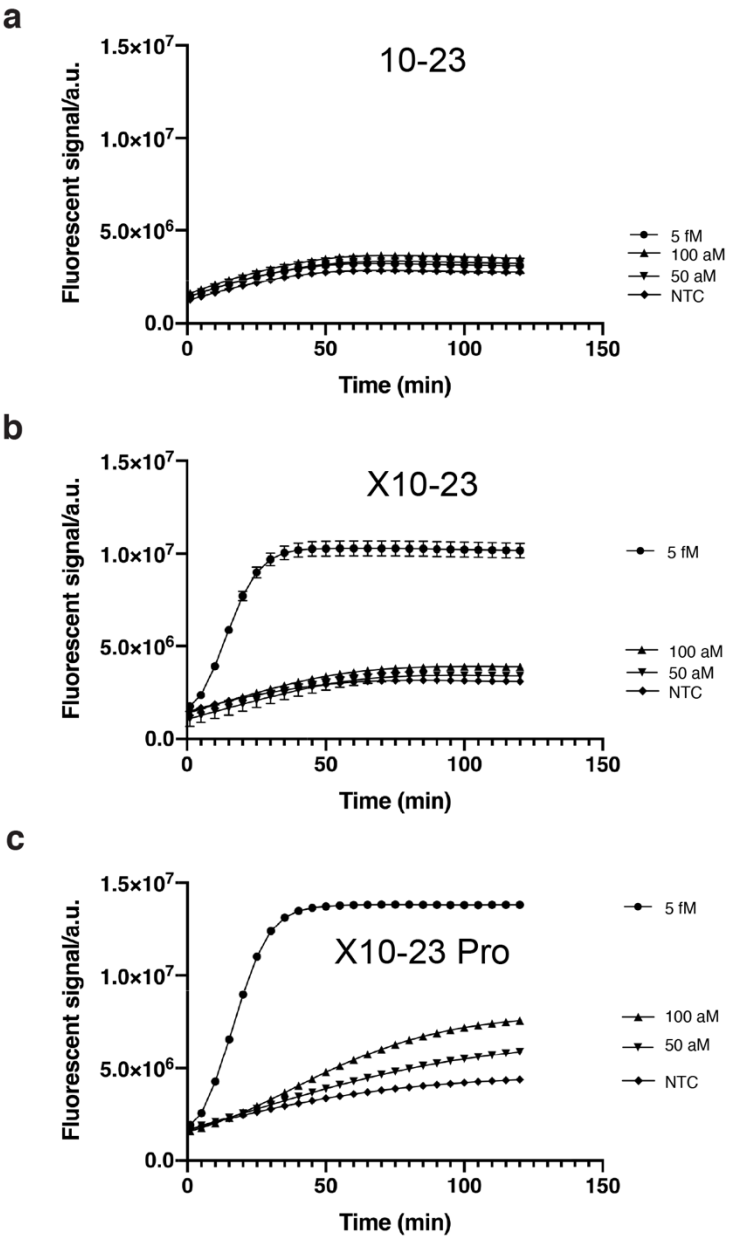

Figure S2.4. Kinetic comparison of three multicomponent designs in the REVEALR detection format. Kinetics of fluorescent signal generation for (a) split 10-23, (b) split X10-23, and (c) split X10-23 Pro across different serial dilutions of the S gene IVT RNA fragment. n = 3, error bars denote standard error of the mean (SEM). au, arbitrary units. NTC, no template control.

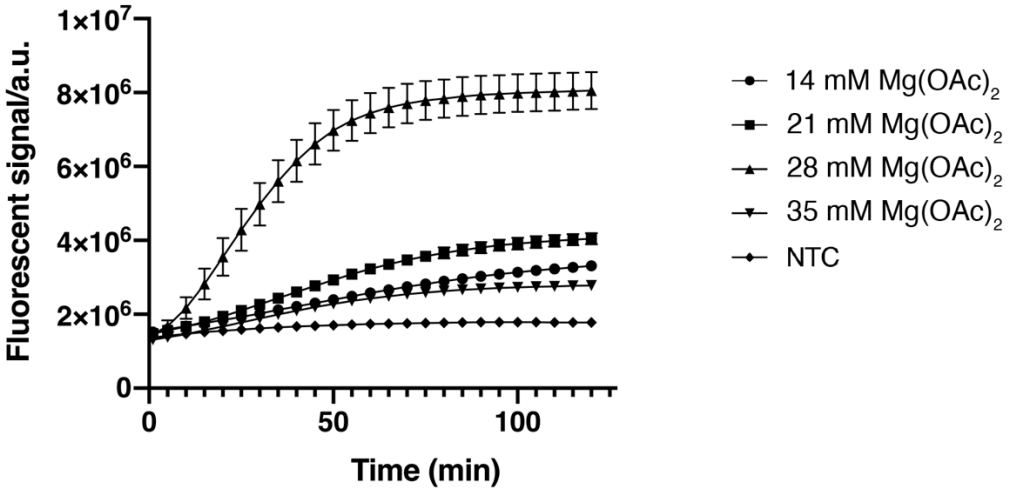

Figure S2.5. Optimization of the magnesium acetate concentration for the RT-RPA step of the REVEALR system. The kinetics of fluorescent signal generation were compared across a range of magnesium acetate concentrations. Signal generation was performed using X10-23 Pro to detect a fixed concentration (50 aM) of the S gene IVT RNA fragment of SARS-CoV-2. n = 3, error bars denote standard error of the mean (SEM). au, arbitrary units. NTC, no template control.

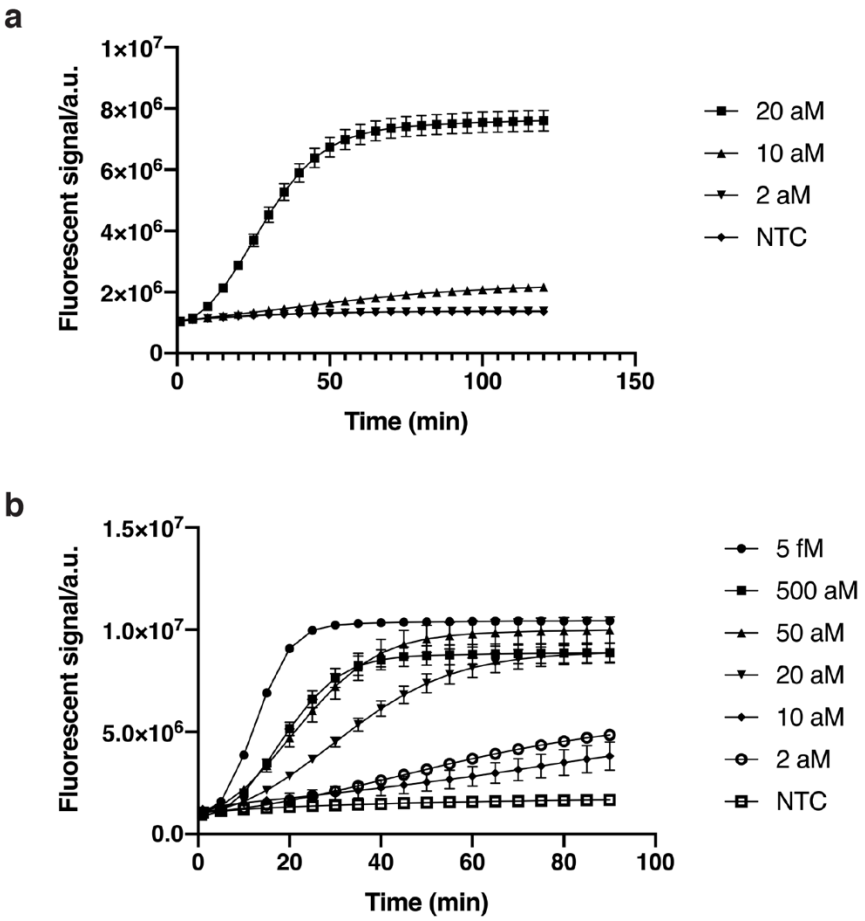

Figure S2.6. **Evaluation of the reverse transcriptase component of the RT-RPA step of the REVEALR system.** The kinetics of fluorescent signal generation were compared using commercial (a) M-MuLV RT and (b) SuperScript IV polymerases to facilitate the initial reverse transcription step of the RT-RPA protocol. Signal generation was performed using X10-23 Pro to detect across different serial dilutions of the S gene IVT RNA fragment of SARS-CoV-2. n = 3, error bars denote standard error of the mean (SEM). au, arbitrary units. NTC, no template control.

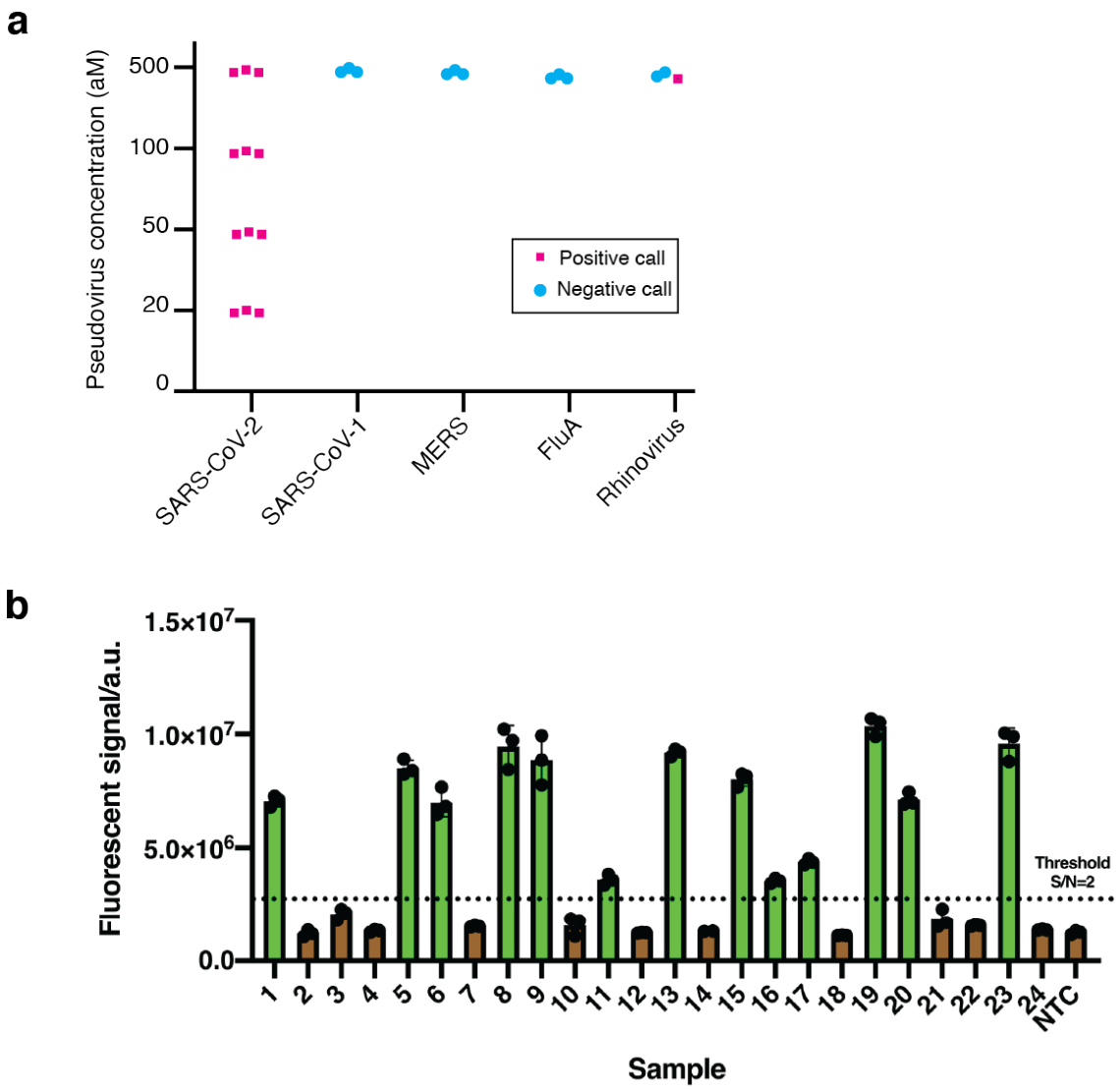

Figure S2.7. Blinded IVT RNA fragment study. (a) Summary of REVEALR test results obtained for a blinded sample of in vitro transcribed RNA IVT RNA fragment samples representing SARS-CoV-2, SARS-CoV-1, MERS, FluA and Rhinovirus. Positive calls (red squares), negative calls (blue circles). (b) Raw fluorescent data of blinded study obtained after 30 min of incubation.

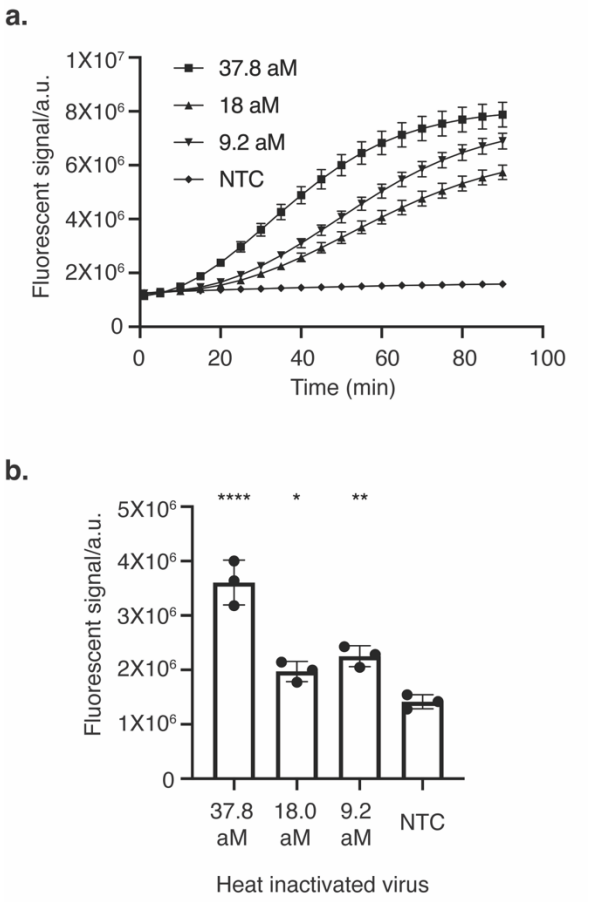

Figure S2.8. Sensitivity test with heat-inactivated SARS-CoV-2. (a) Kinetics of fluorescent signal generation over 90 min across a range of RNA dilutions. au, arbitrary units. (b) Limit of detection for fluorescence-based quantification at 30 min at designated RNA concentrations. Measurements are mean ± standard error (S.E.M), n = 3 for b and c. Two tailed student's t test; *P<0.05, **P<0.01, ***P<0.001, ****P<0.0001.

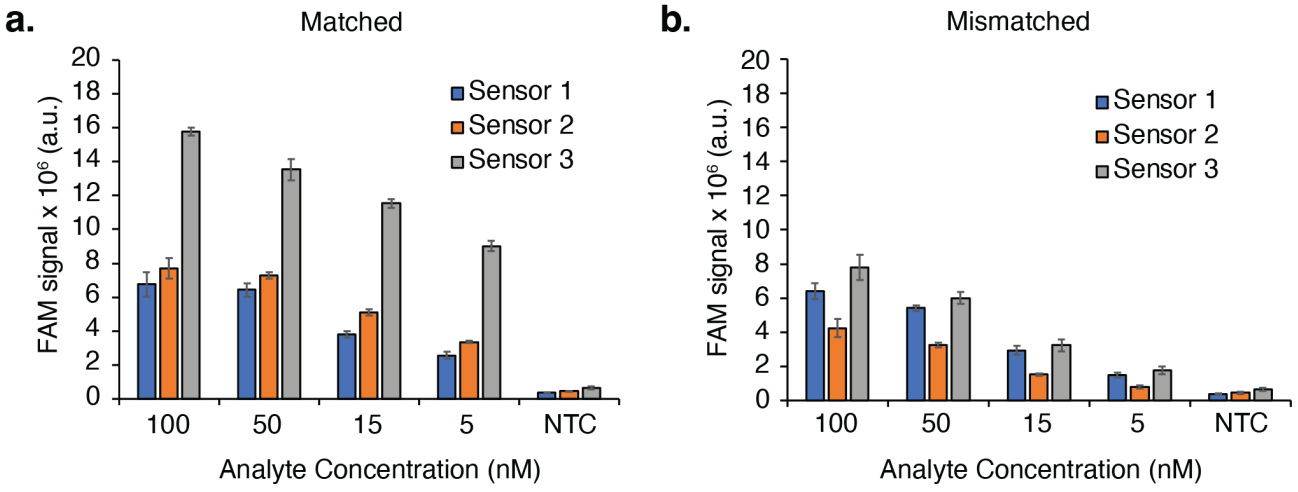

Figure S3.1. DNAzyme sensor design. Fluorescence signal observed for sensor 1-3 against decreasing concentration of the (a) matched and (b) mismatched DNA analyte corresponding to the A570D mutation observed in the S1 protein of the SARS-CoV-2 genome. Error bars represent the standard error of the mean (SEM) with n=3. Abbreviations: au, arbitrary units. This data was used to generate the data presented in Figure 2.

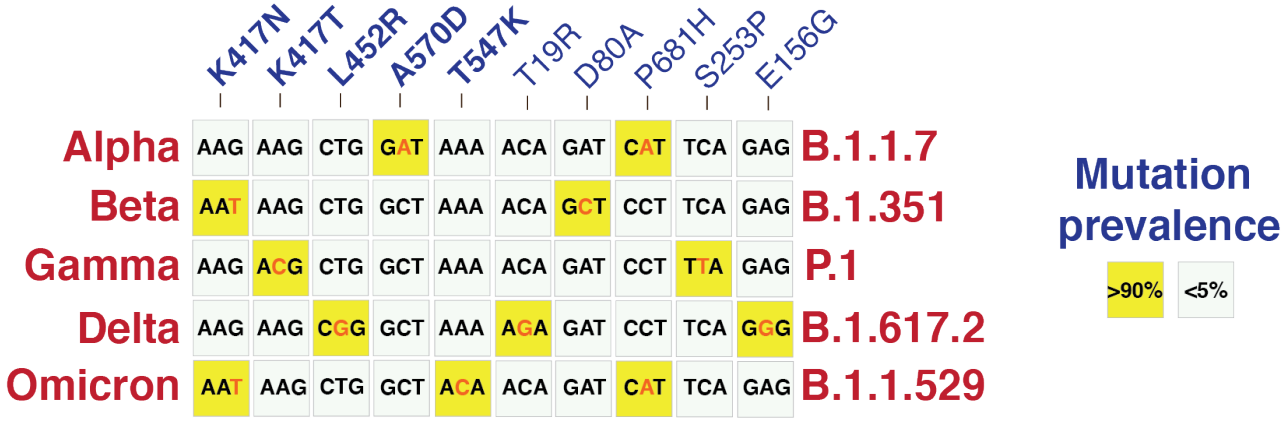

Figure S3.2. Genotype of SARS-CoV-2 variants. Each grouping contains the codon for an amino acid of interest. The single orange colored letter of the codon represents the SNP mutation evaluated. Red labels to the left and right of the table denote the WHO variant name and Pango lineage, respectively. Mutations given in bold font at the top of the table indicate sensors that were chosen for clinical validation, while regular font indicates the back-up sensors.

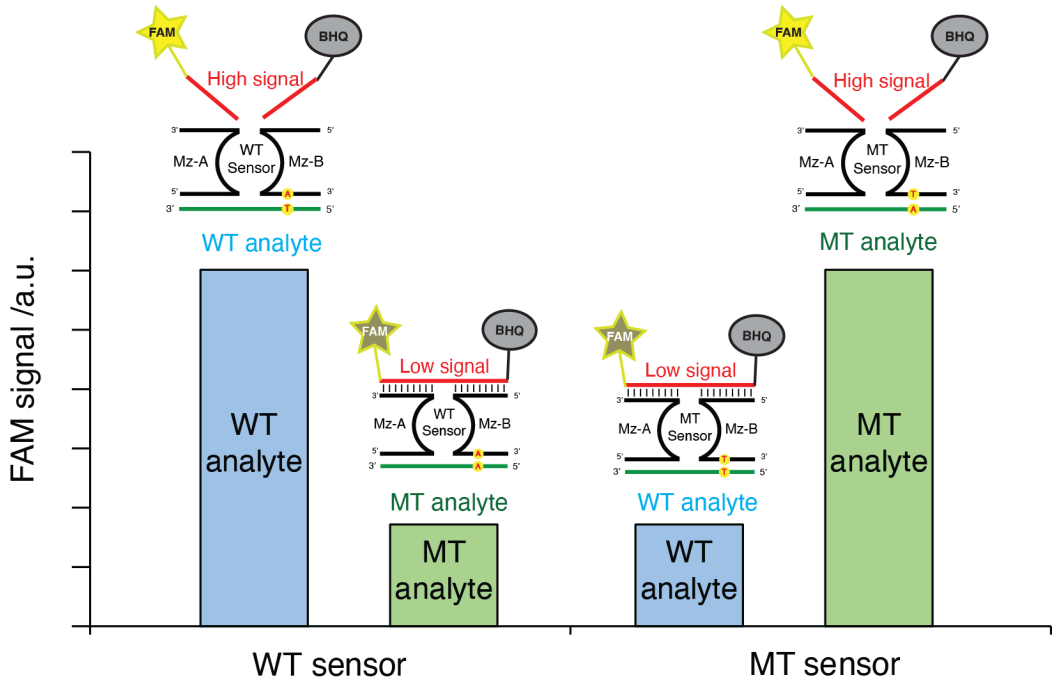

Figure S3.3. Schematic overview of multicomponent enzyme screening. All experiments are performed with 15 nM of the corresponding analyte and incubated at 37°C for 30 min. WT analyte differs from MT analyte by a single nucleotide in the sequence. WT sensor differs from MT sensor by a single nucleotide in the analyte binding arm of Mz-B. n=3. WT, wild type. MT, mutant.

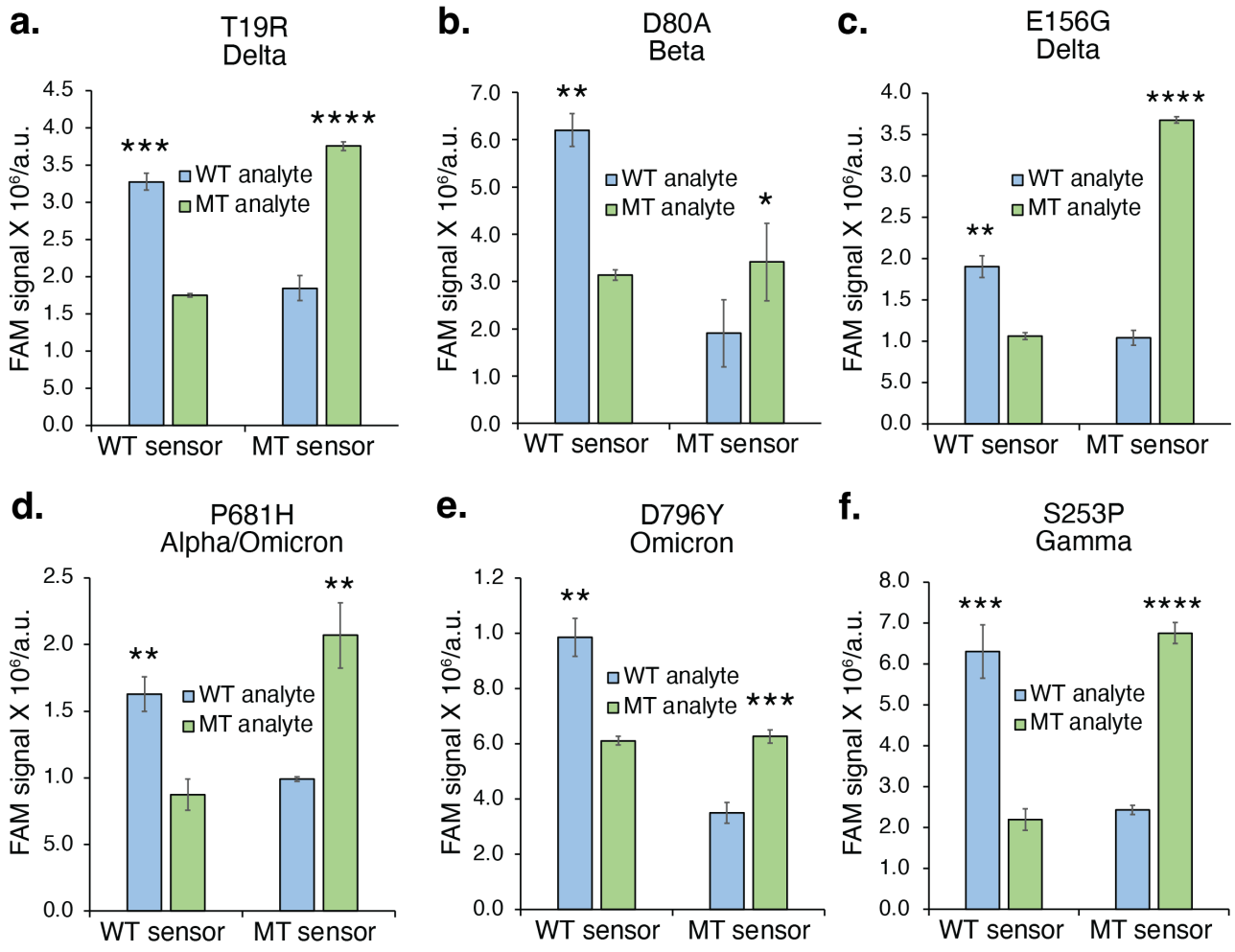

Figure S3.4. Back-up sensors identified for SNP discrimination. Fluorescent signal generation under 15 nM of corresponding IVT RNA fragment and incubated at 37°C for 30 min. Measurements are mean ± standard error (S.E.M), n=3. Two tailed student's t-test; *P<0.05, **P<0.01, ***P<0.001, ****P<0.0001. WT, wild type. MT, mutant.

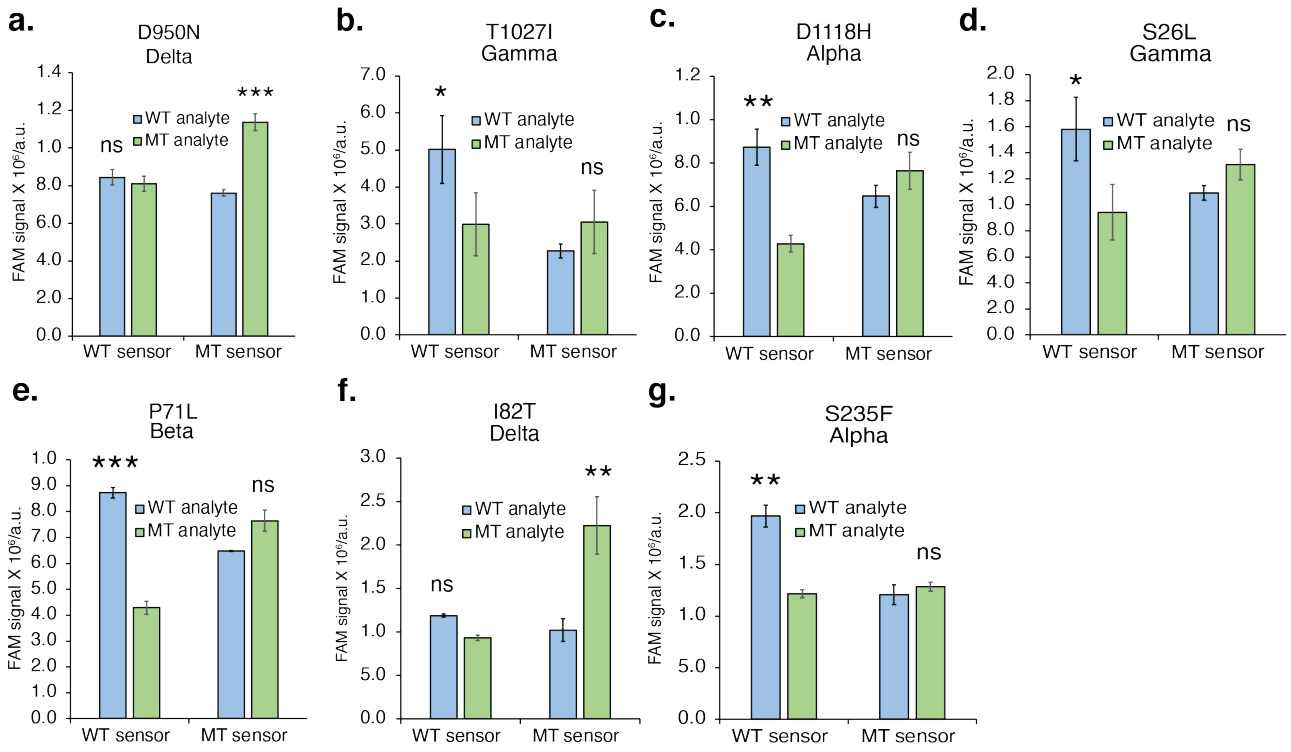

Figure S3.5. Multicomponent sensors that did not qualify for SNP detection. Fluorescent signal generation under 15 nM of corresponding IVT RNA fragment and incubated at 37°C for 30 min. Measurements are mean ± standard error (S.E.M), n=3. Two tailed student's t-test; *P<0.05, **P<0.01, ***P<0.001, ****P<0.0001. ns, not significant. WT, wild type. MT, mutant.

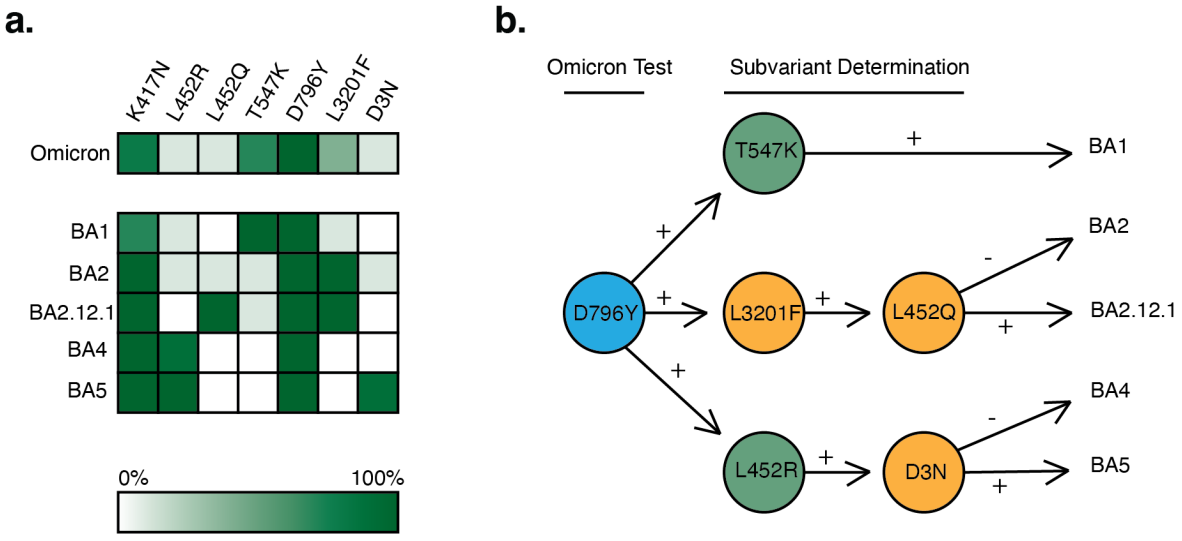

Figure S3.6. Possible REVEALR-based genotyping strategy for omicron subvariants. (a) Mutation prevalence was observed for omicron subvariants. Dark green indicates that the mutation is observed in a higher fraction of the population. Sensors currently exist to recognize the mutations: K417N, L452R, T547K, and D796Y. However, a tiered or direct detection system would also require sensors for the following

mutations: L452Q (S gene), L3201F (ORF1a), and D3N (M gene). (b) Schematic for a tiered detection system used to identify omicron subvariants. Green circles indicate validated sensors used in our clinical study, blue circles represent backup sensors, and orange circles denote sensors that would need to be created. In this hierarchical scheme, an initial positive test (blue) would be followed with additional sensors to elucidate the identity of the precise subvariant in the patient sample.

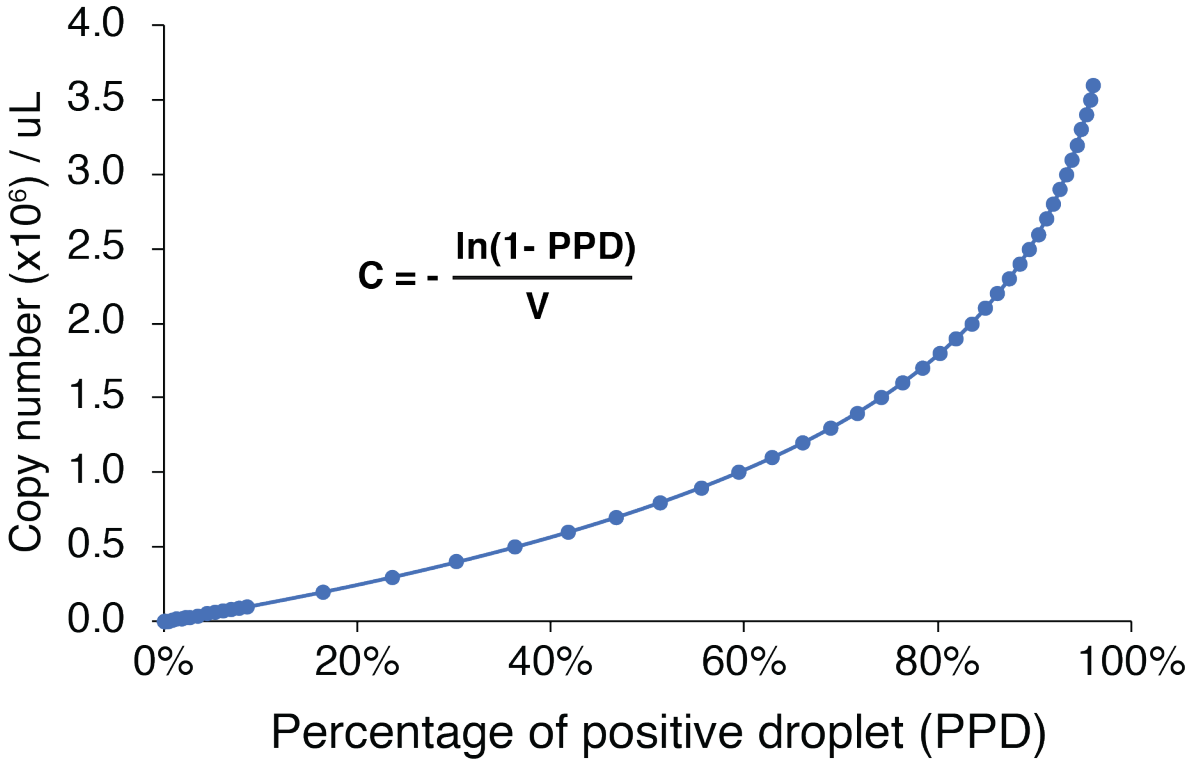

Figure S4.1. Poisson distribution calculating the percentage of positive droplet (PPD) as a function of sample concentration. Data were calculated using the formula of concentration (copies per uL) = -ln(1-PPD)/V, where PPD stands for the percentage of positive droplet and V stands for the average volume (uL) of the droplet.

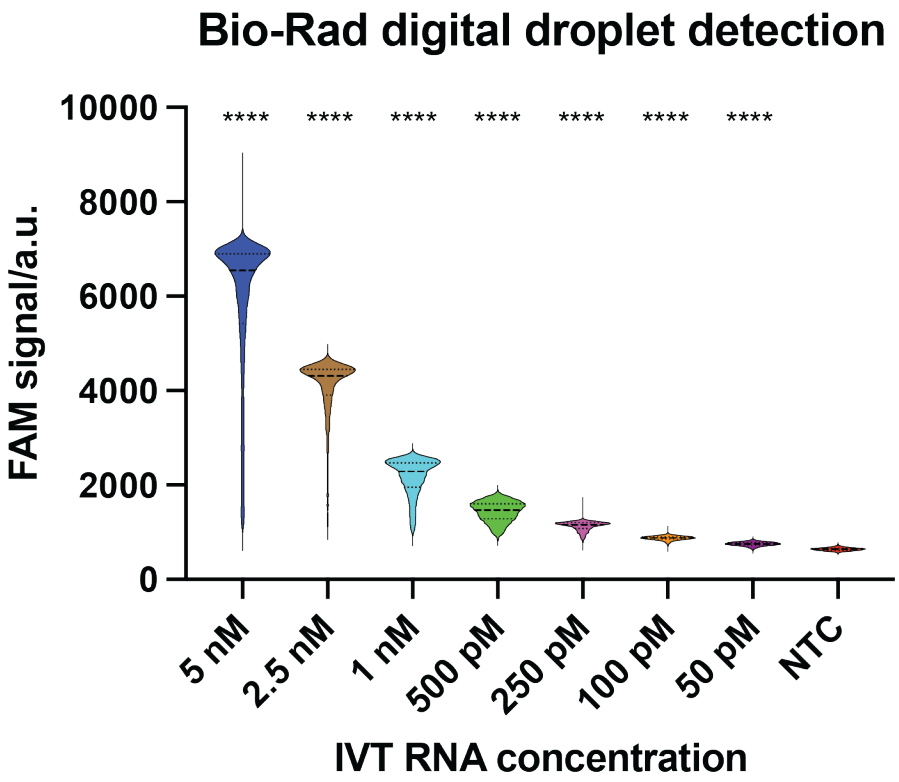

Figure S4.2. Sensitivity test of multicomponent DNAzyme in a Bio-Rad digital droplet system. Assays were performed in Bio-Rad droplets generated from buffer containing 50 mM $MgCl_2$, 50 mM Tris (pH 8.5), 150 mM NaCl, 500 nM FAM-labeled RNA substrate and 500 nM unmodified multicomponent DNAzyme, gradient concentration of in vitro transcribed RNA analyte, 1X Bio-Rad ddPCR Supermix. Droplet populations were evaluated after a 1-hour incubation at 25°C using a Bio-Rad ddPCR droplet reader. Dash lines represent the medians, and the dot lines represent the two quartile lines. Two-tailed Student's t test: *, $P < 0.05$; **, $P < 0.01$; ***, $P < 0.001$; ****, $P < 0.0001$. Abbreviations: au, arbitrary units.

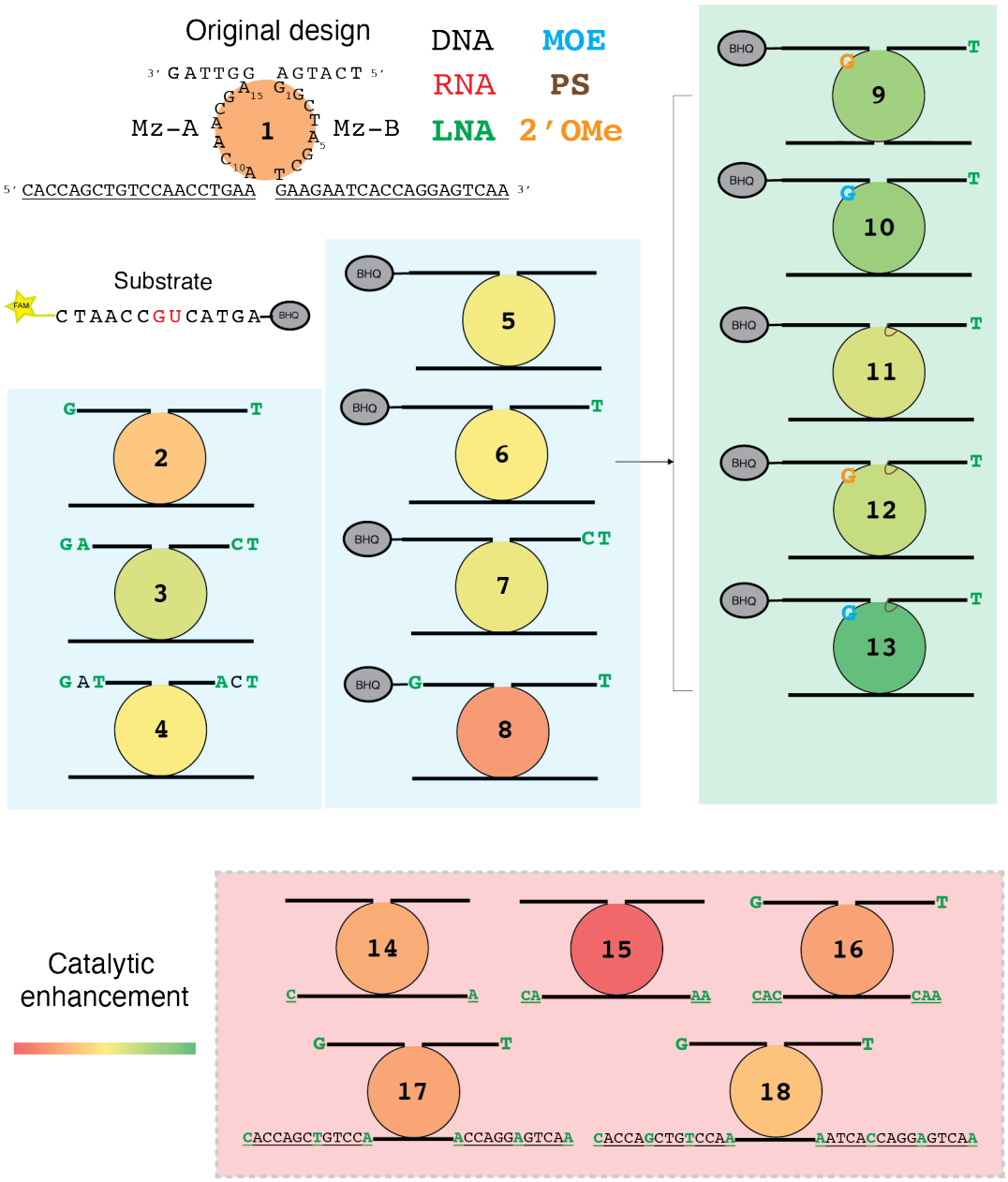

Figure S4.3. Chemical modifications evaluated for optimal DNAzyme activity**.** The catalytic core of each DNAzyme design is colored according to activity as referenced in the heat map (bottom left). Chemical modifications are indicated by color and residue. Assays were performed in Bio-Rad droplets generated from buffer containing 200 mM $MgCl_2$, 50 mM Tris (pH 8.5), 150 mM NaCl, 500 nM FAM-labeled RNA substrate and 500 nM DNAzyme, 100 pM of in vitro transcribed RNA analyte, 1X Bio-Rad ddPCR Supermix. Droplet populations were evaluated after a 1-hour incubation using a Bio-Rad ddPCR droplet reader. Abbreviations: 2'-*O*-methylribonucleic acid (2'-OMe), 2'-*O*-methoxyethylribonucleic acid (MOE), locked nucleic acid (LNA), phosphonothioate (PS), and black hole quencher (BHQ).

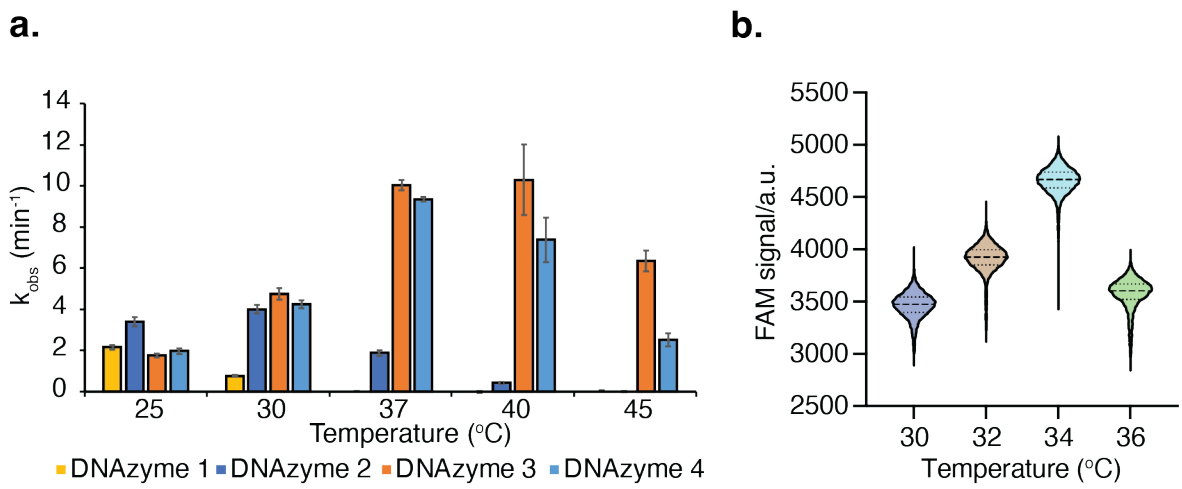

Figure S4.4. Temperature optimization of DNAzyme sensor. (a) Temperature course of DNAzymes 1 to 4 in bulk solution. Assays were performed in buffer containing 100 mM $MgCl_2$, 50 mM Tris (pH 8.5), 150 mM NaCl, 500 nM FAM-labeled whole RNA substrate, and 500 nM DNAzyme 2, 5 nM of single strand DNA analyte. Signal were evaluated after a 10 min under different temperature. Error bars denote ± standard deviation of the mean for 3 independent replicates. (b) Temperature course of DNAzyme 13 in a Bio-Rad digital droplet system. Reactions were performed in droplets generated from buffer containing 200 mM $MgCl_2$, 50 mM Tris (pH 9.0), 150 mM NaCl, 1 uM FAM labeled RNA substrate, 20 nM of each multicomponent DNAzyme 13 shown in figure 2c, 10 pM in vitro transcribed RNA analyte and 1X Bio-Rad ddPCR Supermix. Droplet populations were evaluated after 1 hour at different temperatures using a Bio-Rad ddPCR droplet reader.

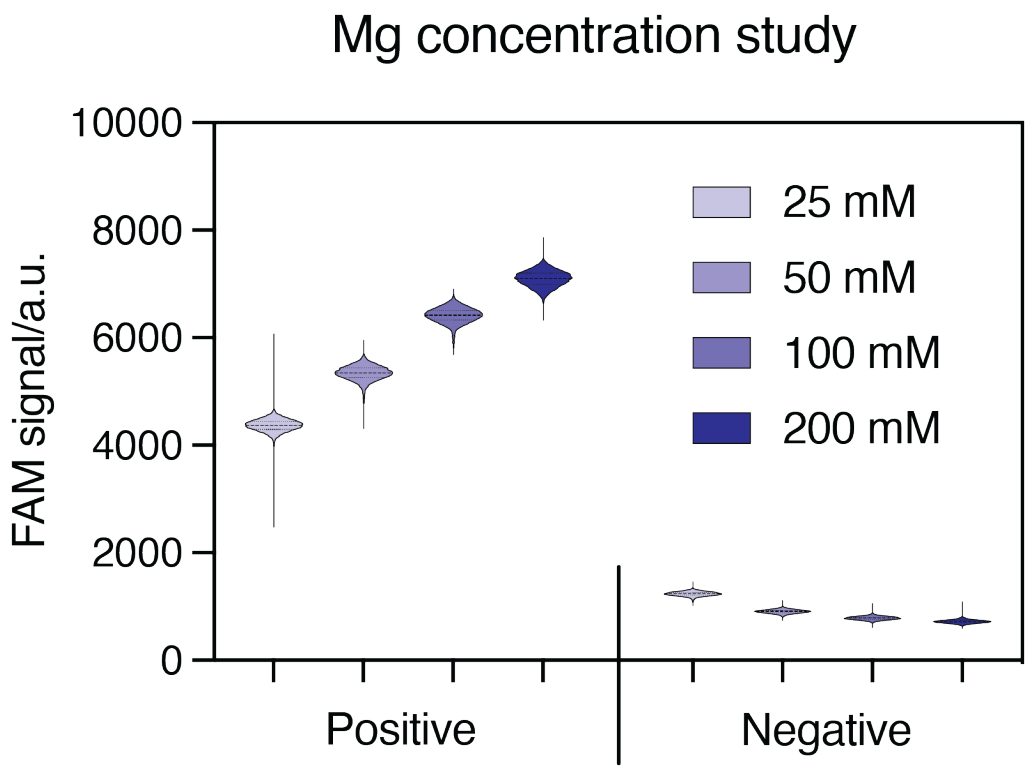

Figure S4.5. Mg concentration study in droplet system. Assays were performed in Bio-Rad droplets generated from buffer containing gradient concentration of $MgCl_2$, 50 mM Tris (pH 8.5), 150 mM NaCl, 500 nM FamQ RNA substrate, and 500 nM DNAzyme 2, 500 pM of single strand DNA analyte, 1X Bio-Rad ddPCR Supermix. Droplet populations were evaluated after a 1 hour incubation at 25°C using a Bio-Rad ddPCR droplet reader.

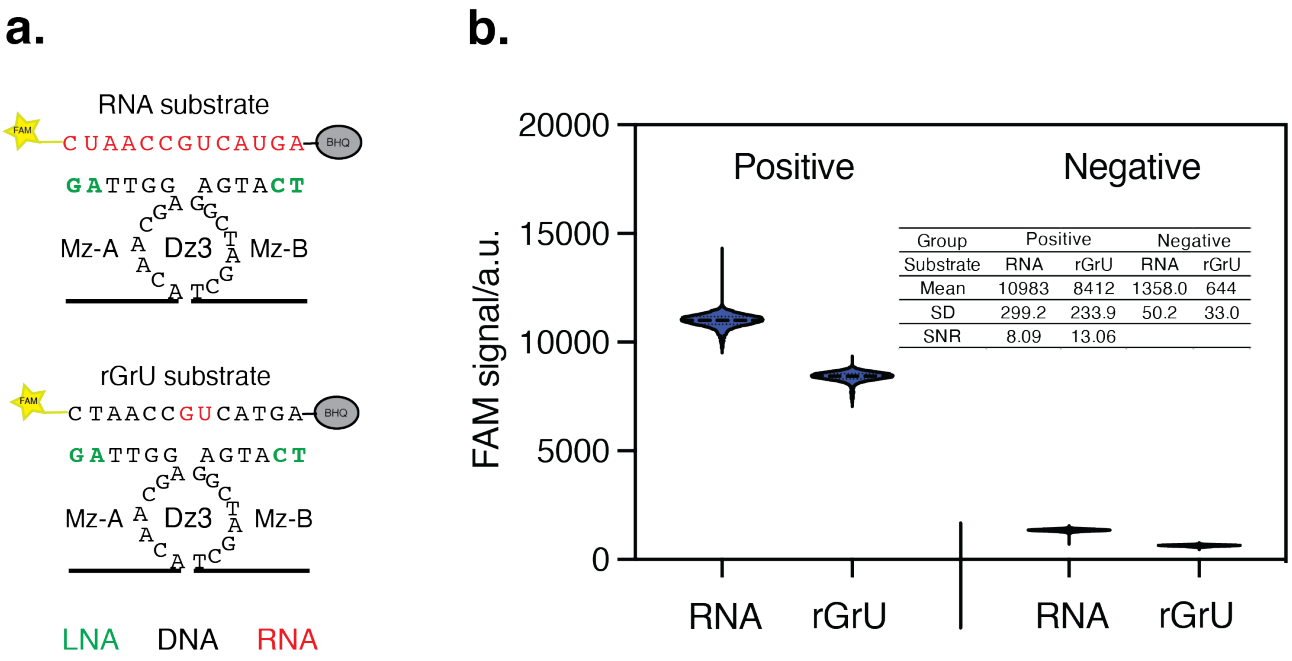

Group	Positive		Negative	
Substrate	RNA	rGrU	RNA	rGrU
Mean	10983	8412	1358.0	644
SD	299.2	233.9	50.2	33.0
SNR	8.09	13.06		

Figure S4.6. Substrate comparison. (a) Cartoon representation of the DNAzyme 3 recognizing a quenched whole RNA substrate (top) or rGrU chimeric substrate (bottom). (b) Comparison in Bio-Rad digital droplet system. Assays were performed in Bio-Rad droplets generated from buffer containing 200 mM $MgCl_2$, 50 mM Tris (pH 8.5), 150 mM NaCl, 500 nM FAM-labeled whole RNA substrate or rGrU chimeric substrate, and 500 nM DNAzyme 3, 500 pM of single strand DNA analyte, 1X Bio-Rad ddPCR Supermix. Droplet populations were evaluated after a 1 hour incubation at 37°C using a Bio-Rad ddPCR droplet reader. Abbreviations: DNAzyme 3 (Dz3); locked nucleic acid (LNA); Signal to noise ratio (SNR); Standard Deviation (SD). RNA in b panel specifically stands for whole RNA substrate.

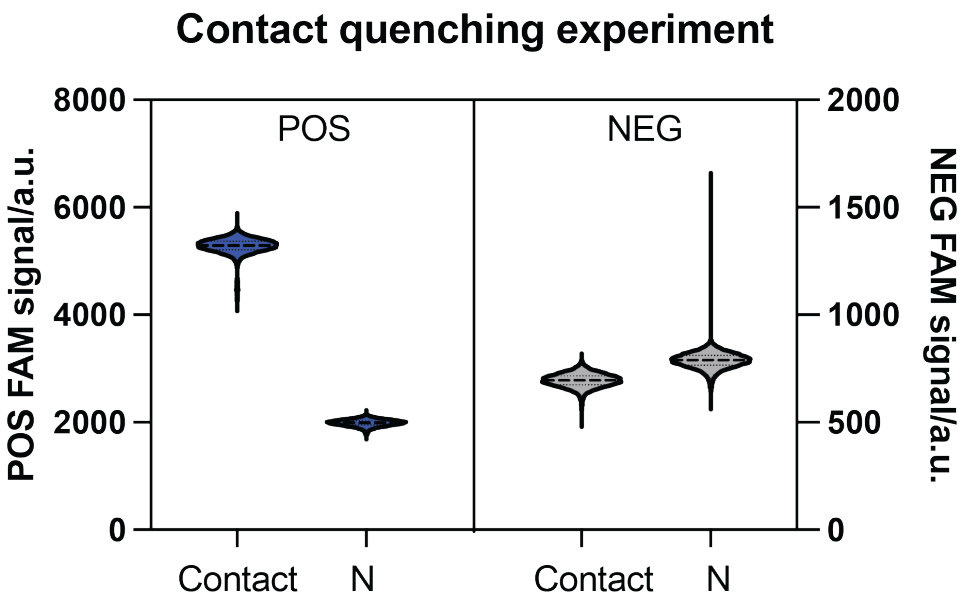

Figure S4.7. Contact quenching experiment. Experiments were performed with 500 nM DNAzyme sensor, 50 mM Tris (pH 8.5), 150 mM NaCl, 200 mM $MgCl_2$, 1X Bio-Rad ddPCR Supermix, 500 nM substrate and incubated at 25°C for 60 min. Contact quenching group (used sign "Contact") was used DNAzyme 5 and control group (used sign "N") was used DNAzyme 1. 500 pM in vitro transcribed RNA added for positive groups.

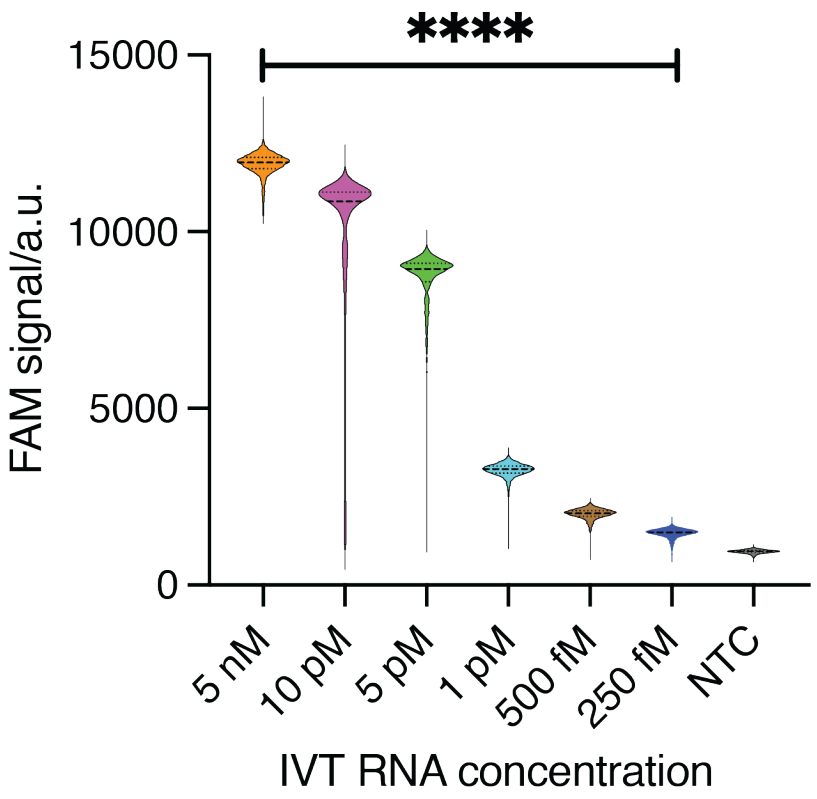

Figure S4.8. Multiplex DNAzyme sensor in Bio-Rad digital droplet system. The DNAzyme sensor used in this experiment were the "All" shown in Figure 2c. Data was collected after 3 hours of incubation at 34°C using Bio-Rad ddPCR reader. Experiments were performed with 20 nM of each DNAzyme 13 sensor shown in Figure 2c (5 in total), 50 mM Tris (pH 8.5), 150 mM NaCl, 200 mM $MgCl_2$, 1X Bio-Rad ddPCR Supermix, 500 nM rGrU substrate, gradient concentration of in vitro transcription RNA and incubated at 34°C for 60 min.

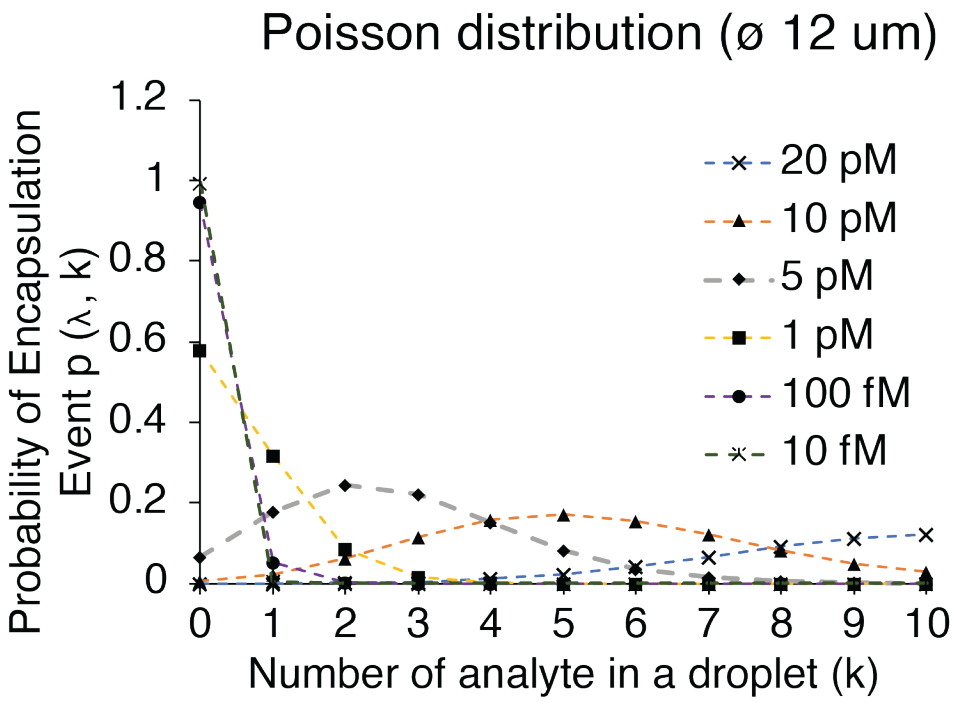

Figure S4.9. Poisson distribution of the number of analyte molecules in the droplet based on sample concentration. Calculations were based on the droplet diameter of 12 μm. The proportion of droplets *p(λ, k)* was calculated based on the average number of events (λ) for a given number of analytes in a droplet (k).

a.

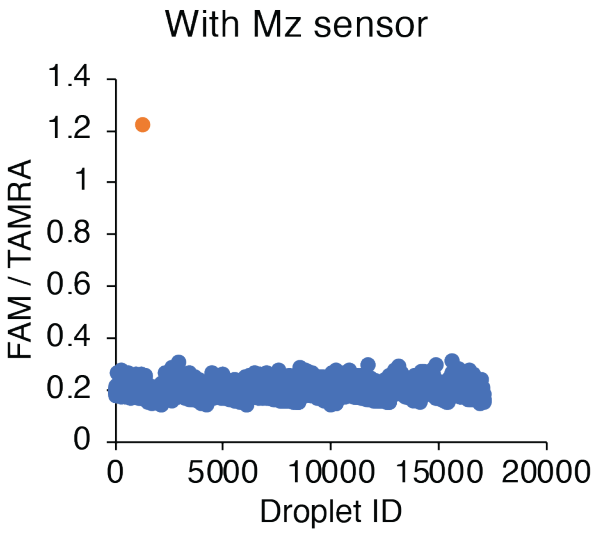

b.

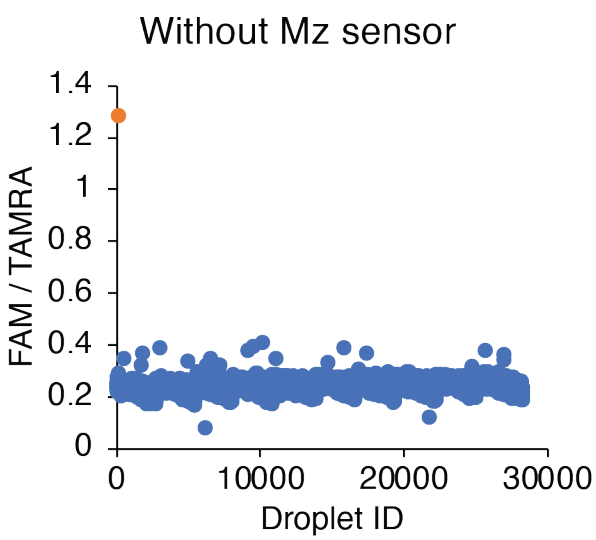

c.

Experiment	Positive droplet	Negative droplet	Total droplet	PPD
With Mz	1	17089	17090	0.0059%
No Mz	1	28259	28260	0.0035%

Figure S4.10. Empirically observed droplet false-positive rate. Blue data points represent negative droplets and orange data points represent positive droplets. PPD stands for positive percentage droplet. Mz stands for multicomponent DNAzyme. Experiments were performed with or without 20 nM of each Mz sensor (5 Mz in total), 50 mM Tris (pH 9.0), 150 mM NaCl, 200 mM $MgCl_2$, 1X Bio-Rad ddPCR Supermix, 500 nM rGrU substrate, gradient concentration of in vitro transcription RNA and incubated for 60 minutes at 34°C. Ten images were analyzed for each experiment. The FAM/TAMRA represents the signal intensity of each droplet with the normalization about its size.

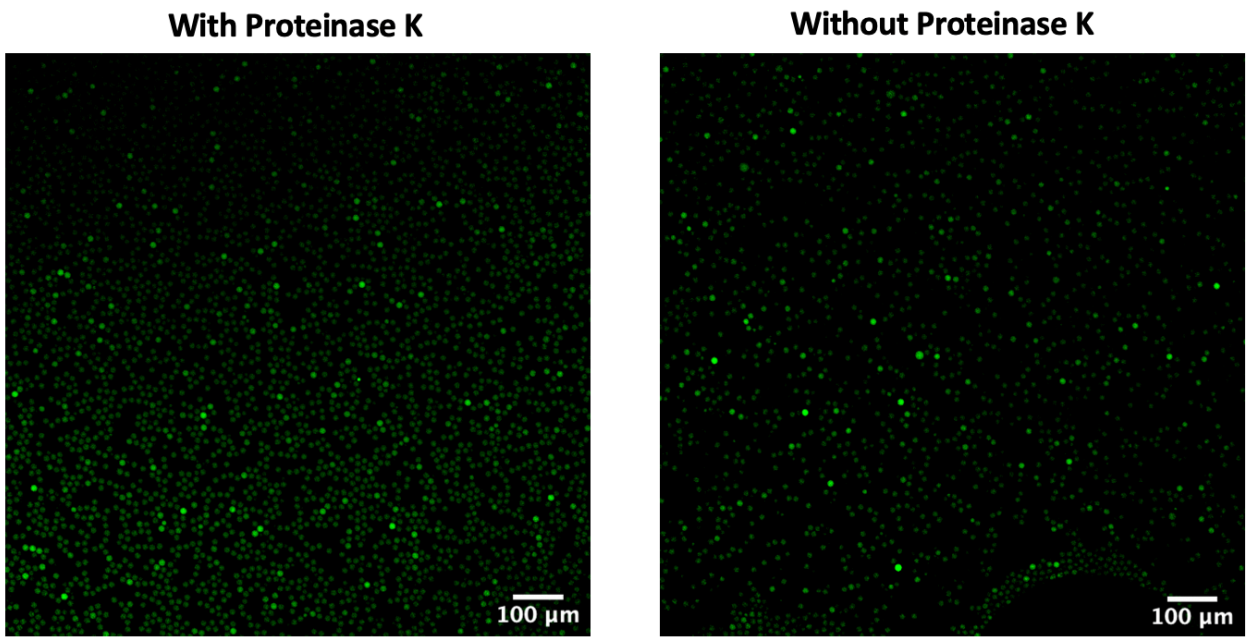

Figure S4.11. Validation of a protein-free assay using proteinase K. Data were collected after 3 hours of incubation at 34°C with 100 fM of IVT RNA analyte. Experiments were performed with 20 nM of each Mz sensor (5 Mz in total), 50 mM Tris (pH 9.0), 150 mM NaCl, 200 mM $MgCl_2$, 1X Bio-Rad ddPCR Supermix, 500 nM rGrU substrate, with or without 1 uL Proteinase K (NEB P8107S), 100 fM in vitro transcription RNA and incubated for 60 minutes at 34°C.

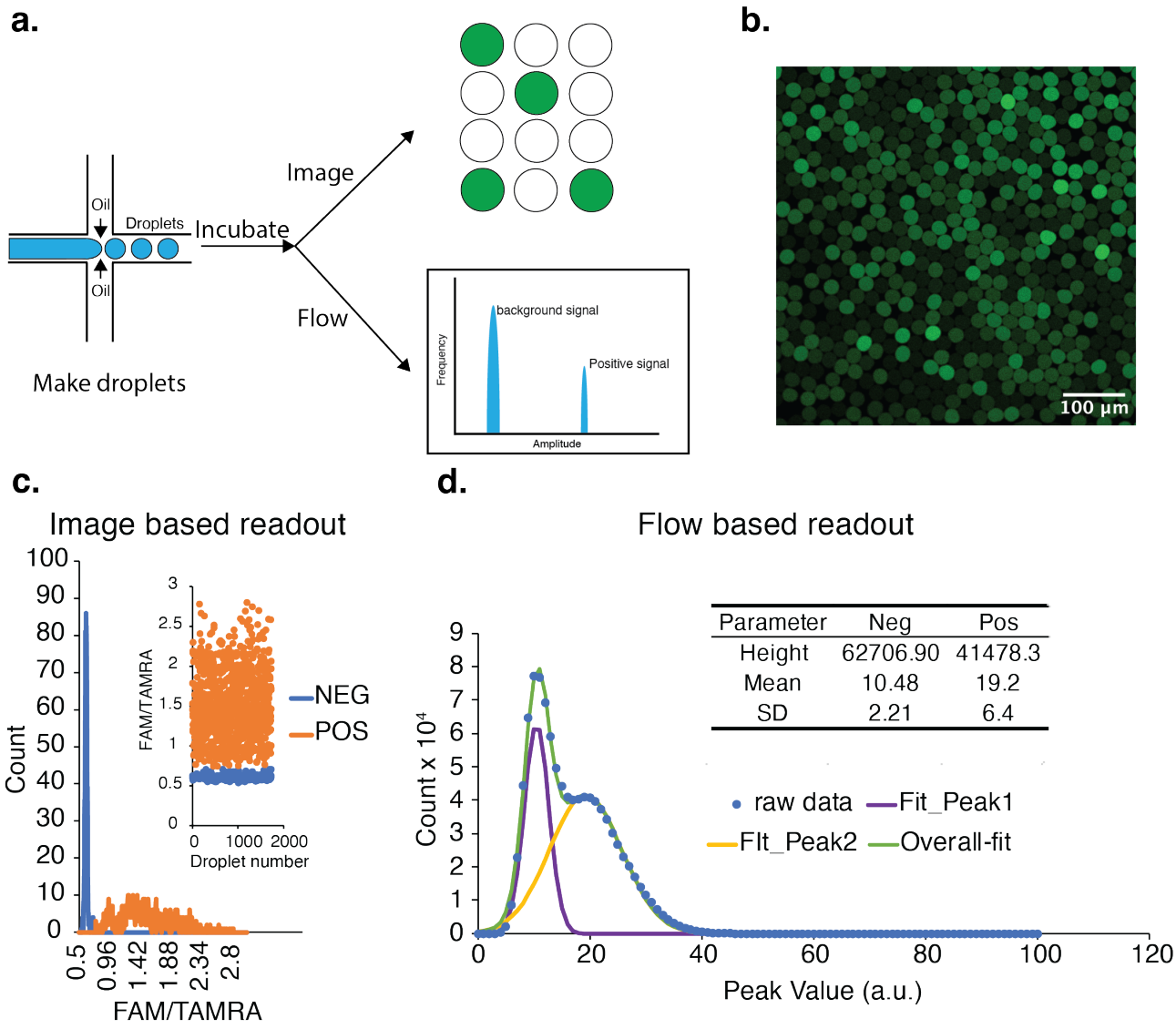

Figure S4.12. Comparison of image-based readout to flow-based readout. (a) Overview of droplet readout methods. (b) Raw data. Experiments were performed with 20 nM of each Mz sensor (5 Mz in total), 50 mM Tris (pH 8.5), 150 mM NaCl, 200 mM $MgCl_2$, 1X Bio-Rad ddPCR Supermix, 500 nM rGrU substrate, 1 pM of in vitro transcription RNA and incubated overnight incubation at 30°C. (c) Data analysis using image-based readout. (d) Data analysis using flow-based readout. The fit curve was calculated using Gaussian fitting. The detection limit was calculated as 17.10 based on LOD = mean + 3SD. Abbreviations: SD, standard deviation.

Reference

(1) Yang, K.; Chaput, J. C. REVEALR : A Multicomponent XNAzyme-Based Nucleic Acid Detection System for SARS-CoV-2 REVEALR : A Multicomponent XNAzyme-Based Nucleic Acid Detection System for SARS-CoV-2. **2021**. https://doi.org/10.1021/jacs.1c02664.

(2) Yang, K.; Schuder, D. N.; Ngor, A. K.; Chaput, J. C. REVEALR-Based Genotyping of SARS-CoV-2 Variants of Concern in Clinical Samples. *J Am Chem Soc* **2022**, *144* (26), 11685–11692. https://doi.org/10.1021/jacs.2c03420.

(3) Zhao, Y.; Chen, F.; Li, Q.; Wang, L.; Fan, C. Isothermal Amplification of Nucleic Acids. *Chem Rev* **2015**, *115* (22), 12491–12545. https://doi.org/10.1021/acs.chemrev.5b00428.

(4) Grandien, M. *Viral Diagnosis by Antigen Detection Techniques*; 1996; Vol. 5.

(5) Arumugam, A.; Wong, S. The Potential Use of Unprocessed Sample for RT-QPCR Detection of COVID-19 without an RNA Extraction Step. https://doi.org/10.1101/2020.04.06.028811.

(6) Wee, S. K.; Sivalingam, S. P.; Yap, E. P. H. Rapid Direct Nucleic Acid Amplification Test without Rna Extraction for Sars-Cov-2 Using a Portable Pcr Thermocycler. *Genes (Basel)* **2020**, *11* (6), 1–13. https://doi.org/10.3390/genes11060664.

(7) Wu, Q.; Suo, C.; Brown, T.; Wang, T.; Teichmann, S. A.; Bassett, A. R. *INSIGHT: A Population-Scale COVID-19 Testing Strategy Combining Point-of-Care Diagnosis with Centralized High-Throughput Sequencing*; 2021; Vol. 7. https://www.science.org.

(8) Broughton, J. P.; Deng, X.; Yu, G.; Fasching, C. L.; Servellita, V.; Singh, J.; Miao, X.; Streithorst, J. A.; Granados, A.; Sotomayor-Gonzalez, A.; Zorn, K.; Gopez, A.; Hsu, E.; Gu, W.; Miller, S.; Pan, C. Y.; Guevara, H.; Wadford, D. A.; Chen, J. S.; Chiu, C. Y. CRISPR–Cas12-Based Detection of SARS-CoV-2. *Nat Biotechnol* **2020**, *38* (July). https://doi.org/10.1038/s41587-020-0513-4.

(9) Shanmugakani, R. K.; Wu, M. An Isothermal Amplification-Coupled Dipstick for the Rapid Detection of COVID-19. *J Med Microbiol* **2022**, *71* (4). https://doi.org/10.1099/jmm.0.001519.

(10) Qian, J.; Boswell, S. A.; Chidley, C.; Lu, Z. xiang; Pettit, M. E.; Gaudio, B. L.; Fajnzylber, J. M.; Ingram, R. T.; Ward, R. H.; Li, J. Z.; Springer, M. An Enhanced Isothermal Amplification Assay for Viral Detection. *Nat Commun* **2020**, *11* (1), 1–10. https://doi.org/10.1038/s41467-020-19258-y.

(11) Friedrich, R.; Rappold, E.; Bogdan, C.; Held, J. Comparative Analysis of the Wako B-Glucan Test and the Fungitell Assay for Diagnosis of Candidemia and Pneumocystis Jirovecii Pneumonia. *J Clin Microbiol* **2020**, *56* (9). https://doi.org/10.1128/JCM.

(12) Pham, J.; Meyer, S.; Nguyen, C.; Williams, A.; Hunsicker, M.; Mchardy, I.; Gendlina, I.; Goldstein, D. Y.; Fox, A. S.; Hudson, A.; Darby, P.; Hovey, P.; Morales, J.; Mitchell, J.; Harrington, K.; Majlessi, M.; Moberly, J.; Shah, A.; Worlock, A.; Walcher, M.; Eaton, B.; Getman, D.; Clark, C. *Performance Characteristics of a High-Throughput Automated Transcription-Mediated Amplification Test for SARS-CoV-2 Detection*; 2020. https://journals.asm.org/journal/jcm.

(13) K. MULLIS; F. FALOONA; S. SCHARF; R. SAIKI; G. HORN; H. ERLICH. Specific Enzymatic Amplification of DNA In Vitro: The Polymerase Chain Reaction. *Cold Spring Harb Symp Quant Biol* **1986**.

(14) Khan, P.; Aufdembrink, L. M.; Engelhart, A. E. Isothermal SARS-CoV - 2 Diagnostics: Tools for Enabling Distributed Pandemic Testing as a Means of Supporting Safe Reopenings. *ACS Synth Biol* **2020**, *9* (11), 2861–2880. https://doi.org/10.1021/acssynbio.0c00359.

(15) Majumder, J.; Minko, T. Recent Developments on Therapeutic and Diagnostic Approaches for COVID-19. *AAPS Journal*. Springer Science and Business Media Deutschland GmbH January 1, 2021. https://doi.org/10.1208/s12248-020-00532-2.

(16) Tomita, N.; Mori, Y.; Kanda, H.; Notomi, T. Loop-Mediated Isothermal Amplification (LAMP) of Gene Sequences and Simple Visual Detection of Products. *Nat Protoc* **2008**, *3* (5), 877–882. https://doi.org/10.1038/nprot.2008.57.

(17) Kaneko, H.; Kawana, T.; Fukushima, E.; Suzutani, T. Tolerance of Loop-Mediated Isothermal Amplification to a Culture Medium and Biological Substances. *J Biochem Biophys Methods* **2007**, *70* (3), 499–501. https://doi.org/10.1016/j.jbbm.2006.08.008.

(18) Zheng, Z.; Cheng, Z. Advances in Molecular Diagnosis of Malaria. In *Advances in Clinical Chemistry*; 2017; Vol. 80. https://doi.org/10.1016/bs.acc.2016.11.006.

(19) Piepenburg, O.; Williams, C. H.; Stemple, D. L.; Armes, N. A. DNA Detection Using Recombination Proteins. *PLoS Biol* **2006**, *4* (7), 1115–1121. https://doi.org/10.1371/journal.pbio.0040204.

(20) Lobato, I. M.; O'Sullivan, C. K. Recombinase Polymerase Amplification: Basics, Applications and Recent Advances. *TrAC - Trends in Analytical Chemistry* **2018**, *98*, 19–35. https://doi.org/10.1016/j.trac.2017.10.015.

(21) Compton, J. Nucleic Acid Sequence-Based Amplification. *Nature* **1991**, *354*, 56–58.

(22) Zhao, Y.; Chen, F.; Li, Q.; Wang, L.; Fan, C. Isothermal Amplification of Nucleic Acids. *Chem Rev* **2015**, *115* (22), 12491–12545. https://doi.org/10.1021/acs.chemrev.5b00428.

(23) Vincent, M.; Xu, Y.; Kong, H. Helicase-Dependent Isothermal DNA Amplification. *EMBO Rep* **2004**, *5* (8), 795–800. https://doi.org/10.1038/sj.embor.7400200.

(24) Barreda-García, S.; Miranda-Castro, R.; de-los-Santos-Álvarez, N.; Miranda-Ordieres, A. J.; Lobo-Castañón, M. J. Helicase-Dependent Isothermal Amplification: A Novel Tool in the Development of Molecular-Based Analytical Systems for Rapid Pathogen Detection. *Analytical and Bioanalytical Chemistry*. Springer Verlag January 1, 2018, pp 679–693. https://doi.org/10.1007/s00216-017-0620-3.

(25) Ness, J. van; Ness, L. K. van; Galas, D. J. *Isothermal Reactions for the Amplification of Oligonucleotides*; 2003; Vol. 15. www.pnas.orgcgidoi10.1073pnas.0730811100.

(26) Khan, P.; Aufdembrink, L. M.; Engelhart, A. E. Isothermal SARS-CoV-2 Diagnostics: Tools for Enabling Distributed Pandemic Testing as a Means of Supporting Safe Reopenings. *ACS Synth Biol* **2020**, *9* (11), 2861–2880. https://doi.org/10.1021/acssynbio.0c00359.

(27) Reid, M. S.; Le, X. C.; Zhang, H. Exponential Isothermal Amplification of Nucleic Acids and Assays for Proteins , Cells , Small Molecules , and Enzyme Activities : An EXPAR Example Angewandte. **2018**, 11856–11866. https://doi.org/10.1002/anie.201712217.

(28) Jinek, M.; Chylinski, K.; Fonfara, I.; Hauer, M.; Doudna, J. A.; Charpentier, E. *A Programmable Dual-RNA-Guided DNA Endonuclease in Adaptive Bacterial Immunity*. https://www.science.org.

(29) Abudayyeh, O. O.; Gootenberg, J. S.; Konermann, S.; Joung, J.; Slaymaker, I. M.; Cox, D. B. T.; Shmakov, S.; Makarova, K. S.; Semenova, E.; Minakhin, L.; Severinov, K.; Regev, A.; Lander, E. S.; Koonin, E. v.; Zhang, F. C2c2 Is a Single-Component Programmable RNA-Guided RNA-Targeting CRISPR Effector. *Science (1979)* **2016**, *353* (6299). https://doi.org/10.1126/science.aaf5573.

(30) Gootenberg, J. S.; Abudayyeh, O. O.; Lee, J. W.; Essletzbichler, P.; Dy, A. J.; Joung, J.; Verdine, V.; Donghia, N.; Daringer, N. M.; Freije, C. A.; Myhrvold, C.; Bhattacharyya, R. P.; Livny, J.; Regev, A.; Koonin, E. v; Hung, D. T.; Sabeti, P. C.; Collins, J. J.; Zhang, † Feng. *Nucleic Acid Detection with CRISPR-Cas13a/C2c2*. https://www.science.org.

(31) Chen, J. S.; Ma, E.; Harrington, L. B.; da Costa, M.; Tian, X.; Palefsky, J. M.; Doudna, J. A. CRISPR-Cas12a Target Binding Unleashes Indiscriminate Single-Stranded DNase Activity. *Science (1979)* **2018**, *360* (6387), 436–439. https://doi.org/10.1126/science.aar6245.

(32) Wang, B.; Wang, R.; Wang, D.; Wu, J.; Li, J.; Wang, J.; Liu, H.; Wang, Y. Cas12aVDet: A CRISPR/Cas12a-Based Platform for Rapid and Visual Nucleic Acid Detection. *Anal Chem* **2019**, *91* (19), 12156–12161. https://doi.org/10.1021/acs.analchem.9b01526.

(33) Safari, F.; Afarid, M.; Rastegari, B.; Borhani-Haghighi, A.; Barekati-Mowahed, M.; Behzad-Behbahani, A. CRISPR Systems: Novel Approaches for Detection and Combating COVID-19. *Virus Research*. Elsevier B.V. March 1, 2021. https://doi.org/10.1016/j.virusres.2020.198282.

(34) Ganbaatar, U.; Liu, C. CRISPR-Based COVID-19 Testing: Toward Next-Generation Point-of-Care Diagnostics. *Frontiers in Cellular and Infection Microbiology*. Frontiers Media S.A. April 30, 2021. https://doi.org/10.3389/fcimb.2021.663949.

(35) Pang, B.; Xu, J.; Liu, Y.; Peng, H.; Feng, W.; Cao, Y.; Wu, J.; Xiao, H.; Pabbaraju, K.; Tipples, G.; Joyce, M. A.; Saffran, H. A.; Tyrrell, D. L.; Zhang, H.; Le, X. C. Isothermal Amplification and Ambient Visualization in a Single Tube for the Detection of SARS-CoV-2 Using Loop-Mediated Amplification and CRISPR Technology. *Anal Chem* **2020**, *92* (24), 16204–16212. https://doi.org/10.1021/acs.analchem.0c04047.

(36) Chandrasekaran, S. S.; Agrawal, S.; Fanton, A.; Jangid, A. R.; Charrez, B.; Escajeda, A. M.; Son, S.; Mcintosh, R.; Tran, H.; Bhuiya, A.; de León Derby, M. D.; Switz, N. A.; Armstrong, M.; Harris, A. R.; Prywes, N.; Lukarska, M.; Biering, S. B.; Smock, D. C. J.; Mok, A.; Knott, G. J.; Dang, Q.; van Dis, E.; Dugan, E.; Kim, S.;

Liu, T. Y.; Hamilton, J. R.; Lin-Shiao, E.; Stahl, E. C.; Tsuchida, C. A.; Giannikopoulos, P.; McElroy, M.; McDevitt, S.; Zur, A.; Sylvain, I.; Ciling, A.; Zhu, M.; Williams, C.; Baldwin, A.; Moehle, E. A.; Kogut, K.; Eskenazi, B.; Harris, E.; Stanley, S. A.; Lareau, L. F.; Tan, M. X.; Fletcher, D. A.; Doudna, J. A.; Savage, D. F.; Hsu, P. D. Rapid Detection of SARS-CoV-2 RNA in Saliva via Cas13. *Nat Biomed Eng* **2022**, *6* (8), 944–956. https://doi.org/10.1038/s41551-022-00917-y.

(37) Lin, M.; Yue, H.; Tian, T.; Xiong, E.; Zhu, D.; Jiang, Y.; Zhou, X. Glycerol Additive Boosts 100-Fold Sensitivity Enhancement for One-Pot RPA-CRISPR/Cas12a Assay. *Anal Chem* **2022**, *94* (23), 8277–8284. https://doi.org/10.1021/acs.analchem.2c00616.

(38) Rauch, J.; Valois, E.; Solley, S.; Rauch, J. N.; Solley, S. C.; Braig, F.; Lach, R. S.; Audouard, M.; Carlos Ponce-Rojas, J.; Costello, M. S.; Baxter, N. J.; Kosik, K. S.; Arias, C.; Acosta-Alvear, D.; Wilson, M. Z. UC Santa Barbara UC Santa Barbara Previously Published Works Title A Scalable, Easy-to-Deploy, Protocol for Cas13-Based Detection of SARS-CoV-2 Genetic Material Permalink Https://Escholarship.Org/Uc/Item/14c5s78p Publication Date A Scalable, Easy-to-Deploy, Protocol for Cas13-Based Detection of SARS-CoV-2 Genetic Material. **2020**. https://doi.org/10.1101/2020.04.20.052159.

(39) Patchsung, M.; Jantarug, K.; Pattama, A.; Aphicho, K.; Suraritdechachai, S.; Meesawat, P.; Sappakhaw, K.; Leelahakorn, N.; Ruenkam, T.; Wongsatit, T.; Athipanyasilp, N.; Eiamthong, B.; Lakkanasirorat, B.; Phoodokmai, T.; Niljianskul, N.; Pakotiprapha, D.; Chanarat, S.; Homchan, A.; Tinikul, R.; Kamutira, P.;

Phiwkaow, K.; Soithongcharoen, S.; Kantiwiriyawanitch, C.; Pongsupasa, V.; Trisrivirat, D.; Jaroensuk, J.; Wongnate, T.; Maenpuen, S.; Chaiyen, P.; Kamnerdnakta, S.; Swangsri, J.; Chuthapisith, S.; Sirivatanauksorn, Y.; Chaimayo, C.; Sutthent, R.; Kantakamalakul, W.; Joung, J.; Ladha, A.; Jin, X.; Gootenberg, J. S.; Abudayyeh, O. O.; Zhang, F.; Horthongkham, N.; Uttamapinant, C. Clinical Validation of a Cas13-Based Assay for the Detection of SARS-CoV-2 RNA. *Nat Biomed Eng* **2020**, *4* (12), 1140–1149. https://doi.org/10.1038/s41551-020-00603-x.

(40) Azhar, M.; Phutela, R.; Kumar, M.; Ansari, A. H.; Rauthan, R.; Gulati, S.; Sharma, N.; Sinha, D.; Sharma, S.; Singh, S.; Acharya, S.; Sarkar, S.; Paul, D.; Kathpalia, P.; Aich, M.; Sehgal, P.; Ranjan, G.; Bhoyar, R. C.; Singhal, K.; Lad, H.; Patra, P. K.; Makharia, G.; Chandak, G. R.; Pesala, B.; Chakraborty, D.; Maiti, S. Rapid and Accurate Nucleobase Detection Using FnCas9 and Its Application in COVID-19 Diagnosis. *Biosens Bioelectron* **2021**, *183*. https://doi.org/10.1016/j.bios.2021.113207.

(41) Joung, J. , L. A. , S. M. , K. N. G. , W. A. E. , S. M. , . . . & Z. F. (2020). D. of S.-C.-2 with S. one-pot testing. N. E. J. of M. 383(15), 1492-1494. *Detection of SARS-CoV-2 with SHERLOCK One-Pot Testing*; 2020.

(42) Ding, X.; Yin, K.; Li, Z.; Lalla, R. v.; Ballesteros, E.; Sfeir, M. M.; Liu, C. Ultrasensitive and Visual Detection of SARS-CoV-2 Using All-in-One Dual CRISPR-Cas12a Assay. *Nat Commun* **2020**, *11* (1). https://doi.org/10.1038/s41467-020-18575-6.

(43) Ali, Z.; Aman, R.; Mahas, A.; Rao, G. S.; Tehseen, M.; Marsic, T.; Salunke, R.; Subudhi, A. K.; Hala, S. M.; Hamdan, S. M.; Pain, A.; Alofi, F. S.; Alsomali, A.; Hashem, A. M.; Khogeer, A.; Almontashiri, N. A. M.; Abedalthagafi, M.; Hassan, N.; Mahfouz, M. M. ISCAN: An RT-LAMP-Coupled CRISPR-Cas12 Module for Rapid, Sensitive Detection of SARS-CoV-2. *Virus Res* **2020**, *288*. https://doi.org/10.1016/j.virusres.2020.198129.

(44) Guo, L.; Sun, X.; Wang, X.; Liang, C.; Jiang, H.; Gao, Q.; Dai, M.; Qu, B.; Fang, S.; Mao, Y.; Chen, Y.; Feng, G.; Gu, Q.; Wang, R. R.; Zhou, Q.; Li, W. SARS-CoV-2 Detection with CRISPR Diagnostics. *Cell Discovery*. Springer Nature December 1, 2020. https://doi.org/10.1038/s41421-020-0174-y.

(45) Gootenberg, J. S.; Abudayyeh, O. O.; Lee, J. W.; Essletzbichler, P.; Dy, A. J.; Joung, J.; Verdine, V.; Donghia, N.; Daringer, N. M.; Freije, C. A.; Myhrvold, C.; Bhattacharyya, R. P.; Livny, J.; Regev, A.; Koonin, E. v. Nucleic Acid Detection with CRISPR-Cas13a/C2c2. **2017**, *442* (April), 438–442.

(46) Gootenberg, J. S.; Abudayyeh, O. O.; Kellner, M. J.; Joung, J.; Collins, J. J.; Zhang, F. Multiplexed and Portable Nucleic Acid Detection Platform with Cas13, Cas12a and Csm6. *Science (1979)* **2018**, *360* (6387), 439–444. https://doi.org/10.1126/science.aaq0179.

(47) Santoro, S. W.; Joyce, G. F. A General Purpose RNA-Cleaving DNA Enzyme. *Proc Natl Acad Sci U S A* **1997**, *94* (9), 4262–4266. https://doi.org/10.1073/pnas.94.9.4262.

(48) Santoro, S. W.; Joyce, G. F. Mechanism and Utility of an RNA-Cleaving DNA Enzyme. *Biochemistry* **1998**, *37* (38), 13330–13342. https://doi.org/10.1021/bi9812221.

(49) Borggräfe, J.; Victor, J.; Rosenbach, H.; Viegas, A.; Gertzen, C. G. W.; Wuebben, C.; Kovacs, H.; Gopalswamy, M.; Riesner, D.; Steger, G.; Schiemann, O.; Gohlke, H.; Span, I.; Etzkorn, M. Time-Resolved Structural Analysis of an RNA-Cleaving DNA Catalyst. *Nature* **2022**, *601* (7891), 144–149. https://doi.org/10.1038/s41586-021-04225-4.

(50) Kolpashchikov, D. M. A Binary DNA Probe for Highly Specific Nucleic Acid Recognition. *J Am Chem Soc* **2006**, *128* (32), 10625–10628. https://doi.org/10.1021/ja0628093.

(51) Deng, M.; Zhang, D.; Zhou, Y.; Zhou, X. Highly Effective Colorimetric and Visual Detection of Nucleic Acids Using an Asymmetrically Split Peroxidase DNAzyme. *J Am Chem Soc* **2008**, *130* (39), 13095–13102. https://doi.org/10.1021/ja803507d.

(52) Kolpashchikov, D. M. A Binary Deoxyribozyme for Nucleic Acid Analysis. *ChemBioChem* **2007**, *8* (17), 2039–2042. https://doi.org/10.1002/cbic.200700384.

(53) Mokany, E.; Bone, S. M.; Young, P. E.; Doan, T. B.; Todd, A. v. MNAzymes, a Versatile New Class of Nucleic Acid Enzymes That Can Function as Biosensors and Molecular Switches. *J Am Chem Soc* **2010**, *132* (3), 1051–1059. https://doi.org/10.1021/ja9076777.

(54) Gao, J.; Shimada, N.; Maruyama, A. MNAzyme-Catalyzed Nucleic Acid Detection Enhanced by a Cationic Copolymer. *Biomater Sci* **2015**, *3* (5), 716–720. https://doi.org/10.1039/c4bm00449c.

(55) Hanpanich, O.; Saito, K.; Shimada, N.; Maruyama, A. One-Step Isothermal RNA Detection with LNA-Modified MNAzymes Chaperoned by Cationic Copolymer. *Biosens Bioelectron* **2020**, *165* (May), 112383. https://doi.org/10.1016/j.bios.2020.112383.

(56) Safdar, S.; Ven, K.; van Lent, J.; Pavie, B.; Rutten, I.; Dillen, A.; Munck, S.; Lammertyn, J.; Spasic, D. DNA-Only, Microwell-Based Bioassay for Multiplex Nucleic Acid Detection with Single Base-Pair Resolution Using MNAzymes. *Biosens Bioelectron* **2020**, *152* (January), 112017. https://doi.org/10.1016/j.bios.2020.112017.

(57) Zagorovsky, K.; Chan, W. C. W. A Plasmonic DNAzyme Strategy for Point-of-Care Genetic Detection of Infectious Pathogens. *Angewandte Chemie - International Edition* **2013**, *52* (11), 3168–3171. https://doi.org/10.1002/anie.201208715.

(58) Diao, W.; Tang, M.; Ding, X.; Zhang, Y.; Yang, J.; Cheng, W.; Mo, F.; Wen, B.; Xu, L.; Yan, Y. Electrochemical DNA Biosensor Based on MNAzyme-Mediated Signal Amplification. *Microchimica Acta* **2016**, *183* (9), 2563–2569. https://doi.org/10.1007/s00604-016-1910-8.

(59) Wang, F.; Elbaz, J.; Orbach, R.; Magen, N.; Willner, I. Amplified Analysis of DNA by the Autonomous Assembly of Polymers Consisting of DNAzyme Wires. *J Am Chem Soc* **2011**, *133* (43), 17149–17151. https://doi.org/10.1021/ja2076789.

(60) Wang, H.; Wang, H.; Wu, Q.; Liang, M.; Liu, X.; Wang, F. A DNAzyme-Amplified DNA Circuit for Highly Accurate MicroRNA Detection and Intracellular Imaging. *Chem Sci* **2019**, *10* (41), 9597–9604. https://doi.org/10.1039/c9sc03552d.

(61) Liu, S.; Cheng, C.; Liu, T.; Wang, L.; Gong, H.; Li, F. Highly Sensitive Fluorescence Detection of Target DNA by Coupling Exonuclease-Assisted Cascade Target Recycling and DNAzyme Amplification. *Biosens Bioelectron* **2015**, *63*, 99–104. https://doi.org/10.1016/j.bios.2014.07.023.

(62) Si, Y.; Li, L.; Wang, N.; Zheng, J.; Yang, R.; Li, J. Oligonucleotide Cross-Linked Hydrogel for Recognition and Quantitation of MicroRNAs Based on a Portable Glucometer Readout. *ACS Appl Mater Interfaces* **2019**, *11* (8), 7792–7799. https://doi.org/10.1021/acsami.8b21727.

(63) Hasick, N. J.; Ramadas, R.; Todd, A. v. Subzymes: Regulating DNAzymes for Point of Care Nucleic Acid Sensing. *Sens Actuators B Chem* **2019**, *297*. https://doi.org/10.1016/j.snb.2019.126704.

(64) Hasick, N.; Lawrence, A.; Ramadas, R.; Todd, A.; Smietana, M.; Arseniyadis, S.; Müller, S. Sensitive Detection of Nucleic Acids Using Subzyme Feedback Cascades. **2020**. https://doi.org/10.3390/molecules25081755.

(65) Mokany, E.; Tan, Y. L.; Bone, S. M.; Fuery, C. J.; Todd, A. v. MNAzyme QPCR with Superior Multiplexing Capacity. *Clin Chem* **2013**, *59* (2), 419–426. https://doi.org/10.1373/clinchem.2012.192930.

(66) Yang, J.; Tang, M.; Diao, W.; Cheng, W.; Zhang, Y.; Yan, Y. Electrochemical Strategy for Ultrasensitive Detection of MicroRNA Based on MNAzyme-Mediated

Rolling Circle Amplification on a Gold Electrode. *Microchimica Acta* **2016**, *183* (11), 3061–3067. https://doi.org/10.1007/s00604-016-1958-5.

(67) Mokany, E.; Bone, S. M.; Young, P. E.; Doan, T. B.; Todd, A. v. MNAzymes, a Versatile New Class of Nucleic Acid Enzymes That Can Function as Biosensors and Molecular Switches. *J Am Chem Soc* **2010**, *132* (3), 1051–1059. https://doi.org/10.1021/ja9076777.

(68) Gao, J.; Shimada, N.; Maruyama, A. MNAzyme-Catalyzed Nucleic Acid Detection Enhanced by a Cationic Copolymer. *Biomater Sci* **2015**, *3* (5), 716–720. https://doi.org/10.1039/c4bm00449c.

(69) Kolpashchikov, D. M. Binary Probes for Nucleic Acid Analysis. *Chem Rev* **2010**, *110* (8), 4709–4723. https://doi.org/10.1021/cr900323b.

(70) Kolpashchikov, D. M. Split DNA Enzyme for Visual Single Nucleotide Polymorphism Typing. *J Am Chem Soc* **2008**, *130* (10), 2934–2935. https://doi.org/10.1021/ja711192e.

(71) Stancescu, M.; Fedotova, T. A.; Hooyberghs, J.; Balaeff, A.; Kolpashchikov, D. M. Nonequilibrium Hybridization Enables Discrimination of a Point Mutation within 5-40 °c. *J Am Chem Soc* **2016**, *138* (41), 13465–13468. https://doi.org/10.1021/jacs.6b05628.

(72) Sando, S.; Narita, A.; Aoyama, Y. Light-up Hoechst-DNA Aptamer Pair: Generation of an Aptamer-Selective Fluorophore from a Conventional DNA-Staining Dye. *ChemBioChem* **2007**, *8* (15), 1795–1803. https://doi.org/10.1002/cbic.200700325.

(73) Safdar, S.; Ven, K.; van Lent, J.; Pavie, B.; Rutten, I.; Dillen, A.; Munck, S.; Lammertyn, J.; Spasic, D. DNA-Only, Microwell-Based Bioassay for Multiplex Nucleic Acid Detection with Single Base-Pair Resolution Using MNAzymes. *Biosens Bioelectron* **2020**, *152*. https://doi.org/10.1016/j.bios.2020.112017.

(74) Bengtson, H. N.; Homolka, S.; Niemann, S.; Reis, A. J.; da Silva, P. E.; Gerasimova, Y. v.; Kolpashchikov, D. M.; Rohde, K. H. Multiplex Detection of Extensively Drug Resistant Tuberculosis Using Binary Deoxyribozyme Sensors. *Biosens Bioelectron* **2017**, *94*, 176–183. https://doi.org/10.1016/j.bios.2017.02.051.

(75) Vester, B.; Lundberg, L. B.; Sørensen, M. D.; Babu, B. R.; Douthwaite, S.; Wengel, J. LNAzymes: Incorporation of LNA-Type Monomers into DNAzymes Markedly Increases RNA Cleavage. *J Am Chem Soc* **2002**, *124* (46), 13682–13683. https://doi.org/10.1021/ja0276220.

(76) Cairns, M. J.; King, A.; Sun, L. Q. Optimisation of the 10-23 DNAzyme-Substrate Pairing Interactions Enhanced RNA Cleavage Activity at Purine-Cytosine Target Sites. *Nucleic Acids Res* **2003**, *31* (11), 2883–2889. https://doi.org/10.1093/nar/gkg378.

(77) Schubert, S.; Gül, D. C.; Grunert, H. P.; Zeichhardt, H.; Erdmann, V. A.; Kurreck, J. RNA Cleaving “10-23” DNAzymes with Enhanced Stability and Activity. *Nucleic Acids Res* **2003**, *31* (20), 5982–5992. https://doi.org/10.1093/nar/gkg791.

(78) Wang, Y.; Nguyen, K.; Spitale, R. C.; Chaput, J. C. A Biologically Stable DNAzyme That Efficiently Silences Gene Expression in Cells. *Nat Chem* **2021**, *13* (4), 319–326. https://doi.org/10.1038/s41557-021-00645-x.

(79) Nawrot, B.; Widera, K.; Wojcik, M.; Rebowska, B.; Nowak, G.; Stec, W. J. Mapping of the Functional Phosphate Groups in the Catalytic Core of Deoxyribozyme 10-23. *FEBS Journal* **2007**, *274* (4), 1062–1072. https://doi.org/10.1111/j.1742-4658.2007.05655.x.

(80) Hanpanich, O.; Saito, K.; Shimada, N.; Maruyama, A. One-Step Isothermal RNA Detection with LNA-Modified MNAzymes Chaperoned by Cationic Copolymer. *Biosens Bioelectron* **2020**, *165* (June), 112383. https://doi.org/10.1016/j.bios.2020.112383.

(81) Cairns, M. J.; King, A.; Sun, L. Q. Optimisation of the 10-23 DNAzyme-Substrate Pairing Interactions Enhanced RNA Cleavage Activity at Purine-Cytosine Target Sites. *Nucleic Acids Res* **2003**, *31* (11), 2883–2889. https://doi.org/10.1093/nar/gkg378.

(82) Petersen, M.; Wengel, J. LNA: A Versatile Tool for Therapeutics and Genomics. *Trends Biotechnol* **2003**, *21* (2), 74–81. https://doi.org/10.1016/S0167-7799(02)00038-0.

(83) Schubert, S.; Fürste, J. P.; Werk, D.; Grunert, H. P.; Zeichhardt, H.; Erdmann, V. A.; Kurreck, J. Gaining Target Access for Deoxyribozymes. *J Mol Biol* **2004**, *339* (2), 355–363. https://doi.org/10.1016/j.jmb.2004.03.064.

(84) Jadhav, V. M.; Scaria, V.; Maiti, S. Antagomirzymes: Oligonucleotide Enzymes That Specifically Silence MicroRNA Function. *Angewandte Chemie - International Edition* **2009**, *48* (14), 2557–2560. https://doi.org/10.1002/anie.200805521.

(85) Schubert, S.; Gül, D. C.; Grunert, H. P.; Zeichhardt, H.; Erdmann, V. A.; Kurreck, J. RNA Cleaving “10-23” DNAzymes with Enhanced Stability and Activity. *Nucleic Acids Res* **2003**, *31* (20), 5982–5992. https://doi.org/10.1093/nar/gkg791.

(86) Fokina, A. A.; Meschaninova, M. I.; Durfort, T.; Venyaminova, A. G.; François, J. C. Targeting Insulin-like Growth Factor i with 10-23 DNAzymes: 2′-O-Methyl Modifications in the Catalytic Core Enhance MRNA Cleavage. *Biochemistry* **2012**, *51* (11), 2181–2191. https://doi.org/10.1021/bi201532q.

(87) Liu, Y.; Li, Z.; Liu, G.; Wang, Q.; Chen, W.; Zhang, D.; Cheng, M.; Zheng, Z.; Liu, K.; He, J. Breaking the Conservation of Guanine Residues in the Catalytic Loop of 10-23 Dnazyme by Position-Specific Nucleobase Modifications for Rate Enhancement. *Chemical Communications* **2013**, *49* (44), 5037–5039. https://doi.org/10.1039/c3cc42067a.

(88) Robaldo, L.; Berzal-Herranz, A.; Montserrat, J. M.; Iribarren, A. M. Activity of Core-Modified 10-23 DNAzymes against HCV. *ChemMedChem* **2014**, *9* (9), 2172–2177. https://doi.org/10.1002/cmdc.201402222.

(89) Zhu, J.; Li, Z.; Wang, Q.; Liu, Y.; He, J. The Contribution of Adenines in the Catalytic Core of 10-23 DNAzyme Improved by the 6-Amino Group Modifications. *Bioorg Med Chem Lett* **2016**, *26* (18), 4462–4465. https://doi.org/10.1016/j.bmcl.2016.07.076.

(90) Cutler, D. M.; Summers, L. H. The COVID-19 Pandemic and the $16 Trillion Virus. *JAMA* **2020**, *324* (3), 1495–1496. https://doi.org/10.1257/pol.20170046.

(91) Mina, B. M. J.; Andersen, K. G. COVID-19 Testing: One Size Does Not Fit All. **2021**, *37* (6525), 126–128.

(92) Notomi, T.; Okayama, H.; Masubuchi, H.; Yonekawa, T.; Watanabe, K.; Amino, N.; Hase, T. Loop-Mediated Isothermal Amplification of DNA. *Nucleic Acids Res* **2000**, *28* (12), e63.

(93) Becherer, L.; Borst, N.; Bakheit, M.; Frischmann, S.; Zengerle, R.; von Stetten, F. Loop-Mediated Isothermal Amplification (LAMP)-Review and Classification of Methods for Sequence-Specific Detection. *Analytical Methods* **2020**, *12* (6), 717–746. https://doi.org/10.1039/c9ay02246e.

(94) Kellner, M. J.; Koob, J. G.; Gootenberg, J. S.; Abudayyeh, O. O.; Zhang, F. SHERLOCK: Nucleic Acid Detection with CRISPR Nucleases. *Nat Protoc* **2019**, *14* (10), 2986–3012. https://doi.org/10.1038/s41596-019-0210-2.

(95) Damha, M. J.; Wilds, C. J.; Noronha, A.; Brukner, I.; Borkow, G.; Arion, D.; Parniak, M. A. Hybrids of RNA and Arabinonucleic Acids (ANA and 2'F-ANA) Are Substrates of Ribonuclease H [11]. *J Am Chem Soc* **1998**, *120* (49), 12976–12977. https://doi.org/10.1021/ja982325+.

(96) Pan, Y.; Zhang, D.; Yang, P.; Poon, L. L. M.; Wang, Q. Viral Load of SARS-CoV-2 in Clinical Samples. *Lancet Infect Dis* **2020**, *20* (4), 411–412. https://doi.org/10.1016/S1473-3099(20)30113-4.

(97) Chan, K. H.; Sridhar, S.; Zhang, R. R.; Chu, H.; Fung, A. Y. F.; Chan, G.; Chan, J. F. W.; To, K. K. W.; Hung, I. F. N.; Cheng, V. C. C.; Yuen, K. Y. Factors Affecting

Stability and Infectivity of SARS-CoV-2. *Journal of Hospital Infection* **2020**, *106* (2), 226–231. https://doi.org/10.1016/j.jhin.2020.07.009.

(98) Robson, F.; Khan, K. S.; Le, T. K.; Paris, C.; Demirbag, S.; Barfuss, P.; Rocchi, P.; Ng, W. L. Coronavirus RNA Proofreading: Molecular Basis and Therapeutic Targeting. *Molecular Cell*. Cell Press September 3, 2020, pp 710–727. https://doi.org/10.1016/j.molcel.2020.07.027.

(99) Otto, S. P.; Day, T.; Arino, J.; Colijn, C.; Dushoff, J.; Li, M.; Mechai, S.; van Domselaar, G.; Wu, J.; Earn, D. J. D.; Ogden, N. H. The Origins and Potential Future of SARS-CoV-2 Variants of Concern in the Evolving COVID-19 Pandemic. *Current Biology*. Cell Press July 26, 2021, pp R918–R929. https://doi.org/10.1016/j.cub.2021.06.049.

(100) Korber, B.; Fischer, W. M.; Gnanakaran, S.; Yoon, H.; Theiler, J.; Abfalterer, W.; Hengartner, N.; Giorgi, E. E.; Bhattacharya, T.; Foley, B.; Hastie, K. M.; Parker, M. D.; Partridge, D. G.; Evans, C. M.; Freeman, T. M.; de Silva, T. I.; Angyal, A.; Brown, R. L.; Carrilero, L.; Green, L. R.; Groves, D. C.; Johnson, K. J.; Keeley, A. J.; Lindsey, B. B.; Parsons, P. J.; Raza, M.; Rowland-Jones, S.; Smith, N.; Tucker, R. M.; Wang, D.; Wyles, M. D.; McDanal, C.; Perez, L. G.; Tang, H.; Moon-Walker, A.; Whelan, S. P.; LaBranche, C. C.; Saphire, E. O.; Montefiori, D. C. Tracking Changes in SARS-CoV-2 Spike: Evidence That D614G Increases Infectivity of the COVID-19 Virus. *Cell* **2020**, *182* (4), 812-827.e19. https://doi.org/10.1016/j.cell.2020.06.043.

(101) Tao, K.; Tzou, P. L.; Nouhin, J.; Gupta, R. K.; de Oliveira, T.; Kosakovsky Pond, S. L.; Fera, D.; Shafer, R. W. The Biological and Clinical Significance of Emerging SARS-CoV-2 Variants. *Nature Reviews Genetics*. Nature Research December 1, 2021, pp 757–773. https://doi.org/10.1038/s41576-021-00408-x.

(102) Cai, Y.; Zhang, J.; Xiao, T.; Lavine, C. L.; Rawson, S.; Peng, H.; Zhu, H.; Anand, K.; Tong, P.; Gautam, A.; Lu, S.; Sterling, S. M.; Walsh, R. M.; Rits-Volloch, S.; Lu, J.; Wesemann, D. R.; Yang, W.; Seaman, M. S.; Chen, B. *Structural Basis for Enhanced Infectivity and Immune Evasion of SARS-CoV-2 Variants*. https://www.science.org.

(103) Gobeil, S. M. C.; Janowska, K.; McDowell, S.; Mansouri, K.; Parks, R.; Stalls, V.; Kopp, M. F.; Manne, K.; Li, D.; Wiehe, K.; Saunders, K. O.; Edwards, R. J.; Korber, B.; Haynes, B. F.; Henderson, R.; Acharya, P. Effect of Natural Mutations of SARS-CoV-2 on Spike Structure, Conformation, and Antigenicity. *Science (1979)* **2021**, *373* (6555). https://doi.org/10.1126/science.abi6226.

(104) Mccallum, M.; Walls, A. C.; Sprouse, K. R.; Bowen, J. E.; Rosen, L. E.; Dang, H. v; de Marco, A.; Franko, N.; Tilles, S. W.; Logue, J.; Miranda, M. C.; Ahlrichs, M.; Carter, L.; Snell, G.; Pizzuto, M. S.; Chu, H. Y.; van Voorhis, W. C.; Corti, D.; Veesler, D. *Molecular Basis of Immune Evasion by the Delta and Kappa SARS-CoV-2 Variants*. https://www.science.org.

(105) Callaway, E. The Coronavirus Is Mutating - Does It Matter? *Nature* **2020**, *585* (7824), 174–177. https://doi.org/10.1038/d41586-020-02544-6.

(106) Cao, Y.; Wang, J.; Jian, F.; Xiao, T.; Song, W.; Yisimayi, A.; Huang, W.; Li, Q.; Wang, P.; An, R.; Wang, J.; Wang, Y.; Niu, X.; Yang, S.; Liang, H.; Sun, H.; Li, T.; Yu, Y.; Cui, Q.; Liu, S.; Yang, X.; Du, S.; Zhang, Z.; Hao, X.; Shao, F.; Jin, R.; Wang, X.; Xiao, J.; Wang, Y.; Xie, X. S. Omicron Escapes the Majority of Existing SARS-CoV-2 Neutralizing Antibodies. *Nature* **2022**, *602* (7898), 657–663. https://doi.org/10.1038/s41586-021-04385-3.

(107) Cyranoski, D. Alarming COVID Variants Show Vital Role of Genomic Surveillance. *Nature* **2021**, 337–339.

(108) World Health Organization. *Methods for the detection and characterisation of SARS-CoV-2 variants: first update*. World Health Organization. Regional Office for Europe.

(109) Bal, A.; Destras, G.; Gaymard, A.; Stefic, K.; Marlet, J.; Eymieux, S.; Regue, H.; Semanas, Q.; d'Aubarede, C.; Billaud, G.; Laurent, F.; Gonzalez, C.; Mekki, Y.; Valette, M.; Bouscambert, M.; Gaudy-Graffin, C.; Lina, B.; Morfin, F.; Josset, L. Two-Step Strategy for the Identification of SARS-CoV-2 Variant of Concern 202012/01 and Other Variants with Spike Deletion H69–V70, France, August to December 2020. *Eurosurveillance* **2021**, *26* (3). https://doi.org/10.2807/1560-7917.ES.2021.26.3.2100008.

(110) Bechtold, P.; Wagner, P.; Hosch, S.; Siegrist, D.; Ruiz-Serrano, A.; Gregorini, M.; Mpina, M.; Ondó, F. A.; Obama, J.; Ayekaba, M. O. O.; Engler, O.; Stark, W. J.; Daubenberger, C. A.; Schindler, T. Rapid Identification of SARS-CoV-2 Variants of

Concern Using a Portable PeakPCR Platform. *Anal Chem* **2021**, *93* (49). https://doi.org/10.1021/acs.analchem.1c02368.

(111) Sherrill-Mix, S.; Hwang, Y.; Roche, A. M.; Glascock, A.; Weiss, S. R.; Li, Y.; Haddad, L.; Deraska, P.; Monahan, C.; Kromer, A.; Graham-Wooten, J.; Taylor, L. J.; Abella, B. S.; Ganguly, A.; Collman, R. G.; van Duyne, G. D.; Bushman, F. D. Detection of SARS-CoV-2 RNA Using RT-LAMP and Molecular Beacons. *Genome Biol* **2021**, *22* (1). https://doi.org/10.1186/s13059-021-02387-y.

(112) Kim, S.; Misra, A. SNP Genotyping: Technologies and Biomedical Applications. *Annu Rev Biomed Eng* **2007**, *9*, 289–320. https://doi.org/10.1146/annurev.bioeng.9.060906.152037.

(113) He, C.; Lin, C.; Mo, G.; Xi, B.; Li, A.; Huang, D.; Wan, Y.; Chen, F.; Liang, Y.; Zuo, Q.; Xu, W.; Feng, D.; Zhang, G.; Han, L.; Ke, C.; Du, H.; Huang, L. Rapid and Accurate Detection of SARS-CoV-2 Mutations Using a Cas12a-Based Sensing Platform. *Biosens Bioelectron* **2022**, *198*. https://doi.org/10.1016/j.bios.2021.113857.

(114) Malik, T. N.; Chaput, J. C. XNA Enzymes by Evolution and Design. *Current Research in Chemical Biology* **2021**, *1*. https://doi.org/10.1016/j.crchbi.2021.100012.

(115) Abi, A.; Safavi, A. Targeted Detection of Single-Nucleotide Variations: Progress and Promise. *ACS Sensors*. American Chemical Society April 26, 2019, pp 792–807. https://doi.org/10.1021/acssensors.8b01604.

(116) Kauppinen, S.; Vester, B.; Wengel, J. Locked Nucleic Acid (LNA): High Affinity Targeting of RNA for Diagnostics and Therapeutics. *Drug Discovery Today: Technologies*. 2005. https://doi.org/10.1016/j.ddtec.2005.08.012.

(117) Koshkin, A. A.; Nielsen, P.; Meldgaard, M.; Rajwanshi, V. K.; Singh, S. K.; Wengel, J. LNA (Locked Nucleic Acid): An RNA Mimic Forming Exceedingly Stable LNA:LNA Duplexes [3]. *Journal of the American Chemical Society*. December 23, 1998, pp 13252–13253. https://doi.org/10.1021/ja9822862.

(118) Koshkin, A. A.; Rajwanshi, V. K.; Wengel, J. Novel Convenient Syntheses of LNA [2.2.1]Bicyclo Nucleosides. *Tetrahedron Lett* **1998**, *39* (24), 4381–4384. https://doi.org/10.1016/S0040-4039(98)00706-0.

(119) You, Y.; Moreira, B. G.; Behlke, M. A.; Owczarzy, R. Design of LNA Probes That Improve Mismatch Discrimination. *Nucleic Acids Res* **2006**, *34* (8). https://doi.org/10.1093/nar/gkl175.

(120) Mullen, J. L.; Tsueng, G.; Latif, A. A.; Alkuzweny, M.; Cano, M.; Haag, E.; Zhou, J.; Zeller, M.; Hufbauer, E.; Matteson, N.; Andersen, K. G.; Wu, C.; Su, A. I.; Gangavarapu, K.; Hughes, L. D.; the Center for Viral Systems Biology. Outbreak.Info [Cited August 15 2022]. *outbreak.info* **2020**.

(121) Ulrich, M. P.; Christensen, D. R.; Coyne, S. R.; Craw, P. D.; Henchal, E. A.; Sakai, S. H.; Swenson, D.; Tholath, J.; Tsai, J.; Weir, A. F.; Norwood, D. A. Evaluation of the Cepheid GeneXpert® System for Detecting Bacillus Anthracis. *J Appl Microbiol* **2006**, *100* (5). https://doi.org/10.1111/j.1365-2672.2006.02810.x.

(122) Yu, C. Y.; Chan, K. G.; Yean, C. Y.; Ang, G. Y. Nucleic Acid-Based Diagnostic Tests for the Detection SARS-CoV-2: An Update. *Diagnostics*. MDPI January 1, 2021. https://doi.org/10.3390/diagnostics11010053.

(123) Fredricks, D. N.; Relman, D. A. *Application of Polymerase Chain Reaction to the Diagnosis of Infectious Diseases*; 1999; Vol. 29. https://about.jstor.org/terms.

(124) Chen, Y.; Qian, C.; Liu, C.; Shen, H.; Wang, Z.; Ping, J.; Wu, J.; Chen, H. Nucleic Acid Amplification Free Biosensors for Pathogen Detection. *Biosensors and Bioelectronics*. Elsevier Ltd April 1, 2020. https://doi.org/10.1016/j.bios.2020.112049.

(125) Cao, Y.; Zheng, Z.; Monbouquette, H. G. Nucleic Acid Amplification-Free Detection of DNA and RNA at Ultralow Concentration. *Current Opinion in Biotechnology*. Elsevier Ltd October 1, 2021, pp 145–150. https://doi.org/10.1016/j.copbio.2021.07.022.

(126) Hajian, R.; Balderston, S.; Tran, T.; deBoer, T.; Etienne, J.; Sandhu, M.; Wauford, N. A.; Chung, J. Y.; Nokes, J.; Athaiya, M.; Paredes, J.; Peytavi, R.; Goldsmith, B.; Murthy, N.; Conboy, I. M.; Aran, K. Detection of Unamplified Target Genes via CRISPR–Cas9 Immobilized on a Graphene Field-Effect Transistor. *Nat Biomed Eng* **2019**, *3* (6), 427–437. https://doi.org/10.1038/s41551-019-0371-x.

(127) Fozouni, P.; Son, S.; Díaz de León Derby, M.; Knott, G. J.; Gray, C. N.; D'Ambrosio, M. v.; Zhao, C.; Switz, N. A.; Kumar, G. R.; Stephens, S. I.; Boehm, D.; Tsou, C. L.; Shu, J.; Bhuiya, A.; Armstrong, M.; Harris, A. R.; Chen, P. Y.; Osterloh, J. M.; Meyer-Franke, A.; Joehnk, B.; Walcott, K.; Sil, A.; Langelier, C.; Pollard, K. S.;

Crawford, E. D.; Puschnik, A. S.; Phelps, M.; Kistler, A.; DeRisi, J. L.; Doudna, J. A.; Fletcher, D. A.; Ott, M. Amplification-Free Detection of SARS-CoV-2 with CRISPR-Cas13a and Mobile Phone Microscopy. *Cell* **2021**, *184* (2), 323-333.e9. https://doi.org/10.1016/j.cell.2020.12.001.

(128) Fozouni, P.; Son, S.; Díaz de León Derby, M.; Knott, G. J.; Gray, C. N.; D'Ambrosio, M. v.; Zhao, C.; Switz, N. A.; Kumar, G. R.; Stephens, S. I.; Boehm, D.; Tsou, C.-L.; Shu, J.; Bhuiya, A.; Armstrong, M.; Harris, A. R.; Chen, P.-Y.; Osterloh, J. M.; Meyer-Franke, A.; Joehnk, B.; Walcott, K.; Sil, A.; Langelier, C.; Pollard, K. S.; Crawford, E. D.; Puschnik, A. S.; Phelps, M.; Kistler, A.; DeRisi, J. L.; Doudna, J. A.; Fletcher, D. A.; Ott, M. Amplification-Free Detection of SARS-CoV-2 with CRISPR-Cas13a and Mobile Phone Microscopy. *Cell* **2020**. https://doi.org/10.1016/j.cell.2020.12.001.

(129) Hindson, B. J.; Ness, K. D.; Masquelier, D. A.; Belgrader, P.; Heredia, N. J.; Makarewicz, A. J.; Bright, I. J.; Lucero, M. Y.; Hiddessen, A. L.; Legler, T. C.; Kitano, T. K.; Hodel, M. R.; Petersen, J. F.; Wyatt, P. W.; Steenblock, E. R.; Shah, P. H.; Bousse, L. J.; Troup, C. B.; Mellen, J. C.; Wittmann, D. K.; Erndt, N. G.; Cauley, T. H.; Koehler, R. T.; So, A. P.; Dube, S.; Rose, K. A.; Montesclaros, L.; Wang, S.; Stumbo, D. P.; Hodges, S. P.; Romine, S.; Milanovich, F. P.; White, H. E.; Regan, J. F.; Karlin-Neumann, G. A.; Hindson, C. M.; Saxonov, S.; Colston, B. W. High-Throughput Droplet Digital PCR System for Absolute Quantitation of DNA Copy Number. *Anal Chem* **2011**, *83* (22), 8604–8610. https://doi.org/10.1021/ac202028g.

(130) Thakur, S.; Sasi, S.; Pillai, S. G.; Nag, A.; Shukla, D.; Singhal, R.; Phalke, S.; Velu, G. S. K. SARS-CoV-2 Mutations and Their Impact on Diagnostics, Therapeutics and Vaccines. *Frontiers in Medicine*. Frontiers Media S.A. February 22, 2022. https://doi.org/10.3389/fmed.2022.815389.

(131) Vallejo, D.; Nikoomanzar, A.; Paegel, B. M.; Chaput, J. C. Fluorescence-Activated Droplet Sorting for Single-Cell Directed Evolution. *ACS Synth Biol* **2019**, *8* (6), 1430–1440. https://doi.org/10.1021/acssynbio.9b00103.

(132) Bone, S. M.; Todd, A. v. MNAzymes Provide a Universal Mechanism for Triggering DNAzyme Synthesis Cascades. *Chemical Communications* **2014**, *50* (87), 13243–13246. https://doi.org/10.1039/c4cc05919k.

(133) Ghouneimy, A.; Mahas, A.; Marsic, T.; Aman, R.; Mahfouz, M. CRISPR-Based Diagnostics: Challenges and Potential Solutions toward Point-of-Care Applications. *ACS Synthetic Biology*. American Chemical Society 2022. https://doi.org/10.1021/acssynbio.2c00496.

(134) Vallejo, D.; Nikoomanzar, A.; Chaput, J. C. *Directed Evolution of Custom Polymerases Using Droplet Microfluidics*, 1st ed.; Elsevier Inc., 2020. https://doi.org/10.1016/bs.mie.2020.04.056.

(135) Kaur, N.; Thota, N.; Toley, B. J. A Stoichiometric and Pseudo Kinetic Model of Loop Mediated Isothermal Amplification. *Comput Struct Biotechnol J* **2020**, *18*, 2336–2346. https://doi.org/10.1016/j.csbj.2020.08.020.

(136) Da Silva, S. J. R.; Pardee, K.; Pena, L. Loop-Mediated Isothermal Amplification (LAMP) for the Diagnosis of Zika Virus: A Review. *Viruses* **2019**, *12* (1), 1–20. https://doi.org/10.3390/v12010019.

(137) Zyrina, N. V.; Antipova, V. N.; Zheleznaya, L. A. Ab Initio Synthesis by DNA Polymerases. *FEMS Microbiol Lett* **2014**, *351* (1), 1–6. https://doi.org/10.1111/1574-6968.12326.

(138) Tanner, N. A.; Zhang, Y.; Evans, T. C. Simultaneous Multiple Target Detection in Real-Time Loop-Mediated Isothermal Amplification. *Biotechniques* **2012**, *53* (2), 81–89. https://doi.org/10.2144/0000113902.

(139) Esbin, M. N.; Whitney, O. N.; Chong, S.; Maurer, A.; Darzacq, X.; Tjian, R. Overcoming the Bottleneck to Widespread Testing: A Rapid Review of Nucleic Acid Testing Approaches for COVID-19 Detection. *Rna* **2020**, *26* (7), 771–783. https://doi.org/10.1261/rna.076232.120.

(140) Hafner, G. J.; Yang, I. C.; Woiter, L. C.; Stafford, M. R.; Giffard, P. M. Isothermal Amplification and Multimerization of Dna by Bst DNA Polymerase. *Biotechniques* **2001**, *30* (4), 852–867. https://doi.org/10.2144/01304rr03.

(141) Ma, L.; Liu, J. Catalytic Nucleic Acids: Biochemistry, Chemical Biology, Biosensors, and Nanotechnology. https://doi.org/10.1016/j.isci.

(142) Lyu, M.; Kong, L.; Yang, Z.; Wu, Y.; McGhee, C. E.; Lu, Y. PNA-Assisted DNAzymes to Cleave Double-Stranded DNA for Genetic Engineering with High Sequence Fidelity. *J Am Chem Soc* **2021**, *143* (26), 9724–9728. https://doi.org/10.1021/jacs.1c03129.

(143) Safdar, S.; Lammertyn, J.; Spasic, D. RNA-Cleaving NAzymes: The Next Big Thing in Biosensing? *Trends in Biotechnology*. Elsevier Ltd December 1, 2020, pp 1343–1359. https://doi.org/10.1016/j.tibtech.2020.04.012.